

# Structure and dynamics of new intelligent copolymer hydrogels and hydrogel nanoparticle hybrids

Dissertation

zur Erlangung des akademischen Grades eines  
Doktor der Naturwissenschaft (Dr. rer. nat.)

im Fach Chemie an der Fakultät für Biologie,  
Chemie und Geowissenschaften der  
Universität Bayreuth

vorgelegt von

**Yvonne Hertle**

geboren in Augsburg

Bayreuth, der 15. Dezember 2010



Die vorliegende Arbeit wurde in der Zeit von Oktober 2007 bis Dezember 2010 an der Universität Bayreuth am Lehrstuhl für Physikalische Chemie I unter Betreuung von Herrn Prof. Dr. Thomas Hellweg angefertigt.

Vollständiger Abdruck der von der Fakultät für Biologie, Chemie und Geowissenschaften der Universität Bayreuth genehmigten Dissertation zur Erlangung des akademischen Grades eines Doktors der Naturwissenschaften (Dr. rer. nat.).

Dissertation eingereicht am: 15. Dezember 2010

Zulassung durch die Prüfungskommission: 22. Dezember 2010

Wissenschaftliches Kolloquium: 05. April 2011

Amtierender Dekan:

*Prof. Dr. Stephan Clemens*

Prüfungsausschuss:

*Prof. Dr. Thomas Hellweg (Erstgutachter)*

*Prof. Dr. Stephan Förster (Zweitgutachter)*

*Prof. Dr. Rainer Schobert (Vorsitz)*

*Prof. Dr. Axel H. E. Müller*



*Der Zweifel ist der Beginn der Wissenschaft.*

*Wer nichts anzweifelt, prüft nichts.*

*Wer nichts prüft, entdeckt nichts.*

*Wer nichts entdeckt, ist blind*

*und bleibt blind.*

*Pierre Teilhard de Chardin*



# Danksagung

An dieser Stelle möchte ich allen dafür danken, die mich in der Zeit meiner Promotion begleitet und unterstützt haben.

Ganz besonderer Dank gilt meinem Doktorvater, Herrn Prof. Dr. Thomas Hellweg, für die Möglichkeit diese Arbeit in seiner Gruppe durchführen zu können. Er hat mich in dieser Zeit stets unterstützt und mit Diskussionen motiviert.

Besonderer Dank für die gute Zusammenarbeit geht auch an meine Kollegen am Lehrstuhl für Physikalische Chemie I der Universität Bayreuth. Ohne eure stete Diskussions- und Hilfsbereitschaft, sowie die zahlreichen heiteren Kaffeepausen, wäre die Arbeit in dieser Form nicht möglich gewesen. Dies gilt auch für meine Kollegen in allen Arbeitsgruppen des Fachbereiches Chemie der Universität Bayreuth.

Bei Michael Zeiser bedanke ich mich für die Hilfe bei theoretischen Fragen und die Unterstützung bei Messzeiten in Garching und Grenoble.

Herzlichen Dank auch an meine ehemaligen Kollegen Stefan Wellert und Matthias Karg, die mich in die Geheimnisse der Licht- und Neutronenstreuung eingeführt haben und mir jederzeit Hilfe zuteil werden ließen.

Karlheinz Lauterbach, Elisabeth Dünfelder und Christa Bächer möchte ich für die gute Zusammenarbeit und Unterstützung bei Arbeiten danken.

Meinen Praktikanten Matthias Bieligmeyer, Tobias Rudolph und Christoph Hasenöhrle danke ich für ihr großes Interesse und ihren Fleiß bei der Bearbeitung ihrer Themen: Alles Gute und viel Erfolg für euren weiteren Lebensweg.

Auch möchte ich mich bei meinen Freunden in Bayreuth sowie in Augsburg, besonders Stefanie Scherer und Simone Wagner, für ihre seelische und moralische Unterstützung bedanken und dafür, dass sie immer an mich geglaubt haben.

Ein sehr großer Dank geht an meine Familie: Ihr habt mir dieses Universitätsstudium

ermöglicht, mir jederzeit und in jeder Hinsicht zur Seite gestanden und mich nicht zuletzt fortlaufend ermuntert, diese Doktorarbeit fertig zu stellen. Ich weiss mein Glück zu schätzen, ich danke euch für alles.

Christian, ich danke dir von ganzem Herzen für deine unglaubliche Geduld und alles was man mit Worten nicht sagen kann.



# ABSTRACT

Polymeric gels consist of a chemically or physically crosslinked polymer network swollen with a certain amount of solvent and most of these gels show an ability of reversible swelling or shrinking due to small changes in their environment (as changes in pH, temperature or electric field). In the group of hydrogels, poly(*N*-isopropylacrylamide) (poly(NIPAM)) crosslinked with *N,N'*-methylenebisacrylamide (BIS) is the most well-known member of the class of thermoresponsive "smart" polymers.

This work covers the characterization of thermoresponsive poly(NIPAM) gels and shows different kinds of possibilities tuning their properties. The first part of this thesis presents different methods for the preparation of crosslinker gradient macroscopic gels with the dimensions of some cubic centimetres. The swelling behaviour from different zones of the macrogel with a varying crosslinker content was studied as a function of temperature. Furthermore, the internal dynamics of a poly(NIPAM-co-butenoic acid) copolymer macrogel was investigated by neutron spin echo and compared to the results for a chemically identical microgel. Due to the different preparation conditions of the macro- and microgel, a difference in the collective diffusion of the network was expected. Beside this, copolymer microgel particles based on NIPAM and *N-tert*-butylacrylamide (NtBAM) were synthesized. The particle size and the swelling behaviour of the obtained colloidal microgels was characterized with respect to the content of the comonomer using different scattering techniques and electron microscopy. In addition, an attempt was made to describe theoretically the temperature induced deswelling with the Flory-Rehner theory.

The latter part of this thesis focuses on hybrid materials based on magnetic nanoparticles and thermoresponsive microgels. First of all, different approaches for the synthesis of cobalt and nickel nanoparticles and their protection against oxidation were made. Furthermore, these magnetic particles were incorporated as an inorganic core in poly(NIPAM) core-shell systems, as well as randomly distributed particles within the gel network.



# ZUSAMMENFASSUNG

Polymergele sind aus chemisch oder physikalisch vernetzten Polymerketten aufgebaut und weisen dabei, bedingt durch ihre Netzwerkstruktur, ein Quellverhalten auf. Die meisten Vertreter dieser Klasse zeigen zusätzlich durch kleine Veränderungen in ihrer Umgebung, wie eine Änderung des pH-Wertes, der Temperatur oder eines elektrischen Feldes, eine reversible Volumenänderung. Das wohlbekannteste Mitglied der sogenannten thermoresponsiven, "intelligenten" Gele ist ein Hydrogel auf der Basis von *N,N'*-Methylenbisacrylamid-vernetztem Poly(*N*-Isopropylacrylamid) (Poly(NIPAM)).

Die vorliegende Arbeit beschäftigt sich mit den charakteristischen Eigenschaften von thermoresponsiven Gelen auf Basis von Poly(NIPAM) und den vielfältigen Möglichkeiten diese Eigenschaften gezielt zu steuern. Im ersten Teil der Arbeit werden unterschiedliche Methoden zur Herstellung von Makrogelen basierend auf Poly(NIPAM) mit einem Quervernetzergradient entwickelt, wobei die hier synthetisierten Gele eine Größe von einigen Kubikzentimetern aufweisen. Für eine anschließende Charakterisierung des Quellverhaltens wurde das Quellverhältnis  $\alpha$  in Abhängigkeit von der Temperatur für unterschiedliche Bereiche des Makrogels bestimmt. Die so erhaltenen Quellkurven konnten dann anhand des Quellvermögens den jeweiligen Bereichen mit unterschiedlichem Quervernetzergehalt zugeordnet werden. Zusätzlich wurde die interne Dynamik eines Poly(NIPAM-co-Butensäure) Copolymer-Makrogels mit Hilfe von Neutronen Spin-Echo Experimenten analysiert. Die durch die Messungen erhaltenen Ergebnisse konnten mit denen chemisch-identischer Mikrogele verglichen werden. Dabei wurde aufgrund der unterschiedlichen Synthesebedingungen von Makro- und Mikrogele ein Unterschied in der kollektiven Netzwerkdifffusion erwartet. Der gefundene Unterschied in der Netzwerkdynamik war allerdings geringer als erwartet und liegt im Bereich von etwa 10%.

Ein weiterer Teil der vorliegenden Arbeit beschäftigt sich mit der Synthese von Mikrogele-Copolymeren auf Basis von NIPAM und *N-tert*-Butylacrylamid (NtBAM). Mit Hilfe unterschiedlicher Streumethoden, sowie durch Elektronenmikroskopie, wurde sowohl Partikelgröße, als auch Quellverhalten der erhaltenen kolloidalen Mikrogele charakterisiert. Dabei galt es zu bestimmen, welchen Einfluss der Comonomergehalt auf die

Eigenschaften des Mikrogels hat. Weiterhin wurde das thermoresponsive Quellen des Gelnetzwerks mit den Vorhersagen der Flory-Rehner Theorie verglichen.

Hybridmaterialien aus magnetischen Nanopartikeln und thermoresponsiven Poly(NIPAM) Mikrogelen werden im letzten Teil der Arbeit vorgestellt. Zuerst wurden unterschiedliche Syntheseansätze für Cobalt- und Nickel-Nanopartikel, sowie deren Schutz vor Oxidation, verfolgt. Des Weiteren wurde ein Kern-Schale System angestrebt, in welchem die magnetischen Partikel als Kern vorliegen. Zum anderen wurde beabsichtigt, eine statistische Verteilung der Nanopartikel im Gelnetzwerk zu erreichen.

# Contents

<b>1</b>	<b>Introduction</b>	<b>1</b>
<b>2</b>	<b>Theory and characterization methods</b>	<b>7</b>
2.1	General aspects of responsive hydrogels based on NIPAM . . . . .	7
2.2	Hybrid microgels materials . . . . .	10
2.3	Investigation of structure and dynamics . . . . .	12
2.3.1	Dynamic light scattering (DLS) . . . . .	12
2.3.2	Swelling behaviour of gels described by Flory-Rehner theory and its limitations . . . . .	16
2.3.3	Neutron Scattering . . . . .	21
2.3.3.1	Introduction . . . . .	21
2.3.3.2	Small angle neutron scattering . . . . .	21
2.3.3.3	Neutron spin-echo spectroscopy . . . . .	25
<b>3</b>	<b>Experimental part</b>	<b>29</b>
3.1	Chemicals . . . . .	29
3.1.1	Macro- and microgels . . . . .	29
3.1.2	Nanoparticles . . . . .	29
3.2	Synthesis . . . . .	30
3.2.1	Macrogels . . . . .	30
3.2.1.1	Macrogels for the NSE experiment . . . . .	30
3.2.1.2	Macrogels with crosslinker gradient . . . . .	30

---

3.2.2	Microgels . . . . .	32
3.2.2.1	Poly(NIPAM-co-NtBAM) . . . . .	32
3.2.2.2	Poly(NIPAM-co-BAC) . . . . .	32
3.2.3	Synthesis of magnetic cobalt nanoparticles . . . . .	32
3.2.3.1	Cobalt@SiO <sub>2</sub> nanoparticles . . . . .	32
3.2.3.2	MPS-fuctionalization of Co@SiO <sub>2</sub> nanoparticles . . . . .	33
3.2.4	Synthesis of different nickel nanoparticles . . . . .	33
3.2.4.1	Pt@Ni nanoparticle synthesis . . . . .	33
3.2.4.2	Silica-coating of nickel nanoparicles using a LbL technique . . . . .	34
3.2.4.3	Nickel nanoparticles coated with polystyrene . . . . .	35
3.3	Characterization Methods . . . . .	35
3.3.1	DLS measurements . . . . .	35
3.3.2	Small angle neutron scattering . . . . .	35
3.3.3	Neutron spin-echo experiment . . . . .	36
3.3.4	Electron microscopy . . . . .	36
3.3.5	Macrogel swelling kinetics via image prosscossing . . . . .	37
<b>4</b>	<b>Marcogels with an internal crosslinker gradient</b>	<b>39</b>
4.1	General aspects of macroscopic gels based on NIPAM and BIS . . . . .	40
4.2	Macroscopic gels with a crosslinker gradient . . . . .	41
4.3	Swelling curves determined with a constant heating rate . . . . .	46
4.4	Deswelling kinetics of a crosslinker-gradient macrogel . . . . .	48
<b>5</b>	<b>Internal network dynamics of micro- and macrogels based on poly(NIPAM)</b>	<b>57</b>
5.1	Characterization of the microgel particles and their VPT . . . . .	58
5.2	A comparative NSE study . . . . .	59
<b>6</b>	<b>NIPAM-co-NtBAM Copolymer Microgels</b>	<b>67</b>
6.1	Overall size and shape of the microgel particles . . . . .	67
6.2	Swelling behaviour . . . . .	71
6.3	Internal structure of the NIPAM-co-NtBAM copolymer microgels . . . . .	76

---

<b>7</b>	<b>Microgels and magnetic particles</b>	<b>81</b>
7.1	Co-Nanoparticles . . . . .	81
7.2	Ni-Nanoparticles . . . . .	86
7.2.1	Magnetic nickel nanoparticle . . . . .	86
7.2.2	Coating techniques of Pt@Ni nanoparticles . . . . .	89
7.2.2.1	Silica-coating . . . . .	89
7.2.2.2	PS-coating . . . . .	91
7.2.3	Direct synthesis of Ni-nanoparticles in microgels . . . . .	93
<b>8</b>	<b>Summary and future perspectives</b>	<b>95</b>





# 1 Introduction

During the last 40 years there was enormous interest in the study of polymer gels and networks. From the physico-chemical point of view, a polymer gel consists of long and flexible macromolecules, which are crosslinked to a three-dimensional structure dissolved in a solvent. The junction points introduced into the polymer to build up the network structure, can either be physical (entanglement of the polymer chains, hydrogen bonding or electrostatic interactions ) or chemical crosslinks (covalent or ionic bondings). Their unique properties arising from the fact that gels can be regarded as intermediates between solids and liquids, make them interesting for statistical physics.<sup>1-3</sup> If water is used as solvent for the crosslinked polymer network, the gels are classified as hydrogels and can adsorb or retain large amounts of water. This type of gels is widely used in scientific and industrial applications. Moreover, they found also wide applications in the biomedical field, because of their similar physical properties to the human body (high water content, permeability, mechanical properties and low interfacial tension with water). Their applications range from chemical separation media,<sup>4</sup> drying agents, soft contact lenses,<sup>5</sup> controlled drug release systems<sup>6</sup> and many others. In addition to polymer gels also other gels like e.g. xerogels mainly based on inorganic materials should not be mentioned here. However, these materials are not subject of the present work and will not be discussed in more detail.

Of outstanding importance in the variety of gels are the so-called "intelligent" hydrogels. These gels are sensitive to different external stimuli. Upon changes of an external parameter they exhibit an abrupt change in volume. Depending on the composition of the gel, the volume phase transition (VPT) can be caused by changes in temperature,<sup>7-10</sup> solvent

composition,<sup>11</sup> ionic strength<sup>12</sup> or pH.<sup>13,14</sup> Among these polymers, the thermoresponsive hydrogels made of crosslinked poly(*N*-isopropylacrylamide) (poly(NIPAM)) are the most extensively studied. These gels undergo a temperature induced VPT at about 32°C in water,<sup>15–17</sup> due to the lower critical solution temperature (LCST) of poly(NIPAM).

With respect to their size, gels can be divided into two groups: macrogels (bulk gels with a size larger than 10  $\mu\text{m}$ ) and microgels (smaller than 10  $\mu\text{m}$ ). A microgel particle is an internally crosslinked colloidal particle and it can be characterized in terms of its water content, the average crosslinking density or characteristic time constants for swelling or shrinking.<sup>9</sup> For a macrogel the properties are similar,<sup>18,19</sup> but due to the difference in size some characteristics can have a different length and time scale.<sup>20,21</sup>

Generally the formation process (amount of components and solvent, temperature, etc.)

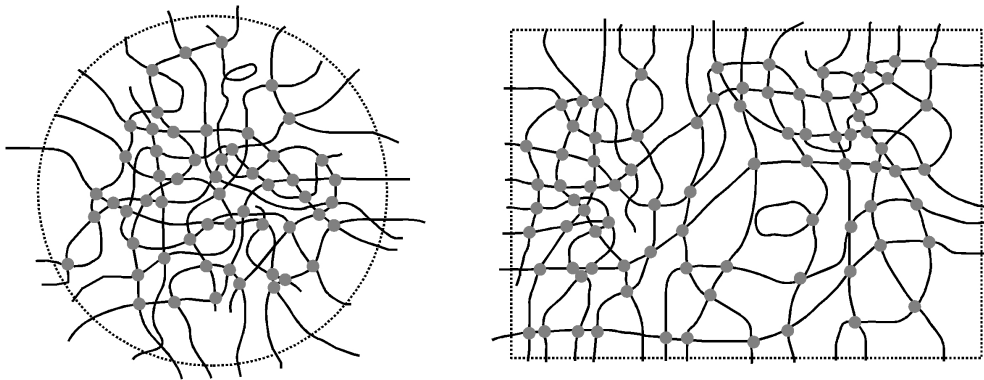


Figure 1.1: Schematic drawings of the internal network structure of a microgel (left) and a macrogel (right) with a heterogeneous microstructure such as loops, dangling chain ends and a heterogeneous crosslinking density

has a strong influence on the network structure of a macro- or microgel. For example, it has been shown in the literature that during the synthesis of NIPAM based microgels using batch methods, the crosslinker *N,N'*-methylenebisacrylamide (BIS) is consumed faster than the NIPAM monomer.<sup>22</sup> In this way colloidal particles with a non-uniform morphology, i.e. particles with a highly crosslinked core and a less crosslinked outer shell, are obtained.<sup>23</sup> In contrast to this, macrogels show a statistical distribution of the monomer and crosslinker.<sup>24</sup> Beside this, the temperature during the gel synthesis also

---

has an effect on the homogeneity of the gel network. Microgel particles are generally made by an emulsion polymerization at temperatures above the LCST of NIPAM. Hence, the network is created nearly under bulk conditions. In contrast to this, macrogels are made under good solvent conditions at temperatures below the LCST of NIPAM. Due to this, it was expected to have a significantly higher network inhomogeneity in a microgel compared to a macrogel.

For the characterization of macrogels as well as for microgel particles in solution and for the study of their volume phase transition, a lot of different techniques have been used. First of all, imaging techniques such as transmission or scanning electron microscopy (TEM and SEM)<sup>25</sup> and atomic force microscopy (AFM)<sup>26,27</sup> provide a good overview of the investigated sample and in the case of microgels, these methods deliver additional information about the homogeneity of the particles in the swollen and collapsed state. Secondly, scattering techniques including static and dynamic light scattering (SLS and DLS)<sup>16,28-30</sup> and neutron scattering (elastic or inelastic)<sup>7,16,30,31</sup> give access to information about dynamics (translational or rotational) and the global or local structure of the gel network.

Beside homopolymer gels based on the temperature sensitive poly(NIPAM), there exists a large number of publications on copolymer systems or on hybrid materials. Using a simple copolymerization of NIPAM with another polymerizable monomer the phase transition can be modified or an additional sensitivity to pH or ionic strength can be generated. With the introduction of charged comonomers, such as allyl-acetic acid,<sup>13</sup> acrylic acid (AAc),<sup>26,32-34</sup> vinylacetic acid<sup>10,14</sup> or methacrylic acid<sup>35,36</sup> the volume phase transition temperature (VPTT) can be shifted to higher values and the resulting gels show an additional sensitivity to pH. Furthermore, the copolymerization with uncharged comonomers can also influence the VPTT of poly(NIPAM).<sup>37</sup> In the case of hybrid NIPAM materials, often inorganic nanoparticles are incorporated into the gel network, either as core-shell particles or randomly distributed. Often metal nanoparticles such as gold,<sup>38-42</sup> silver,<sup>43,44</sup> palladium<sup>43,45</sup> or magnetite<sup>46</sup> are used. But also the incorporation of silica particles into a poly(NIPAM) network has been shown in literature.<sup>47,48</sup>

The aim of this work was to synthesize new microgels and microgel nanoparticle hybrids, to understand their exceptional properties and in some cases to compare these properties to their macroscopic homologous.

Within the present work, we first tried to describe in detail the temperature induced collapse of a macroscopic three-dimensional gel network. To study the influence of the crosslinker density on the swelling behaviour, a NIPAM based macrogel with a crosslinker gradient has been synthesized. The collapse of this network was analyzed by an image processing method in terms of different swelling curves with respect to a varying amount of crosslinker.

The present work also aims at comparing the internal dynamics of two chemically identical NIPAM based gels synthesized in different ways. Due to the different synthesis conditions in the preparation of macro- and microgels a different local network structure is expected. This should also lead to differences in the local network motion. An ideal experimental tool to study such local dynamics on the nanometer scale is neutron spin-echo (NSE). This technique was already previously applied to study gels<sup>24,31,49</sup> or NIPAM based amphiphilic triblock copolymers.<sup>50</sup> However, a comparative study between macro- and microgels is still missing.

Beside the characterization of macrogels, we synthesized copolymer microgel particles based on NIPAM and *N-tert*-butylacrylamide (NtBAM) similar to the work of Bae et al.<sup>51</sup> Further, Lyon et al.<sup>52</sup> prepared poly(NIPAM-co-NtBAM-co-AAc) microgels also using an emulsion polymerization process and the main result of these two works was the decrease of the transition temperature in comparison to the volume phase transition temperature (VPTT) of pure poly(NIPAM) with increasing amount of NtBAM. Here, the main focus was to characterize the VPT by using different scattering techniques (DLS, small angle neutron scattering (SANS)) and to quantitatively analyse the swelling/de-swelling by the Flory-Rehner theory (FRT).

The seventh chapter focuses on poly(NIPAM) hybrid materials containing a magnetic component. Therefore, different synthetical approaches have been employed, to create core-shell particles with an oxidation protected cobalt or nickel core and a thermorespon-

sive poly(NIPAM) shell. Further, a direct synthesis of small nickel nanoparticles inside a pre-prepared microgel has been under investigation.



## 2 Theory and characterization methods

### 2.1 General aspects of responsive hydrogels based on NIPAM

During the last decades, thermo-sensitive polymer networks have been the subject of many investigations owed to their potential use as drug delivery systems, chemical separation media,<sup>4</sup> nanoactuators or sensors.<sup>53,54</sup> In particular, polyacrylamides are potential candidates for this purpose because they exhibit thermoresponsive behaviour. In this group, poly(*N*-isopropylacrylamide) (poly(NIPAM)) is the most well known member of the class of thermoresponsive "intelligent" polymers. The following section briefly reviews the unique temperature responsive properties of poly(NIPAM) systems.

Pure poly(NIPAM) exhibits a sharp transition from a hydrophilic to a more hydrophobic structure at the temperature known as the volume phase transition temperature (VPTT), which is related to the lower critical solution temperature (LCST) of poly(NIPAM). The normal range of the VPTT for poly(NIPAM) is typically found to be around 32°C in aqueous media.<sup>15-17</sup> The change in the hydrophilic character of the polymer is due to the presence of the hydrophilic amide groups and the hydrophobic isopropyl group on its side chain (see figure 2.1). If the temperature is below the VPTT, the hydrophilic chains are hydrated and the hydrogel is in the swollen state. With an increase in temperature above the VPTT, the hydrophobic interactions become stronger and the equilibrium between the hydrophilic/hydrophobic interactions is disturbed. Therefore, the solvent (in the case of hydrogels the solvent is water) inside the network is expelled and the poly(NIPAM) network collapses.

The swelling capacity of a gel network strongly depends on the crosslinking density of

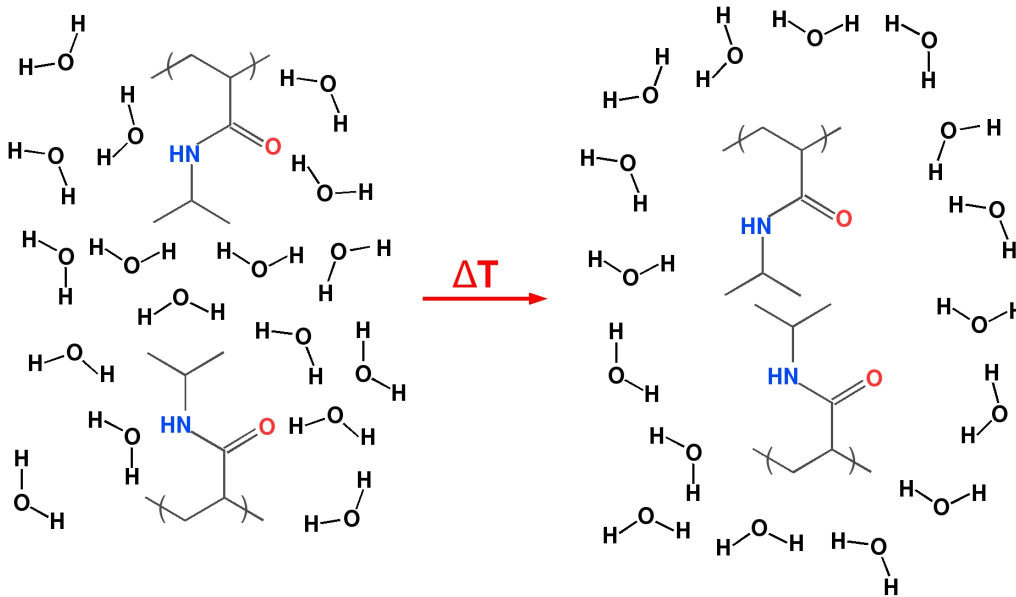


Figure 2.1: Schematic illustration of the structural rearrangement of water molecules around poly(NIPAM) during the VPT

the network.<sup>25,31,55,56</sup> In the case of poly(NIPAM) often *N,N'*-methylenebisacrylamide (BIS) is used as crosslinking agent due to the similarity in the chemical structure between BIS and NIPAM. This is related to the fact, that for the formation of a homogeneous gel the reactivity ratio between monomer and crosslinking agent is very important. If the reactivity of the crosslinker is too high or too small in comparison to the monomer, the rate of the crosslinking reaction at the beginning or at the end of the polymerization is higher compared to the chain growth, resulting in an inhomogeneous network structure. Colloidal microgel particles and macroscopic gels, based on the same chemical composition, differ in a number of aspects. These differences mainly rely on the fact that the gels are prepared using different synthetical methods. In the case of BIS-crosslinked poly(NIPAM) gels, a macrogel is usually synthesized using a bulk solution polymerization at room temperature. Due to this gel preparation at temperatures below the VPTT of poly(NIPAM), which means good solvent conditions, a macrogel with a nearly homogeneous crosslinker distribution is obtained. In contrast to this, microgel particles are prepared using methods such as emulsion polymerization with or without surfactant. There



---

is evidence for a non-homogeneous crosslinker distribution within the microgel particles caused by a faster polymerization of the crosslinker BIS than the monomer NIPAM.<sup>22,23</sup> Like macroscopic gels, colloidal microgel particles are generally characterized by the degree of swelling, the average crosslink density and by a characteristic response time for swelling and deswelling. Since macrogels have dimensions several orders of magnitude higher than microgel particles, the driving force of swelling should be the same, but the time scale for the swelling process is very sensitive to the size of the gels. For colloidal microgel solutions the swelling/deswelling process is fast and the particles achieve their equilibrium state after a temperature change in less than a second. In contrast to this, macroscopic gels need a very long time (minutes to hours) to respond upon a change of an external parameter, because the collapse of the outer parts of the gel prevents the water transport from the inner part of the gel to the outside.<sup>9,20</sup>

Experimentally, the phase transition of gels can be described by the order of transition (first or second order) and whether this transition is continuous or discontinuous. For macroscopic poly(NIPAM) gels the degree of discontinuity depends strongly on the used components for the gel preparation.<sup>54</sup> It was confirmed that with an increase of the crosslinker density inside the macrogel network a change from a discontinuous to a continuous phase transition can be observed.<sup>21</sup> Furthermore, by incorporation of charged groups into the gel network, it was on one hand possible to shift the phase transition to higher temperatures and on the other hand, the degree of discontinuity increased with an increasing content of charged groups.<sup>57</sup> In the case of linear poly(NIPAM) homopolymers it is expected that the volume phase transition is discontinuous if the polymer chains exhibit a totally monodisperse molecular weight distribution.<sup>8,58</sup> Since it is experimentally not possible to prepare such monodisperse linear polymers, the chains with different lengths will collapse at different transition temperatures and hence, the phase transition changes to a continuous one. This relation between the molecular weight ( $M_W$ ) and the phase transition temperature of poly(NIPAM) can be extended to microgels. Due to the fact, that the length of the chains between the crosslinking points inside the gel network is randomly distributed, larger chains will collapse at lower temperatures and shorter chains

at higher temperatures.<sup>8</sup> Thus, the phase transition of microgel solutions is generally continuous and depends strongly on the homogeneity of the crosslinker distribution. A theoretical description of the volume phase transition of gels is given by the Flory-Rehner theory and will be described in detail in section 2.3.2.

## 2.2 Hybrid microgels materials

The term "hybrid material" is used for many different systems including materials, such as clay nanocomposites, porous hybrid materials, sol-gel compounds etc. The most common definition is, that a hybrid material combines the properties of two different materials on a molecular scale. Often one of these compounds is inorganic and the other one is organic. During the last years, there was a growing interest in hybrid systems based on inorganic nanoparticles in combination with organic microgel components.<sup>3,43,59-61</sup> The advantage of using microgels compared to macroscopic gels is that these systems combine the properties of colloidal particles and of stimuli-sensitive gels. Their response time to a change in temperature, pH, ionic strength or an electric field<sup>62,63</sup> is much faster compared to their homologous macrogels as described before and therefore, they are perfect systems for a wide variety of applications. As an example a recent work of Liz-Marzán should be mentioned. In this work such hybrids are used as sensors exploiting the surface enhanced Raman spectroscopy (SERS) effect.<sup>64</sup>

Various types of materials such as silica,<sup>48,65</sup> gold, silver,<sup>43,66,67</sup> quantum dots,<sup>68,69</sup> magnetic materials,<sup>70,71</sup> etc. can be used as the inorganic component of organic-inorganic hybrid microgels. This offers the possibility to prepare well-defined hybrid materials for specific applications. For example, for an application in sensor technology, it is necessary to create a material with a temperature sensitivity and additional optical properties. Therefore, poly(NIPAM), with a VPTT at about 32°C, would be a very suitable organic compound. The additional use of different comonomers, permits to shift the transition temperature to higher or lower values and hence, a tuning of the VPT is possible.<sup>13</sup> For an optically sensitive medium, inorganic materials such as gold or silver nanoparticles can be used. Depending on the particle size and shape, well-defined plasmon bands in the UV

and near-IR region are observable.<sup>13,42,44</sup>

In general, there are many different ways to combine inorganic nanoparticles with microgels. Figure 2.2 shows three main types of nanoparticle/microgel hybrid materials: core-shell particles (core = inorganic; shell = microgel)<sup>13,39,42,44,47,72</sup>, microgels covered with nanoparticles<sup>40,65,73</sup> and microgels, containing nanoparticles inside the polymer network.<sup>38,43,45,46</sup> Beside spherical nanoparticles, there exist a large number of publications

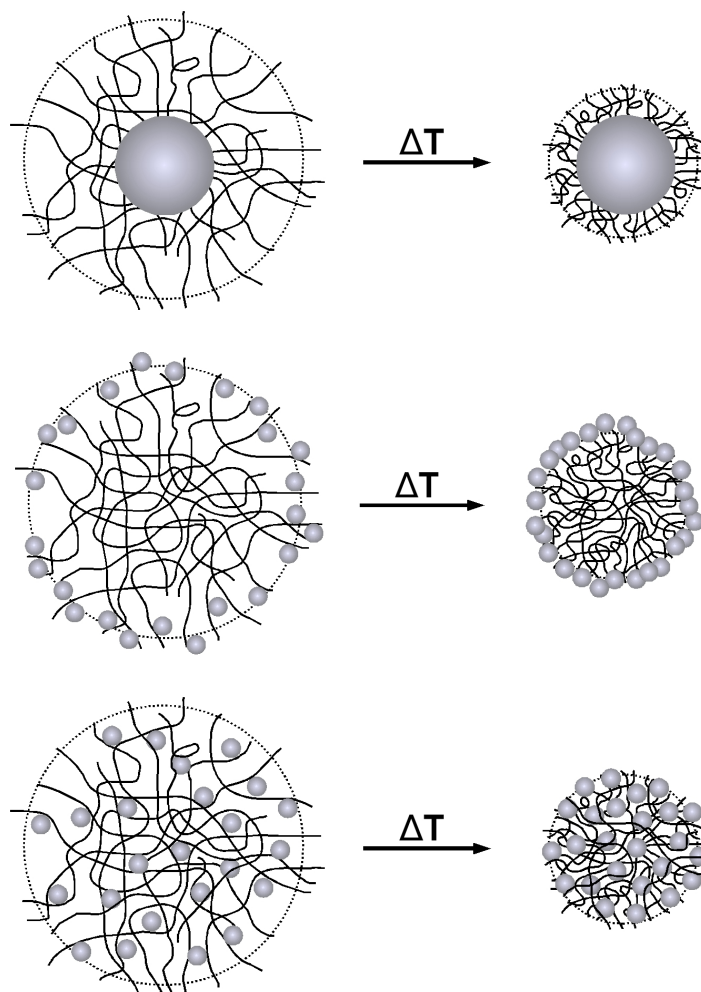


Figure 2.2: Schematic illustration of three types of recently studied thermosensitive hybrid microgels

of different shaped particles, including rods,<sup>41,74</sup> plates<sup>75-77</sup> etc.

From figure 2.2 it is also clear, how a temperature induced collapse of a thermoresponsive microgel influences the distribution of the nanoparticles and the shape of the whole hybrid

system. As already mentioned before, this collapse of the microgel network can change or in the case of catalysis constrain and control the properties of the inorganic component. In the case of gold/poly(NIPAM) core-shell particles it has been shown, that the maximum of the plasmon band is shifted to higher wavelength with an increase in temperature, caused by a collapse of the poly(NIPAM) shell.<sup>42,44</sup> Furthermore, if a catalytically active material like palladium or gold is used as the inorganic part of the hybrid material, then the activity of the metal can be reduced by an increase in temperature.<sup>43</sup> This is due to the change of the mesh size in the network. The mesh size has a strong influence on the accessibility of the catalytic nanoparticles.

## 2.3 Investigation of structure and dynamics

### 2.3.1 Dynamic light scattering (DLS)

Dynamic light scattering is today routinely used to study the movement of colloidal particles, microgels or polymers in a solution.<sup>78</sup> This movement is known as Brownian motion and an analysis of it provides an indication of the average particle size and polydispersity. Moreover, in the case of large colloids like e.g. vesicles also internal modes are resolved. In a typical dynamic light scattering experiment of a highly diluted solution, the time-dependent fluctuations in the scattering intensity  $I(q, t)$  caused by particle motion in the sample (as translation, rotation or vibration) are detected and analyzed by means of correlation functions. The information about the dynamics in the system is available from the normalized electric field autocorrelation function  $g^1(q, t)$  with the sample time  $\tau$ :

$$g^1(q, t) = \frac{\langle E_s^*(t) E_s(t + \tau) \rangle}{\langle I \rangle} \quad (2.1)$$

Here  $E_s(t)$  is the electric field of the scattered light and  $E_s^*(t)$  its complex conjugate. However, the scattered electrical field can not be measured directly and  $g^1(q, t)$  can only be obtained in a so-called heterodyne experiment, where a part of the non-scattered primary beam is interfering with the scattered light. But in general, the analysis of a homodyne experiment is much easier. This measurement provides the time-averaged

intensity correlation function (ICF) of the scattered light:

$$g_T^2(q, t) = \frac{\langle I(q, 0) I(q, \tau) \rangle_T}{\langle I(q, 0) \rangle_T^2} \quad (2.2)$$

where the intensity is proportional to the square of the electric field,  $I(q, t) \sim |E(q, t)|^2$  and  $\langle \dots \rangle_T$  indicates a time average.  $q$  is the magnitude of the scattering vector and defined as

$$q = |\vec{q}| = \frac{4\pi n}{\lambda} \sin\left(\frac{\theta}{2}\right) \quad (2.3)$$

with the wavelength  $\lambda$  of the used laser.  $n$  is the refractive index of the medium. The electric field autocorrelation function  $g^1(q, t)$ , which contains the dynamical information of the system, can be calculated from the ensemble averaged ICF  $g_E^2(q, t)$  using the SIEGERT relation:<sup>29,78</sup>

$$g_E^2(q, t) = 1 + B|g^1(q, t)|^2. \quad (2.4)$$

Here  $B$  is a baseline parameter. In the case of an ergodic system (like fluids) the time-averaged correlation function of the scattered light intensity  $g_T^2(q, t)$  (equation 2.2) is equal to the ensemble-averaged ICF  $g_E^2(q, t)$ . Therefore, a homodyne experiment resulting in  $g_T^2(q, t)$  can be used to estimate  $g^1(q, t)$ . But Pusey and van Meegen<sup>29</sup> pointed out that for solid-like systems, like macrogels and colloidal glasses, the time-average is not equal to the ensemble-average. These systems are non-ergodic. Hence, in the following, the differences between the scattering in DLS from ergodic and non-ergodic media will be explained in more detail.

In general, the term ergodic means that the time-average is identical to the ensemble-average. For example, playing dice is an ergodic process. It does not matter if you throw the dice 100 times (time-average) or if you throw 100 dice only once (ensemble-average), the average value in both cases is the same. Transferring this to a light scattering experiment, highly diluted colloidal suspensions like microgel particles in dilute solution show an ergodic behaviour in a DLS experiment. This means the particles diffuse freely throughout the solvent due to Brownian motion. Given enough time, all possible conformations of the system are observed by only looking at a fixed, small volume fraction. Therefore,

a single experiment over a long enough time period yields the same result as the average of many short experiments. Hence, as mentioned before, the time-averaged ICF is equal to the ensemble-averaged:

$$g_E^2(q, t) = g_T^2(q, t) \quad (2.5)$$

In the case of partly solid-like systems as macroscopic gels, the centers where the scattering in a DLS experiment is created, are fixed or at least limited in their motion. As a result, only a certain range of conformations is scrutinized, but this is not necessarily representative for all possible conformations the system can theoretically adopt. Accordingly, a single measurement over a long time period is not comparable to the average of many different measurement and the system shows a non-ergodic behaviour.

A qualitative description of the light scattering by ergodic and non-ergodic systems is

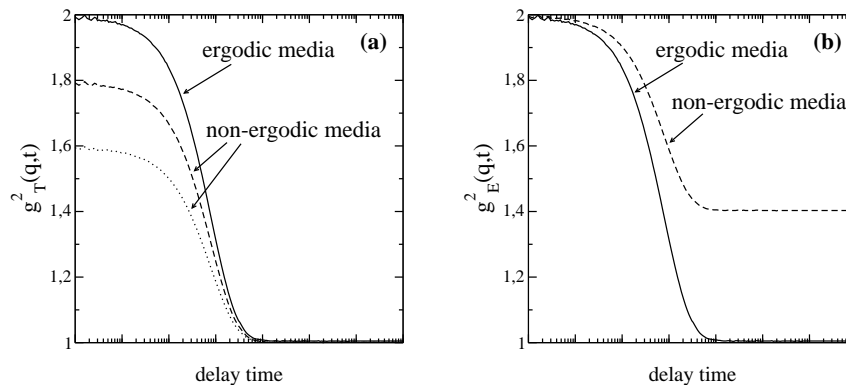


Figure 2.3: Time-averaged ICF  $g_T^2(q, t)$  and ensemble-averaged ICF  $g_E^2(q, t)$  obtained from ergodic and non-ergodic media<sup>79</sup>

given in figure 2.3. The time-averaged as well as the ensemble-averaged ICF of an ergodic medium (see figure 2.3 a and b, black line) starts at a value of two, because the delay or sample time  $\tau$  of the experiment is zero and consequently the ICF has the value two (see equation 2.6). If  $\tau$  takes larger values than the characteristic fluctuation time of the scattered light, both contributions in the numerator of equation 2.2 become uncorrelated

and the ICF is one.

$$\lim_{\tau \rightarrow 0} \frac{\langle I(q, 0) I(q, \tau) \rangle_{E,T}}{\langle I(q) \rangle_{E,T}^2} = \frac{\langle I^2(q) \rangle_{E,T}}{\langle I(q) \rangle_{E,T}^2} = 2 \quad (2.6)$$

$$\lim_{\tau \rightarrow \infty} \frac{\langle I(q) I(q, \tau) \rangle_{E,T}}{\langle I(q, 0) \rangle_{E,T}^2} = \frac{\langle I(q, 0) \rangle_{E,T} \langle I(q, \infty) \rangle_{E,T}}{\langle I(q) \rangle_{E,T}^2} = 1 \quad (2.7)$$

As illustrated in figure 2.3 a and b (dotted lines), the time-averaged and the ensemble-averaged ICF of a non-ergodic media are not equal. This is due to the fact, as already mentioned before, that for example in a macroscopic gel the scattering centers are limited in their motion, because of the nearly solid-like network structure of the gel. Hence, a single DLS measurement, as applied for ergodic systems, represents only one specific part of the gel, which is however not representative for the whole sample.

For a non-ergodic systems,  $g_E^2(q, t)$  will begin at a value of 2, because at  $\tau = 0$  all fluctuations (dynamic and static<sup>80</sup>) contribute to the scattering. Finally, for  $\tau \rightarrow \infty$  the ensemble-averaged ICF decays to a constant value greater than 1, due to remaining static fluctuations, which are caused by the limited motion of the scattering centers in the gel. In contrast to this, the time-averaged ICF will start for  $\tau = 0$  at a value below 2, because only the scattering from a regionally limited conformation of the gel is sampled. For large delay times,  $\tau \rightarrow \infty$ , decays to 1, since the the numerator of equation 2.2 become uncorrelated and equation 2.7 applies.

To solve the problem of inequality of  $g_E^2(q, t)$  and  $g_T^2(q, t)$  of a non-ergodic system in DLS, the sample is moved stepwise during the experiment and at every step the time-averaged ICF is measured. Hence, it is possible to obtain the scattering from many different positions of the gel and a summation of the collected data (followed by normalization) yields the scattering function of the whole sample, which is equal to the normalized ensemble-averaged ICF. Using then the SIEGERT relation (equation 2.4), the normalized electric field autocorrelation function  $g^1(q, t)$  can be determined.

The DLS measurements performed here are limited to diluted microgel solutions, which show an ergodic behaviour. For monodisperse samples the correlation function of the

electrical field can be written as:

$$g^1(\tau) = \exp(-\Gamma t) . \quad (2.8)$$

The relaxation rate  $\Gamma$  is connected to the translational diffusion coefficient  $D^T$  according to<sup>78,81</sup>

$$\Gamma = D^T q^2 . \quad (2.9)$$

But usually colloidal systems are more or less polydisperse. Therefore, the decay of the field time autocorrelation function is given by a weighted sum of exponentials

$$g^1(\tau) = \int_0^\infty G(\Gamma) \exp(-\Gamma\tau) d\Gamma , \quad (2.10)$$

Here,  $G(\Gamma)$  is the distribution function of the relaxation rates. Equation 2.10 can be analyzed by the method of cumulants<sup>82,83</sup> or by inverse Laplace transformation.<sup>84,85</sup> Both methods provide the mean relaxation rate  $\bar{\Gamma}$  of the distribution function and the width of the distribution. With Eq. 2.9, the translational diffusion coefficient  $D^T$  for diluted colloidal dispersions can be calculated. Based on this, the hydrodynamic radius  $R_h$  is obtained using the Stokes-Einstein equation

$$D^T = \frac{k_B T}{6\pi\eta R_h} . \quad (2.11)$$

Here,  $k_B$  is the Boltzmann constant,  $T$  the temperature and  $\eta$  the viscosity of the solvent.

### 2.3.2 Swelling behaviour of gels described by Flory-Rehner theory and its limitations

Gels in general are insoluble in any solvent because of the crosslinking (physically or chemically), but they can swell to a large extent in a good solvent. On the other hand gels collapse to a compact form if they are in a poor solvent. Hence, this so-called volume phase transition is based on the fact that the quality of the solvent for the polymer gel is changed between good and poor. For macroscopic networks, the VPT has been studied in detail by Tanaka and Shibayama<sup>7,86,87</sup> and can be described in terms of the classical



Flory-Rehner theory (FRT).<sup>58,88,89</sup> In two cases the FRT was already applied to also describe the VPT of microgels.<sup>90,91</sup>

To characterize the volume phase transition of spherical microgels, the so-called swelling or de-swelling ratio  $\alpha$  is widely used

$$\alpha = \frac{V_{collapsed}}{V_{swollen}} = \left( \frac{R_h}{R_0} \right)^3 \quad (2.12)$$

where  $R_h$  is the hydrodynamic radius at a certain temperature and  $R_0$  the particle radius at reference conditions (usually the fully swollen state). A detailed description of the swelling behaviour of gels provides the FRT.<sup>58,92</sup> In this approach, it is assumed that thermodynamic equilibrium for a gel is attained, if no net transfer of solvent takes place across the gel-solvent interface. Therefore, the macroscopic state of a homogeneous neutral gel can be described by means of the osmotic pressure in the gel. According to the FRT,<sup>92</sup> the osmotic pressure  $\Pi$  consists of two terms:

$$\Pi = \Pi_m + \Pi_e \quad (2.13)$$

The first contribution  $\Pi_m$  represents the mixing free energy of the polymer and the surrounding solvent; the second term  $\Pi_e$  describes a change in the elastic free energy due to the deformation of the polymer network. They are expressed as

$$\Pi_m = - \frac{N_A k_B T}{v} [\phi + \ln(1 - \phi) + \chi \phi^2] \quad (2.14)$$

$$\Pi_e = \frac{N_c k_B T}{V_0} \left[ \left( \frac{\phi}{2\phi_0} \right) - \left( \frac{\phi}{\phi_0} \right)^{1/3} \right] \quad (2.15)$$

where  $N_A$  is Avogadro's number,  $T$  the absolute temperature,  $v$  the molar volume of the solvent,  $N_c$  the number of chains contained in the gel network,  $V_0$  the volume of the relaxed Gaussian gel network,  $\phi$  the volume fraction of the polymer,  $\phi_0$  the volume fraction at reference conditions and  $\chi$  the polymer-solvent interaction parameter,<sup>54</sup> also called Flory-Huggins interaction parameter.

Assuming that the temperature dependent swelling of the microgels occurs under isobaric

conditions, the osmotic pressure  $\Pi$  within the gel becomes zero.

$$\frac{N_c k_B T}{V_0} \left[ \left( \frac{\phi}{2\phi_0} \right) - \left( \frac{\phi}{\phi_0} \right)^{1/3} \right] - \frac{N_A k_B T}{v} [\phi + \ln(1 - \phi) + \chi \phi^2] = 0 \quad (2.16)$$

The interaction parameter  $\chi$  describes the change in free energy  $\Delta F$  per solvent molecule (divided by  $k_B T$ ) caused by the change from a solvent-solvent contact to a solvent-polymer contact. Using two further parameters  $A = \frac{2\Delta S + k_B}{2k_B}$  and  $\Theta = \frac{2\Delta H}{2\Delta S + k_B}$ , the polymer-solvent interaction parameter  $\chi$  can be defined as

$$\chi = \frac{\Delta F}{k_B T} = \frac{\Delta H - T\Delta S}{k_B T} = \frac{1}{2} - A \left( 1 - \frac{\Theta}{T} \right). \quad (2.17)$$

$\Delta S$  and  $\Delta H$  are the changes in entropy and enthalpy per monomeric unit of the network related to the volume phase transition. It was shown that for good solvents the  $\chi$  parameter has a value smaller than 0.5, and if a poor solvent is used,  $\chi$  is larger than 0.5.<sup>93</sup> For some polymer-solvent systems it was experimentally found, that  $\chi$  depends on the concentration of the polymer in a nonlinear manner.<sup>94</sup> For this case it has been shown that  $\chi$  can be described by a power series of the volume fraction of the polymer  $\phi$  using the equation:

$$\chi(T, \phi) = \chi_1(T) + \chi_2\phi + \chi_3\phi^2 + \dots \quad (2.18)$$

with  $\chi_i$  as temperature dependent coefficients.<sup>93</sup>

A numerical calculation of  $\Pi_e$  and  $-\Pi_m$  for neutral gels as a function of the volume fraction of the polymer  $\phi$  was done by Hirotsu<sup>95</sup> in detail. In the case of a concentration independent polymer-solvent interaction parameter  $\chi$  in equation 2.16, the value of  $\chi_2$  in equation 2.18 is zero. Hence, at different values of  $\chi_1$ , which is equal to  $\chi$  at low concentrations, the two parts of the osmotic pressure show only one intersection at all temperatures and the phase transition is continuous. The calculated curves for this case are presented in figure 2.4 (left side).

As observed from some experiments of polymer-solvent systems, the interaction parameter  $\chi$  depends on the polymer volume fraction. Therefore, the calculated curves for  $\Pi_e$  and  $-\Pi_m$  show at values of  $\chi_1 \sim 0.465$  (with  $\chi_2 = 0.56$ ) three intersection points, which means that the phase transition is discontinuous. Here, the intersections represent the

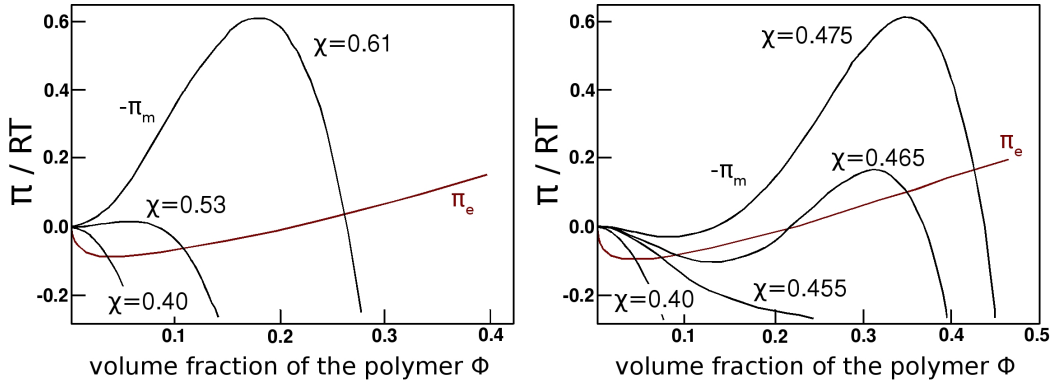


Figure 2.4: Calculated curves for  $\Pi_e$  and  $-\Pi_m$  as a function of the polymer volume fraction; left: polymer-solvent interaction parameter  $\chi$  is independent of the polymer volume fraction, hence only one intersection between  $\Pi_e$  and  $-\Pi_m$ ; right: polymer-solvent interaction parameter depends on the polymer volume fraction, consequently three intersections appear in the intermediate temperature range (redrawn based on the publication of Hirotsu<sup>95</sup>).

stable, unstable and metastable states of the gel.

For the analysis of the temperature dependent swelling of neutral gels, the equations 2.16 and 2.17 have to be combined. The resulting term is solved for the temperature  $T$  and  $\phi$  is redisplayed by the swelling ratio  $\alpha$ .

$$T_{\Pi=0} = \frac{A \alpha^2 \Theta}{\frac{\phi_0}{N_{gel}} \left[ \frac{1}{2} \left( \frac{\alpha}{\phi_0} \right) - \left( \frac{\alpha}{\phi_0} \right)^{\frac{1}{3}} \right] - \alpha - \ln(1 - \alpha) + \left( A - \frac{1}{2} \right) \alpha^2 - \chi_2 \alpha^3}. \quad (2.19)$$

Here,  $N_{gel}$  is the average degree of polymerization of the polymer chain between crosslinks,  $\Theta$  is the temperature at which the hydrodynamic radius approaches its minimum and  $A = \frac{2\Delta S + k_B}{2k_B}$ , which roughly comprises the entropy change of the system.

As described at the beginning of this section, the classical Flory-Rehner theory<sup>92</sup> was developed for neutral homogeneous macroscopic gels. In addition, in the case of electrostatically charged systems, the swelling/deswelling behaviour of a neutral gel by means of the osmotic pressure  $\Pi$  has to be extended by an electrostatic term.<sup>57,93</sup>

$$\Pi_i = \left( \frac{f N_c k_B T}{V_0} \right) \left( \frac{\phi}{\phi_0} \right) \quad (2.20)$$

Here, the parameter  $f$  represents the average number of counter ions per chain. Consequently, the osmotic pressure under isobaric conditions for charged gels can be described by:

$$\Pi = \Pi_m + \Pi_e + \Pi_i = 0. \quad (2.21)$$

The phase behaviour of a ionic gels, based on the thermosensitive poly(NIPAM) in combination with sodium acrylate (NaA), was studied by Hirotsu and Tanaka.<sup>57</sup> They used equation 2.16 and 2.20 to describe the swelling curves of different gels with varying NIPAM/NaA composition. As a result, they found out that with increasing content of sodium acrylate in the gel, the volume phase transition changes from a continuous to a discontinuous transition. Beside this, the gels with a discontinuous phase transition showed an irregular deformation caused by the coexistence of two phases with different densities. A theoretical description of both kinds of phase transitions with the slightly modified FRT resulted only in a good fit of the experimental data by using  $\Delta H$  and  $\nu$  as variable parameters. In general,  $\Delta H$  is a fixed parameter and can be calculated from the slope of a plot of  $\chi$  vs.  $1/T$ .<sup>54</sup> Here,  $\nu = N_c/V_0$  and is the total number of chains in a gel, which should also be constant. The differences between the theory and the experimental data, as Hirotsu et al. mentioned, can be caused by omitting the effects of loops, free branches, non-Gaussian properties or polydispersity of chains, etc.<sup>57</sup> Also charge-charge interaction and counter ion condensation have to be taken into account.

For poly(NIPAM) microgels it is assumed that during the synthesis, which is mostly done under "bad" solvent conditions, the microgel particles exhibit a crosslinker gradient.<sup>22</sup> This is due to the effect that the crosslinker BIS is consumed faster than the monomer NIPAM. In this case, it has been shown in a AFM study on microgels fixed on a surface by Fernandes et al.<sup>96</sup> that indeed a change in volume can be described by the original FRT, but not a change in the Young's modulus. For this, the FRT was modified by taking into account that the microgel particles consist of certain independent layers of different crosslinker density. With this approach it was possible to describe the experimental volume change as well as the Young's modulus.

Finally the FRT is a well suited theoretical model to quantify the phase transition for

---

homogeneous macro- and microgels. By the introduction of inhomogeneities in the gel network, either by ionic groups or an irregular distribution of crosslinker/comonomer, the Floy-Rehner theory has to be modified.

### 2.3.3 Neutron Scattering

#### 2.3.3.1 Introduction

In the field of scattering methods, neutrons allow unique applications due to their special properties. They have a high penetrating power for many different materials, based on their interactions only with the nucleus of atoms and not with the electron shell, as it is observed in x-ray scattering.<sup>97</sup> Beside this, neutrons exhibit a magnetic moment which enables also to study magnetic systems. For cold neutrons, as usually used for experiments with soft matter, the neutron wavelength  $\lambda$  is of the order of atomic distances and their energy is comparable to excitations in these systems. The most important quantity is the scattering vector  $q$ . At low values of  $q$  information about the overall size and shape of a mesoscale system is available (as usually probed in light scattering); at high  $q$ , as observed in neutron scattering, the internal structure can be resolved. Therefore, in the case of soft matter, small angle neutron scattering (SANS) and also neutron spin-echo (NSE) are well suited methods to study internal structures and movements of systems having colloidal dimensions.

In this work mainly SANS and NSE are used to investigate hydrogels and therefore, the following discussion is focused on these techniques and systems.

#### 2.3.3.2 Small angle neutron scattering

Small angle neutron scattering is a quasi-elastic scattering technique, what means that no significant energy transfer between the neutrons and the sample occurs. Only line-broadening of the initial line can be observed. Hence, the neutrons show nearly the same energy before and after the interaction with the sample. However, the direction of the neutrons changes in the scattering process and the intensity of the scattered neutrons as a function of the scattering angle is detected. A standard setup for a SANS experiment

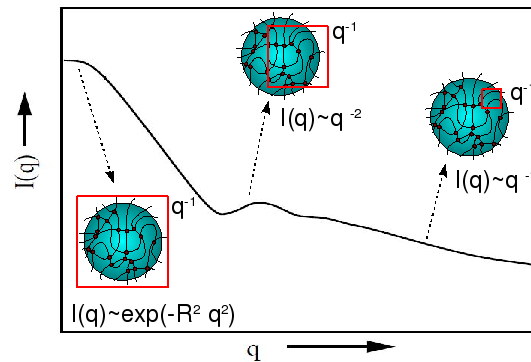


Figure 2.5: Diagram of an exemplary elastic scattering curve of colloidal microgel particles in solution; at low values of  $q$  the overall size and shape of the microgels is seen (red square on the left side) and at high  $q$  values the internal structure of the the particles can be resolved (red square on the right side).

at a research reactor (with a constant neutron flux) is shown in figure 2.6.<sup>97–99</sup>

A central component is the velocity selector made from spinning absorbing blades, which

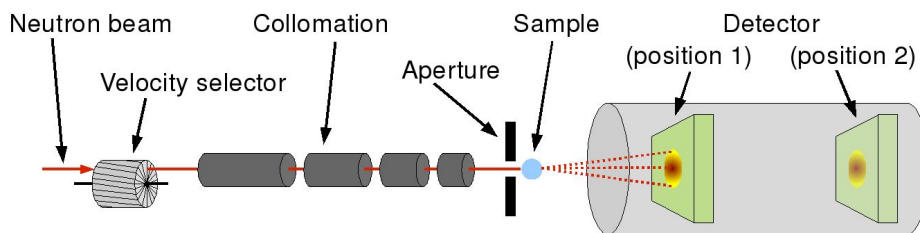


Figure 2.6: Schematical drawing of a typical SANS setup containing a velocity selector, collimation systems, aperture, sample and a detector tube with a movable 2D-detector

will let through neutrons of velocities close to a particular value. This is how a monochromatic neutron beam with a wavelength distribution with  $\Delta\lambda/\lambda = 10\%$  can be generated. The neutron beam is then guided through the collimation system, where its divergence is reduced. The sample is placed directly behind the collimation system and the scattered neutrons are detected by a 2D-multidetector at a variable sample-to-detector distance. Is the detector placed far away from the sample, neutrons scattered in the so-called small angle region can be detected. Hence, the available  $q$ -range (see eq. 2.3) for a certain

SANS setup, follows from the geometry of the experimental settings. In the case of an isotropic scattering sample the obtained 2D-detector pattern can be radially averaged. The obtained scattering curve is then the scattering intensity as a function of  $q$  and can be described by:

$$I(q) \propto S(q) \cdot P(q) \quad (2.22)$$

with  $S(q)$  being the interparticle structure factor and  $P(q)$  being the particle form factor. In the case of colloidal systems or polymer solutions with a low sample concentration, the interparticle structure factor is  $S(q) \sim 1$ .<sup>23</sup> For a solution of monodisperse, independent spherical particles the scattering intensity is given by:<sup>16</sup>

$$I(q) = V \cdot \phi \cdot (\Delta\rho)^2 \cdot \underbrace{\left( \frac{3 \sin(qr) - qr \cdot \cos(qr)}{(qr)^3} \right)^2}_{P(q)} \quad (2.23)$$

Here,  $V$  is the particle volume,  $\phi$  is the volume fraction of the particles,  $\Delta\rho$  is the difference between the scattering length densities of the particle and the solvent and  $r$  is the particle radius.

Extensive SANS studies of poly(NIPAM) macrogels were done by Shibayama and co-workers and also by Geissler et al. in the nineties.<sup>7,87,100,101</sup> These authors showed that the scattering intensity from non-charged networks in solution consists of two contributions. First, static inhomogeneities were taken into account arising from the chemical crosslinking  $I_{solid}(q)$  and secondly, a fluctuation term  $I_{liquid}(q)$  created by the motion of the polymer chains between the junction points is found.<sup>102</sup> In this case the scattering function from a non-charged macroscopic gel in good solvent can be described by

$$I(q) = I_{solid}(q) + I_{liquid}(q). \quad (2.24)$$

The  $I_{liquid}(q)$  contribution can also be found in the description of the elastic scattering from semidilute polymer systems at large  $q$ -values and can be described in terms of an Ornstein-Zernike (OZ) function.<sup>102</sup> Assuming that the static inhomogeneities from the

crosslinking are randomly distributed and exhibit a Gaussian statistics with respect to the spatial position, the  $I_{solid}(q)$  term can be written as a Guinier function and consequently the scattering function of chemically crosslinked gels is given by<sup>7</sup>

$$I(q) = \underbrace{I_G(0) \cdot \exp\left(-\frac{R_g^2 q^2}{3}\right)}_{\text{Guinier function}} + \underbrace{\frac{I_L(0)}{(1 + \xi^2 q^2)}}_{\text{Ornstein-Zernike term}} \quad (2.25)$$

Here,  $R_g$  is the radius of gyration and  $\xi$  is the correlation length, which is considered to be related to the blob size and describes the ensemble-averaged correlation of the polymer network.

In the case of polymer networks containing charged groups an additional electrostatic interaction term has to be taken into account. The original theory was developed for charged polymer solutions by Borue and Erukhimovich<sup>103</sup> and Shibayama showed later that it can also be applied to polymer gel networks for example based on NIPAM and acrylic acid.<sup>100</sup>

By introducing charges into a polymer solution, the scattering intensity becomes less than that of an uncharged polymer solution. This can be described by a modification of the osmotic modulus taking into account the Debye-Hückel interaction energy. So an additional  $q$ -dependency of the osmotic modulus is introduced.

The scattering from spherical colloidal particles like microgels can also be described by equation 2.24 and the condition  $q \cdot R_g \gg 1$  is always fulfilled. However, for microgels it is experimentally not possible to determine  $I_{solid}(q)$  in equation 2.24, because microgels are colloidal particles and their particle form factor,  $P(q)$ , overlaps in this region with the expected Guinier function stemming from the crosslinks. If  $R_g \gg q^{-1}$ , only the Porod part of the particle form factor should contribute significantly to the scattering intensity, and the scattering profiles of microgels in the swollen state can be analyzed by using a combination of a Porod and an OZ contribution<sup>16,104</sup>

$$I(q) = 2\pi(\Delta\rho) \frac{A}{V} \frac{1}{q^4} + \frac{I(0)_L}{1 + \xi^2 q^2}. \quad (2.26)$$

Here  $A$  is the interfacial area in the scattering volume,  $V$  is the scattering volume and  $\xi$  the correlation length.



At temperatures above the transition temperature the hydrophobic interaction between the microgel and the solvent increases and the polymer network collapses. The particles behave then like compact hard spheres and it has to be taken into account that the scattering results from a two-phase system, namely the interface between the collapsed particle and the surrounding liquid phase. In this temperature region, the OZ part in the scattering profile disappears and only Porod scattering remains. For particles with a smooth interface the form factor can be fitted using the Porod law (see Eq. 2.27) in the  $q$ -range probed in the SANS experiments.

$$I(q) \propto \frac{A}{V} \frac{1}{q^4}. \quad (2.27)$$

If the surfaces of the collapsed particles are rough, the Porod law has to be modified.<sup>105</sup>

### 2.3.3.3 Neutron spin-echo spectroscopy

Neutron spin-echo (NSE) spectroscopy is a suitable technique to measure fast motions in soft matter with the highest energy resolution of all types of neutron spectrometers.<sup>106,107</sup>

It was invented by Ferenc Mezei in the 1970's and is based on the magnetic moment of the neutrons,<sup>108</sup> which allows to produce polarized neutron beams.

NSE is a quasi-elastic scattering technique. As shown in figure 2.7 the elastic peak is broadened due to quasi-elastic scattering, for which the average energy transfer is zero. This is due to diffusive processes of atoms and hence, changes in the speed of the quasi-elastically scattered neutrons contain information about the dynamics of the sample. A typical example for inelastic scattering is the Brillouin effect. However, this is beyond the scope of the present discussion.

To describe the setup of a NSE experiment, in figure 2.8 a schematic drawing of a typical instrument, as it is used at the ILL (IN11 A and IN15, Grenoble, France) and at the JCNS at FRM II (Garching, Germany), is shown.<sup>107,109</sup> The incoming neutron beam passes a velocity selector, where a beam with a certain mean wavelength and in the case of NSE a rather broad wavelength distribution is generated. After the velocity selector the neutron beam hits a polarizer (super mirror), producing spin-polarized neutrons. Then passing a so-called  $\pi/2$ -flipper (a magnetic coil) the neutron spin is flipped by  $90^\circ$ . Traveling

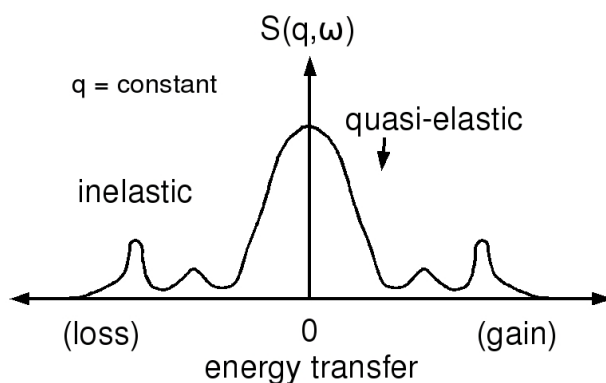


Figure 2.7: Inelastic and quasi-elastic neutron scattering: the inelastic scattering is represented by the peaks at non-zero energy transfer and reflect the vibrational modes of the system; the elastic scattering peak is broadened due to the Doppler effect and offers information about diffusive processes (translation or rotation).

through the first main coil with a magnetic field  $B_0$  the neutrons begin to undergo Larmor precession. This leads to a de-phasing of their spin, due to the different velocities of the neutrons. Faster neutrons reach the end of the first coil earlier with a smaller precession angle, while slower neutrons finally have a higher precession angle. Before the neutron beam is scattered at the sample, the spin is flipped by  $180^\circ$  by a  $\pi$ -flipper, and enters then the second main coil  $B_1$ . This coil has exactly the same magnetic field as the first one. Accordingly, due to the  $\pi$ -flip the dephased neutron spins will be refocused while flying through the second coil. At the end of the second coil the neutrons are flipped again by  $90^\circ$  using a  $\pi/2$ -flipper and subsequently reach the detector. If no energy transfer with the sample occurs (fully elastic scattering), no change in velocity of the neutrons passing the second main coil takes place. In this case the refocusing in the second coil will be complete and all neutrons return to the initial polarization. Moreover, during their flight the neutrons are focused several times by so-called Fresnel coils.

In a NSE experiment the Fourier transform of the scattering function  $S(q, \omega)$ , the so called intermediate scattering function  $S(q, t)$ , is directly measured.  $S(q, t)$  is proportional to  $g^1(\tau)$  and in the NSE experiment the short time part of the motions in microgels is probed.

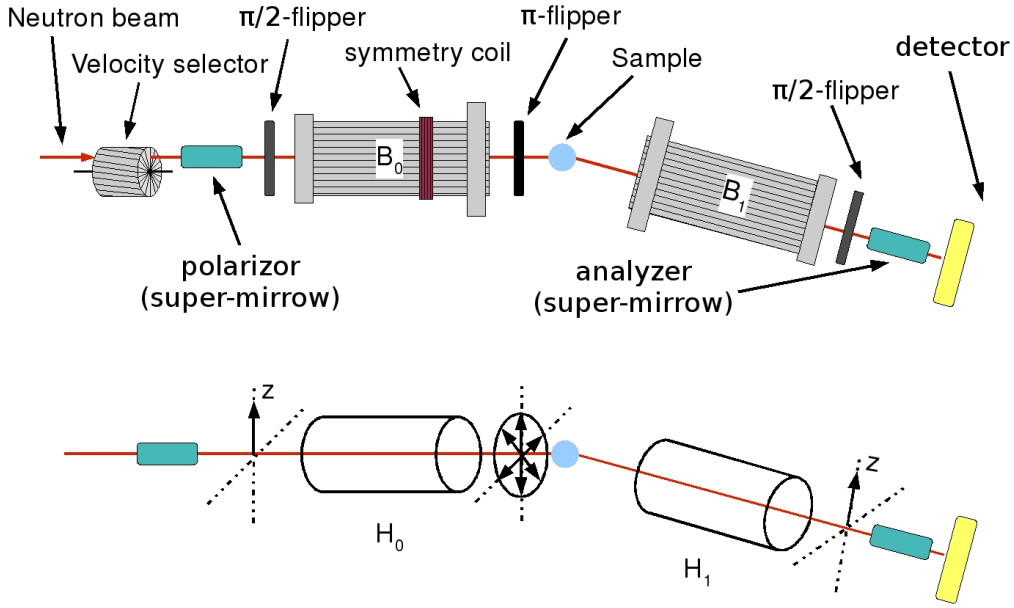


Figure 2.8: Schematical drawing of a typical NSE setup;  $B_0$  and  $B_1$  are the main precession coils and the lower part of the picture displays the spin movements

Gels belong to the group of non-ergodic media. As already mentioned in section 2.3.1 this leads to problems in the analysis of DLS data. In the case of non-ergodic media the process of quasi-elastic scattering was discussed in detail by Pusey and van Meegen.<sup>29</sup> For non-ergodic media the following expression for the ensemble-averaged  $S(q, t)$  was found:

$$\langle S(q, t) \rangle_E \propto \left\langle \exp(-q^2 \langle \xi^2 \rangle) \left( 1 - \exp\left(\frac{-D_G q^2 t}{q^2 \langle \xi^2 \rangle}\right) \right) \right\rangle_E \quad (2.28)$$

where  $q$  is the magnitude of the scattering vector ( $q = (4\pi/\lambda)\sin(\theta/2)$ ). The dynamic correlation length  $\xi$  connected with the network breathing mode is related to  $D_G$ , as the diffusion coefficient of this mode. If  $q^2 \langle \xi \rangle \rightarrow \infty$  the system behaves ergodically, which means that  $\langle S(q, t) \rangle_E$  decays completely to zero and does not exhibit a  $q$ -dependent baseline. The result is, that equation 2.28 becomes

$$\langle S(q, t) \rangle_E \propto \exp(\Gamma t) \quad (2.29)$$

and the decay of the intermediate scattering function can be described by a single exponential decay<sup>31,110,111</sup> with  $\Gamma$  as the relaxation rate. This is a limit, which can usually not be reached in light scattering experiments. However, for neutron scattering experiments  $q$

is very large and even for  $\xi$  values of 5 nm the product can be of the order of 100. In this case within the experimental error  $S(q, t)$  decays to zero and the system shows pseudo-ergodic behaviour. It was already shown before, that this limit can be reached<sup>31</sup> and the data can be treated using a single exponential description leading to a determination of  $\Gamma$ . Plotting  $\Gamma$  vs.  $q^2$  the diffusion coefficient  $D_G$  of the network breathing mode can be calculated by a simple linear regression (eq. 2.9).

## 3 Experimental part

### 3.1 Chemicals

#### 3.1.1 Macro- and microgels

The water for all purposes was purified by a MilliQ system (Millipore, Billerica, USA) and heavy water was purchased from Eurisotop (Groupe CEA, Saclay, France) with an isotopic purity of 99 %. For the macro- and microgels described here the chemicals were obtained from Aldrich. The monomer *N*-isopropylacrylamide (NIPAM, 97 %) was purified by recrystallizing from hexane, the comonomers *N*-*tert*-butylacrylamide (NtBAM, 97 %) and 3-butenic acid (BAc, 97 %) were chromatographically destabilized by using a aluminium oxide B column (MP Biomedicals GmbH, Germany). The crosslinker *N,N'*-methylenebis(acrylamide) (BIS,  $\geq 98$  %), the surfactant sodium dodecyl sulfate (SDS, Merck,  $\geq 97$  %), the initiator potassium peroxydisulfate (KPS, purity 99 %),  $\alpha, \alpha'$ -Azodiisobutyramidine dihydrochloride (V50, 97 %) and the initiator accelerator *N,N,N',N'*-Tetramethylethylenediamine (TMEDA, 99 %) were used as received. For the UV-induced polymerization 2,2'-azobis(2-methylbutyronitrile) (AIBA,  $\geq 98$  %) is used.

#### 3.1.2 Nanoparticles

For the nanoparticle synthesis and the modification procedures the following chemicals were used without further purification: cobalt chloride hexahydrate ( $\text{CoCl}_2 \cdot 6 \text{H}_2\text{O}$ , Riedel-de Haën, puriss.), sodium borohydride ( $\text{NaBH}_4$ , Aldrich,  $> 98$  %), citric acid (Fluka,  $> 99,5$  %), tetraethyl orthosilicate (TEOS, Aldich, 98 %), (3-aminopropyl)trimethoxysilane (APTMS, Aldrich, 97 %), 3-(Trimethoxysilyl)propyl

methacrylate (MPS, Aldrich, 98 %), Potassium hexachloroplatinate ( $K_2PtCl_4$ , Aldrich,  $\geq 99,99$  %), Nickel(II) chloride hexahydrate ( $NiCl_2 \cdot 6 H_2O$ , Aldrich,  $\geq 98$  %), hexadecyltrimethylammonium bromide (CTAB, Merck,  $\geq 97\%$ ), poly(styrene sulphonate) (PSS, Fluka, Mw 14,900), poly(allylamine hydrochloride) (PAH, Aldrich, Mw 15,000), poly(vinylpyrrolidone) (PVP, Aldrich, Mw 10,000), ammonium hydroxide solution (Riedel-de Haën, 33 wt % in water), styrene (Aldrich,  $> 99$  %), divinylbenzene (DVB, Aldrich, 80%), ethanol (VWR, p.a.) and isopropanol (VWR, p.a.).

## 3.2 Synthesis

### 3.2.1 Macrogels

The synthetic approach used for the macrogels, was similar to that described by Shibayama and Tanaka.<sup>7</sup> For some of the experiments it was necessary to systematically prepare gels with a crosslinker gradient. For these macrogels a modified synthesis procedure was applied.

#### 3.2.1.1 Macrogels for the NSE experiment

To obtain enough contrast in the neutron scattering experiments, the macrogels were directly polymerized in  $D_2O$ . For that 50 ml  $D_2O$  was degassed at room temperature (RT) for about 30 minutes in a conventional glass beaker. Then NIPAM, BIS and if necessary comonomers were added and stirred until they were completely dissolved. Subsequently, the monomer solution was cooled down to  $0^\circ C$  and the initiator KPS was added. Directly after the addition of the accelerator TMEDA, the glass beaker was heated up to RT and the polymerization process started immediately. The reaction was allowed to proceed at RT for 24 hours.

#### 3.2.1.2 Macrogels with crosslinker gradient

**Method 1** First of all, two solutions of the main components, the monomer NIPAM (0.7 M in water<sup>7</sup>), and the crosslinker BIS (saturated in water), are prepared. 3.0 ml

---

of the NIPAM solution are mixed with the photoinitiator AIBA (0.5 mol% respective to NIPAM amount) and filled in a small reaction vessel, which is placed in a second tube with icewater. Subsequently, a bottom layer of the concentrated BIS solution is created in the reaction vessel filled with NIPAM under exclusion of light to prevent a prematurely and uncontrolled polymerization. After 10 minutes of cooling, the reaction tube is placed on a rotating plate in front of the UV-light and the exposure time for the polymerization was 14 minutes at maximum. To ensure a complete polymerization of the macrogel, the reaction was continued over night without UV irradiation. The obtained macrogel was carefully taken out of the reaction tube and placed in a Petri dish for storage.

**Method 2** The basic solutions of NIPAM and BIS from method 1 were separately mixed with different ratios (0.4 BIS/1.6 NIPAM; 0.8 BIS/1.2 NIPAM; 1.2 BIS/0.8 NIPAM; 1.6 BIS/0.4 NIPAM) so that the total volume pro phase was 2 ml. Furthermore, the initiator concentration was held constant for every of the four phases. Consequently a gradient was build up under exclusion of light with the low-BIS phase at the top and the BIS-rich phase at the bottom. The polymerization procedure was equal to that of method 1.

**Method 3** For the creation of a continuous crosslinker gradient a peristaltic pump (Heidolph Pumpdrive 5201) and two differnt NIPAM/BIS ratios (5 mol% and 20 mol% respective to NIPAM) with AIBA as initiator (3.8 mg for 4 ml monomer solution) were used. The solution with the low content of BIS was filled in the first tube of the peristaltic pump setup and the mixture with the high amount of BIS in the second (setup is shown in section 4.2). In this way, a gradient from a low crosslinker content (top of the reation tube) to a high crosslinker content (bottom) is created. The reaction vessel is placed in a second tube filled with ice water, cooled for 10 minutes and the exposure time was again 14 minutes at maximum. The polymerization was allowed to proceed over night without UV irradiation.

## 3.2.2 Microgels

### 3.2.2.1 Poly(NIPAM-co-NtBAM)

These copolymer microgels are synthesised using a surfactant-free radical emulsion polymerisation<sup>112</sup> of the monomer NIPAM (100-x mol%) and NtBAM (x mol%) and the cross-linker BIS (5 mol%). In brief, the synthesis was performed in a 100 ml three-neck flask equipped with a mechanical stirrer, thermometer, a reflux condenser and a nitrogen inlet. The two monomers (NIPAM and NtBAM) and BIS were dissolved in 50 ml MilliQ water. The reaction solution was heated up to 40°C under continuous stirring and purged with N<sub>2</sub> in order to remove oxygen. Then the reaction mixture was heated up to 70°C and after 30 minutes equilibration the initiator KPS (dissolved in 1 ml MilliQ water) was added to start the polymerisation.<sup>112</sup> After a few minutes the clear reaction medium turned turbid. The reaction was allowed to proceed at 70°C for 4 h. Then the reaction medium was cooled down to room temperature and subsequently stirred over night. At the end the microgels were purified by centrifugation and ultra-filtration and finally freeze-dried.

### 3.2.2.2 Poly(NIPAM-co-BAc)

These copolymer microgels are synthesised using an emulsion polymerisation with sodium dodecyl sulfate (SDS) as surfactant. The used surfactant concentration was at 0.002 M, which is below the critical micelle concentration (cmc) of SDS in pure water at 25°C (cmc(SDS) = 0.0082 M). The polymerization procedure was similar to that of the poly(NIPAM-co-NtBAM) copolymer microgels. Finally the microgel was freeze-dried and redispersed in D<sub>2</sub>O for the neutron scattering experiments.

## 3.2.3 Synthesis of magnetic cobalt nanoparticles

### 3.2.3.1 Cobalt@SiO<sub>2</sub> nanoparticles

The cobalt nanoparticles have been synthesized analogous to the method of Kobayashi et al.<sup>113</sup> For a standard synthesis, 100 ml degassed aqueous solution of NaBH<sub>4</sub> (4·10<sup>-3</sup> M) with different amounts of citric acid (2·10<sup>-6</sup> M, 4·10<sup>-5</sup> M, 2·10<sup>-5</sup> M, 4·10<sup>-4</sup> M



---

or  $2 \cdot 10^{-4}$  M) were prepared. Under intensively stirring and purging with nitrogen 0.1 ml of a 0.4 M  $\text{CoCl}_2$  solution in water was added. Subsequently, the color of the reaction mixture turned gray indicating the nanoparticle formation. Directly after one minute reaction time, 400 ml of an ethanolic solution with 7,2  $\mu\text{l}$  APTMS and 84  $\mu\text{l}$  TEOS (molar ratio of 1:9) was added to build the silica shell around the magnetic cobalt particles. Finally, the particle solution was purified by centrifugation and redispersion in pure ethanol.

### 3.2.3.2 MPS-fuctionalization of $\text{Co@SiO}_2$ nanoparticles

The magnetic particles were separated using a magnet and redispersed with ultrasonification in a mixture of 120 ml ethanol and 20 ml water. The nanoparticle solution was transferred to a three-neck round flask in an ultrasonic bath equipped with a reflux condenser and a mechanical stirrer with a glass stirring paddle. After the addition of 5 ml ammonium hydroxide (33% in water), the dispersion was stirred for 5 minutes under ultrasonic treatment. Then 150  $\mu\text{l}$  MPS were injected dropwise and the reaction mixture was stirred over night. The flask with equipment was transferred to an oil bath and the dispersion was refluxed for 2 hours. Afterwards, the particles were cleaned by centrifugation and redispersed in ethanol.

## 3.2.4 Synthesis of different nickel nanoparticles

### 3.2.4.1 Pt@Ni nanoparticle synthesis

Basically, the preparation of the nanoparticles was done according to a synthesis published by Grzelczak et. al.<sup>114</sup> At first a 0.1 M CTAB solution was prepared. To make sure that CTAB is completely dissolved in water, the solution was heated up to  $40^\circ\text{C}$ . Then 9.63 ml of the 0.1 M CTAB solution was mixed under stirring at  $40^\circ\text{C}$  with 50  $\mu\text{l}$  of a 0.05 M  $\text{K}_2\text{PtCl}_4$ . For the reduction of the platinum salt 0.3 ml of a 0.06 M  $\text{NaBH}_4$  solution was added and the reaction tube was immediately capped. After 10 minutes the vessel was opened and the solution stirred for several minutes. In order to grow a nickel shell around the seed particles, 47.5 ml of an aqueous solution of  $\text{NiCl}_2$  (0.5 mM) and  $\text{N}_2\text{H}_4$  (15 mM) was mixed with 2.5 ml of the platinum seed particles. The reaction was continued for

2-3 h at 40°C and if needed for further applications, the product was separated from the solvent with a magnet.

#### **3.2.4.2 Silica-coating of nickel nanoparticles using a LbL technique**

10 ml of the original Pt@Ni nanoparticle solution was centrifuged at 5000 rpm for 30 minutes (Centricon T-1080, Sorvall Surespin 630), then the excess of solvent was removed and the precipitate redispersed in 5 ml of de-ionised water (MilliQ water). In the meantime an aqueous solution of PSS (2 g/l, 6 mM NaCl) was sonicated for 30 minutes. Afterwards, 5 ml of this PSS solution was added dropwise to the nanoparticle solution under vigorous stirring and the reaction was continued over night. The Pt@Ni@PSS solution was centrifuged at 8000 rpm (Centricon T-1080 with rotor Surespin 630, Sorvall) for 30 minutes and the precipitate redispersed in 5 ml of MilliQ water.

An aqueous solution of PAH (2 g/l, 6 mM NaCl) was sonicated for 30 minutes and then 5 ml of this solution were added dropwise to Pt@Ni@PSS under vigorous stirring. The stirring was continued over night, the Pt@Ni@PSS@PAH solution was centrifuged at 8000 rpm for 30 minutes and redispersed in 5 ml of MilliQ water.

5 ml of the Pt@Ni@PSS@PAH solution was mixed with 5 ml of PVP aqueous solution (Mw 10000, 4 g/l) and stirred overnight. The resulting Pt@Ni@PSS@PAH@PVP was centrifuged 30 minutes at 8000 rpm and the precipitate was redispersed in 0.2 ml water. Under vigorous stirring the Pt@Ni@PSS@PAH@PVP solution was added dropwise to 1 ml of isopropanol.

For the silica coating at first an ammonia solution in isopropanol (3.84 vol.% ammonia (33 wt% in water) in isopropanol) was prepared. The Pt@Ni@PSS@PAH@PVP (1.2 ml) was added under vigorous stirring to 0.46 ml of water and subsequently an addition of 1.43 ml of the pre-prepared ammonia solution followed. Finally, 0.40 ml of a solution of TEOS in isopropanol (0.97 vol% of TEOS) was added under gentle stirring. The reaction mixture was allowed to react for 2 hours and two further additions of TEOS were carried out to grow the silica shells.

---

### 3.2.4.3 Nickel nanoparticles coated with polystyrene

5 ml of the original Pt@Ni nanoparticle solution was separated from the solvent using a magnet. The residue was redispersed in 30 ml MilliQ water using ultrasonification. The Pt@Ni solution was then heated to 30°C (in an ultrasonic bath; DT 103H, Bandelin; 140W), followed by the addition of destabilized styrene (4  $\mu$ l) and destabilized DVB (4  $\mu$ l) under stirring and ultrasonification. After 15 minutes, the temperature was increased to 70°C and the polymerization was initiated by adding 4  $\mu$ l KPS solution (0.1 M in water). The polymerization was allowed to proceed for 2 hours, than cooled down to RT and the Pt@Ni@PS particles were separated with a magnet.

## 3.3 Characterization Methods

### 3.3.1 DLS measurements

The dynamic light scattering (DLS) measurements were performed using an ALV goniometer setup (ALV-Laservertriebsgesellschaft, Langen, Germany) with an argon ion laser as light source ( $\lambda = 514,5$  nm, Spectra Physics 2017), operating with a variable output power (10-400 mW). The correlation function was generated using an ALV-5000/E multiple- $\tau$  digital correlator and subsequently analysed by inverse Laplace transformation (CONTIN<sup>84</sup>). Decaline served as an index matching bath. Measurements for each angle and temperature were repeated three times and averaged afterwards. The microgel swelling curves were recorded at a constant scattering angle of 60° and over a temperature range between 10-44°C. A microgel particle concentration of about 0.01 wt% (dry polymer particles) was employed and to avoid aggregation. The pH value was adjusted to 2-3 using dropwise addition of hydrochloric acid (HCl).

### 3.3.2 Small angle neutron scattering

The SANS experiments for the poly(NIPAM-co-NtBAM) microgels, were carried out using the KWS2 instrument of the JCNS outstation at the FRM II (Garching, Germany).

For details of the setup, see the respective publications of the JCNS.<sup>115</sup> The neutron wavelength was 7 Å for all experiments and the sample-to-detector distances were chosen to be 2 m and 8 m, covering a  $q$ -range from 0.007 to 0.2 Å<sup>-1</sup>. The microgel particle concentration employed for these measurements was 2 wt% in D<sub>2</sub>O and standard Hellma quartz cells (1 x 20 mm) were used. The scattering intensity data were collected using a two-dimensional multi-detector. The experimental data obtained using the two sample-to-detector distances were corrected for electronic background and empty cell scattering. Detector sensitivity corrections and transformation to absolute scattering cross sections  $d\Sigma/d\Omega$  were made with a secondary Plexiglass<sup>®</sup> standard according to a standard procedure.<sup>116,117</sup> After this procedure the data obtained from the two different detector positions overlapped within the experimental error and no further adjustment was necessary.

### 3.3.3 Neutron spin-echo experiment

The NSE experiments presented here, were done using the IN11-A instrument at the Institute Laue-Langevin (Grenoble, France).<sup>118</sup> To generate scattering contrast the macrogels have been synthesized in D<sub>2</sub>O as mentioned before. The microgels were freeze dried in the last step of the purification and were redispersed in D<sub>2</sub>O for the measurements. To adjust the pH of the gels to a value of 2, deuterated hydrochloric acid was used.

To obtain different  $q$ -values ( $0.05 \leq q \leq 0.2$ ) the wavelength of the neutrons ( $\lambda = 5.5, 8.5$  and 10.0 Å) as well as the scattering angle ( $4.6^\circ$  to  $15.5^\circ$ ) was changed. The resolution function of the instrument was determined for the different experimental conditions using the elastic scattering of graphite. More details related to the setup can be found in the literature.<sup>107,109</sup>

### 3.3.4 Electron microscopy

The transmission electron micrographs were taken using a LEO 922 O microscope (Zeiss, acceleration voltage of 200 kV) and the specimen for the room temperature (RT) images were prepared on copper-grids (Science services, carbon only, 200 mesh). The scanning

---

electron microscopy (SEM) experiments were performed with a Zeiss LEO 1530 GEMINI FE-SEM (acceleration voltage of 3 kV) and the samples were prepared on silicon wafers. For the microgels the freeze-dried samples were re-dispersed in water to obtain a highly diluted dispersion. The nanoparticle solutions were used as synthesized or in some cases diluted with the respective solvent.

For the standard transmission electron microscopy (TEM) measurements 3  $\mu\text{l}$  of the diluted solution were dropped on the copper-grid and after one minute the residual solvent was blotted off with a filter paper. The SEM sample was prepared by putting one drop of the solution on a silicon wafer, which was allowed to dry overnight. Afterwards, the specimen were coated with a 1 nm layer of platinum or carbon.

The cryogenic transmission electron microscopy (cryo-TEM) preparation was also done using highly dilute samples. A few microlitres of diluted dispersion were placed on a bare copper grid and the excess liquid was removed with filter paper. This sample was cryo-fixed by rapid dipping into liquid ethane at  $\sim 170^\circ\text{C}$  in a cryo-box (Carl Zeiss NTS GmbH, Germany). Afterwards, the specimen was transferred into a cryo-transfer holder (CT 3500, Gatan, Germany) and placed in the microscope.

### **3.3.5 Macrogel swelling kinetics via image processing**

For the determination of the swelling curves and the swelling ratio  $\alpha$  of the macrogels with a crosslinker gradient the image analysis software 'ImageTool' (UTHSCSA ImageTool, Version 3.0<sup>119</sup>) was used. Therefore, the scale bar of the digital pictures and of the video sequence was transferred to the corresponding amount of pixels, which allows a more precise evaluation of the gel dimensions. The temperature induced changes in width and length of the gel were analyzed at a high magnification by measuring the width or length in pixel and hence, the swelling ratio was calculated.



## 4 Macrogels with an internal crosslinker gradient

Although, macro- and microgels consist of the same components including monomers, crosslinker and initiator, they might differ in their internal network structure. As already mentioned in the introduction, this is due to the formation process of the gels. Hence, macroscopic gels show a rather homogeneous crosslinker distribution inside the network compared to microgels, it would be interesting to see how a macroscopic network with the dimensions of some centimeters and an artificial crosslinker gradient may react on an external stimulus.

A suitable thermoresponsive polymer for such studies is poly(NIPAM) crosslinked with BIS. It has been shown in literature that colloidal poly(NIPAM) microgel particles exhibit a non-uniform crosslinker distribution.<sup>9,22,23,96</sup> Additionally, homogeneous poly(NIPAM) macrogels have been subject of various studies by Shibayama and Tanaka<sup>7,21,120,121</sup> in the nineties.

In the following chapter the influence of the crosslinker density on the swelling behaviour of poly(NIPAM) macrogels is studied. Therefore, different techniques for the preparation of a crosslinker gradient inside the gel have been developed and an attempt was made to quantify the kinetics of the volume phase transition of such a gradient macrogel as a function of the scrutinized position inside the gel.

## 4.1 General aspects of macroscopic gels based on NIPAM and BIS

As a first step, it was important to determine in which way the different components, here the monomers NIPAM and BIS, homopolymerize. As already known from literature, poly(NIPAM) exhibits a phase transition at a temperature of 32° C, in contrast to this a homopolymer only made of the crosslinker agent BIS does not exhibit temperature sensitivity.

Both monomers were independently mixed with an equal amount of photoinitiator (5 mol%) and polymerized under identical conditions using UV-irradiation at RT. The obtained homopolymers are shown in figure 4.1. The image clearly illustrates, that poly(NIPAM) shows no apparent turbidity below the VPTT (here at RT) and forms a transparent semi-viscous solution. Here, the viscosity of the poly(NIPAM) solution is caused by entanglements and by so-called self-crosslinking of the polymer chains. In the case of poly(NIPAM), this effect of self-crosslinking has been reported in the literature before by Gao et al.<sup>122,123</sup> These authors assume that due to chain transfer reactions, the hydrogen atom on the *tert*-C atom of the isopropyl group as well as the *tert*-C atom of the polymer backbone can be attacked by a free radical. Subsequently, the free *tert*-C radical can react with a vinyl group or with another active hydrogen to create junction points. The homopolymer obtained from the polymerization of BIS shows a real gel-like structure and a strong turbidity. Usually, the monomer BIS, due to its two polymerizable end groups, is used as crosslinking agent. Here, the homopolymerization of BIS finally results in a strongly crosslinked network, which exhibits no flow in the steady-state.

By heating up both homopolymers, poly(BIS) shows no visually observable change in turbidity as expected, while poly(NIPAM) changes significantly above 32° C. This temperature-induced effect is based on the LCST of linear poly(NIPAM). Below 32° C, the polymer chains are more or less in a stretched form, since water is a good solvent for the polymer. Above a temperature of 32° C the hydrophobic interactions between the polymer and the solvent increase, while the solubility in water decreases and the polymer



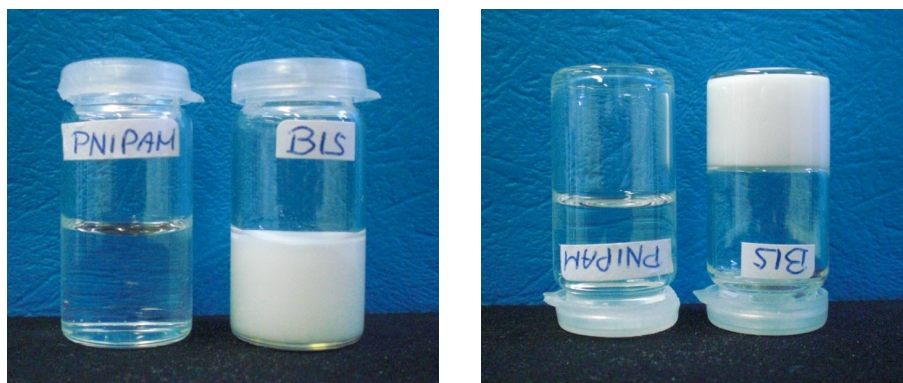


Figure 4.1: Photographs of a pure poly(NIPAM) solution and a poly(BIS) gel prepared by UV initiated polymerization below the LCST of NIPAM at room temperature

chains start to coil. This aggregation of the chains leads to an increase of the turbidity of the poly(NIPAM) solution.

In order to prepare macroscopic gels based on poly(NIPAM) with a density gradient of crosslinker, different preparation techniques have been applied. The aim of the experiments was to synthesize a gel network that is already in the totally swollen state during the preparation (at RT) and shows a temperature induced collapse. Due to the produced crosslinker gradient it is likely that different zones of the gel exhibit different swelling capacities. Moreover, areas with a high crosslinker content should only decrease slightly in volume, while lower amounts of BIS should result in a more flexible network with a high swelling capacity.

## 4.2 Macroscopic gels with a crosslinker gradient

Recently, a new approach to describe the swelling behaviour of gels with a crosslinker gradient was introduced by Fernandes et al.<sup>96</sup> This approach is based on a modification of the Flory-Rehner theory and divides the gel in discrete layers of different crosslinker densities. Doing so, a crosslinker gradient as observed for example in microgels can be approximated. For microgels this approach leads to a satisfying description of the swelling behaviour. However, macrogels are usually homogeneous and only exhibit heterogeneities on a very local scale. Therefore, the aim of this section was to produce

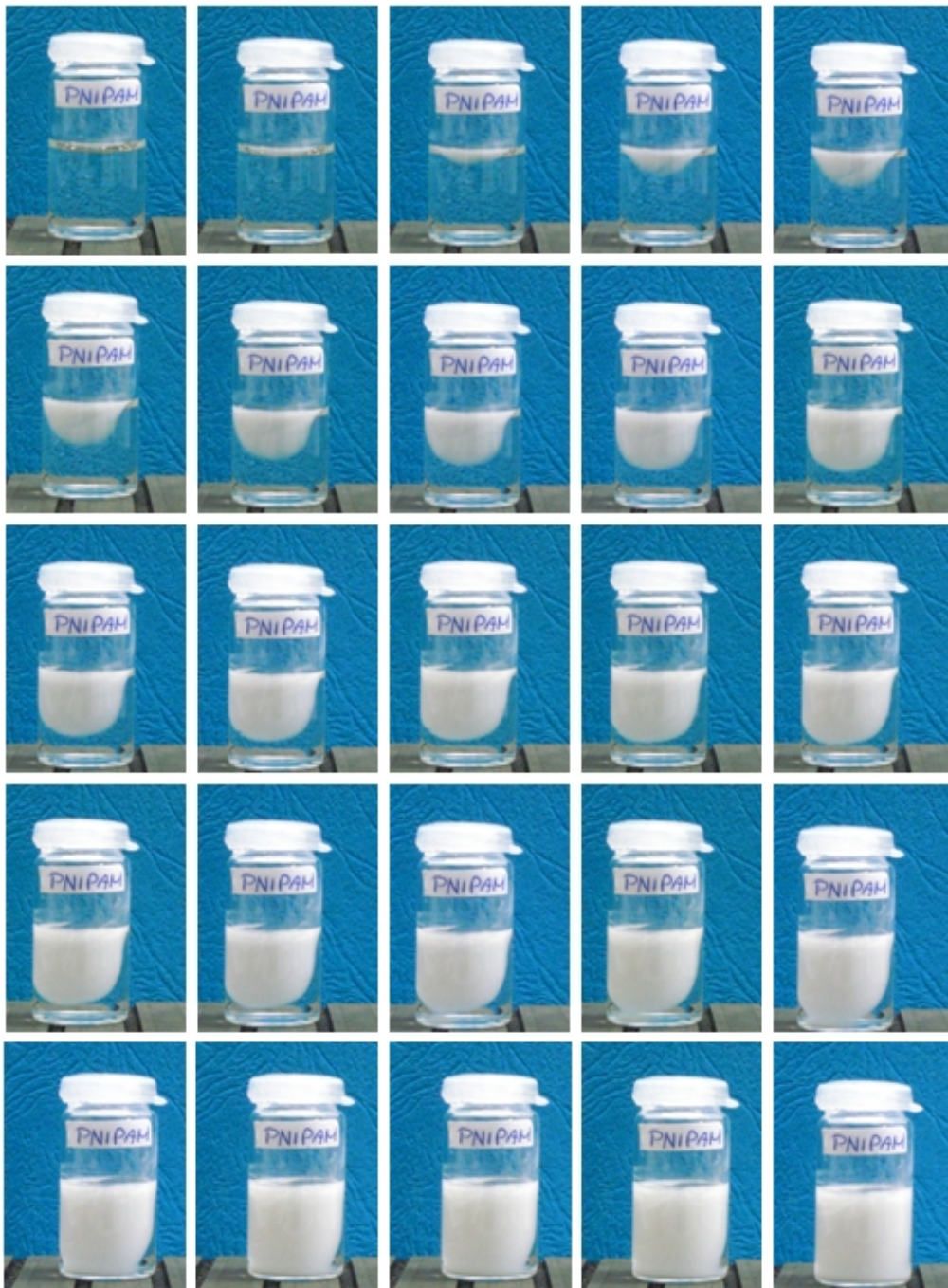


Figure 4.2: Temperature dependent turbidity of a non-crosslinked poly(NIPAM) solution; with increasing temperature above the VPTT the sample shows a white colouration.

macroscopic gels, which exhibit exactly the gradient structure used in the new model.

For the preparation of the crosslinker-gradient macrogels the following three different methods have been used:

- \* A NIPAM solution is sub-layered by a concentrated BIS solution.
- \* Four different solutions with varying NIPAM/BIS ratio are prepared and filled layer-wise into the reaction tube.
- \* Build-up of a crosslinker gradient using a commercial peristaltic pump.

It has been shown in various experiments, that using the sub-layer technique, the formation of a BIS gradient in the macrogel is limited in some way. The distribution of the crosslinker in the initial NIPAM/initiator solution is diffusion controlled and a long time period (more than 24 hours) is required to build up the gradient. After the UV-light induced polymerization, a macroscopic gel was obtained, but only with a low degree of crosslinking and thus no good form stability.

The second preparation method is based on the fact that four solutions with different ratios of NIPAM/BIS have been prepared and gradually layered. The concentration of UV initiator AIBA was kept constant for all four stock solutions. To ensure that the polymerization of poly(NIPAM) occurs below the VPTT, the reaction vessel is cooled with ice water and the exposure time was 14 minutes at maximum. A schematic drawing as well as a result of preparation method 2 is shown in figure 4.3.

Using this preparation method macroscopic gels with an optically visible crosslinker

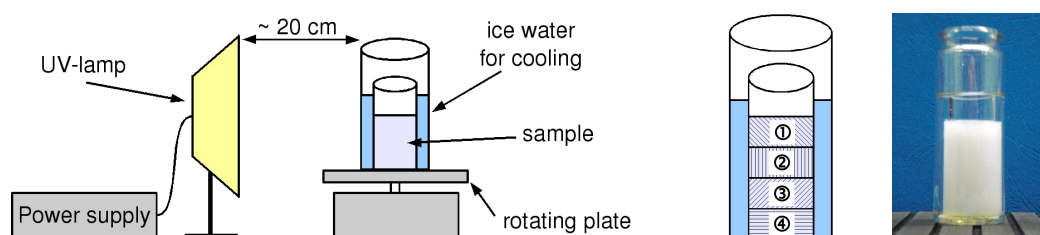


Figure 4.3: Sketch of the UV-induced polymerization setup and a photograph of a macrogel polymerized this way

gradient could be obtained. On the photograph given in figure 4.4 it is obvious that the

gel has well-separated areas. On the right side a higher turbidity is observable, compared to areas with lower turbidity (left). Taking into account the previous experiments on the homopolymerization of NIPAM (clear gel) and BIS (white gels), the more turbid areas can be identified as highly crosslinked polymer, while the more transparent gel contains a lower amount of crosslinker. In addition, the upper part of the gel was peeled away during extraction out of the reaction tube. This indicates that the top layer of the macrogel consist of a very weakly crosslinked network.

The last and most successful method for the crosslinker gradient preparation was carried

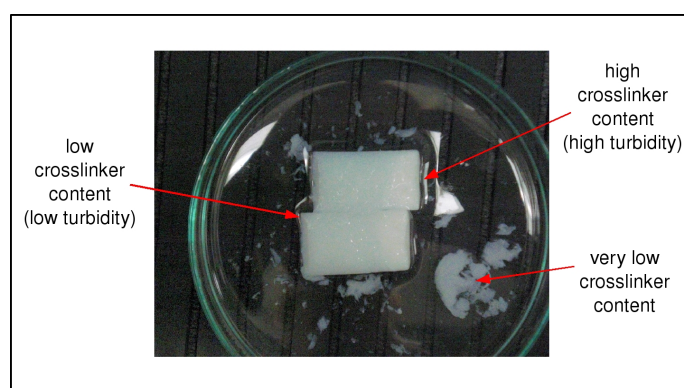


Figure 4.4: Photograph of a macrogel prepared by the layer-technique using four solutions with different NIPAM/BIS ratios; the areas with a high turbidity consist of a high crosslinked network (right side), while a low BIS content is represented by a low turbidity of the gel (left side)

out using a commercially available peristaltic pump (Heidolph Pumpdrive 5201). For this experiment, two solutions with the same amount of initiator, but different NIPAM/BIS ratios are prepared (5 mol% and 20 mol% respective to the total monomer amount). Using this peristaltic pump technique it was possible to synthesize a mechanically stable macroscopic gel with a continuously changing crosslinker gradient. In contrast to this, the gels obtained by the layer technique with the four different mixing solutions of NIPAM/BIS showed well-defined and separable areas of varying crosslinker content, but no continuous BIS gradient.

The schematic structure of the setup for the gel synthesis using a peristaltic pump is

depicted in Figure 4.5. Caused by the construction of the setup, the solution with a low concentration of BIS (right glass tube) is first pumped through the peristaltic pump into the reaction vessel. Followed by a continuous addition of the solution with high BIS amount to the low-BIS solution, a gradient is created in the reaction vessel (top: low BIS content; bottom: high BIS content). After the UV light induced polymerization, a macroscopic gel with a continuous crosslinker gradient was obtained. Its macroscopic structure is shown in figure 4.5 on the right hand side. From the different areas of the gel with varying turbidity it is clear, that the crosslinker content changes continuously from high to low.

For fundamental studies on the temperature-dependent swelling behaviour the 4-zone

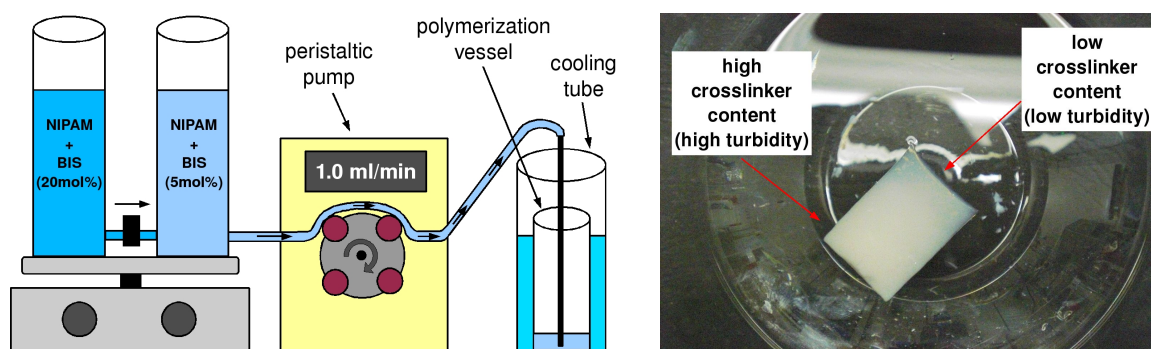


Figure 4.5: Schematic drawing of the used peristaltic pump setup to generate macrogels with a continuous crosslinker gradient (left) and a photograph of a macrogel with a visible crosslinker gradient obtained by the preparation method with a commercial peristaltic pump

gels were used. In the following chapters, only the results of the swelling of macrogels with a continuous BIS gradient are shown, since here, swelling curves with well-defined heating rate and additionally kinetic studies are performed.

### 4.3 Swelling curves determined with a constant heating rate

Due to the dimensions of the network, macroscopic gels based on NIPAM show a much slower response upon changes of temperature compared to microgels. With respect to this, for the determination of the swelling curves under equilibrium conditions, a heating rate of  $1^{\circ}\text{C}$  per 30 minutes was chosen. Thus, it is assumed that the macrogel reaches its equilibrium state within 30 minutes after an increase in temperature. For the experiment described here, a setup consisting of a computer-controlled thermostat, a temperature-controlled vessel with a thermometer, a timer and digital camera is used (see figure 4.6). It should be mentioned that the temperature of the thermostat differs slightly from the measured temperature in a water bath. Therefore, in the following discussion the water bath temperature is used. The images for the swelling analysis of the macrogel were taken after the equilibration phase, just before the next temperature step. To determine the swelling ratio  $\alpha$  the image analysis software 'ImageTool' (UTHSCSA ImageTool, Version 3.0<sup>119</sup>) was used.

In figure 4.7 different snapshots of the macrogel with a continuous BIS gradient during

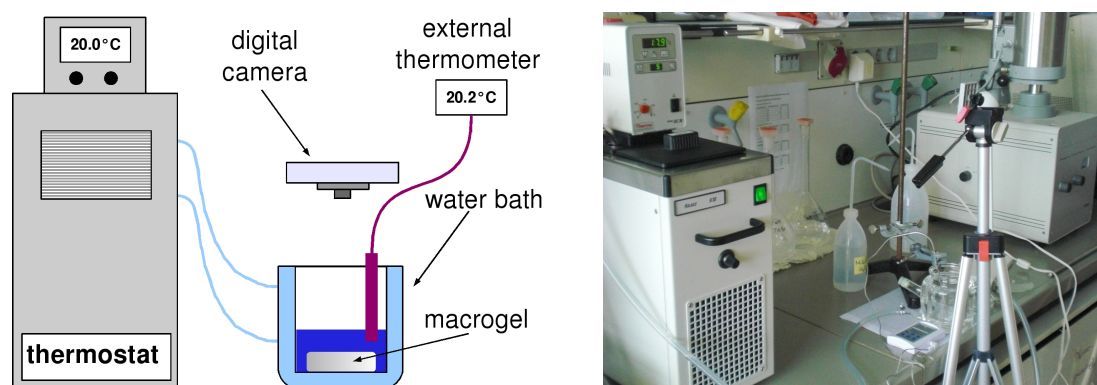


Figure 4.6: Schematic drawing and picture of the used self-constructed setup for the swelling curve measurement with a constant heating rate of  $1^{\circ}\text{C}/30$  min

the determination of the swelling curve with a constant heating rate are shown. From the pictures it is clear that below the volume phase transition temperature (VPTT) of

crosslinked poly(NIPAM) ( $\sim 32^\circ\text{C}$ ) the macrogel does not change in its dimensions within the experimental errors. At temperatures above the VPTT a visible deswelling of the gel was observed. In this case the areas with a low crosslinker content exhibit a strong deswelling behaviour, while the network areas with a high BIS content decrease only slightly in volume.

Based on a detailed image analysis of the pictures obtained from the deswelling measure-

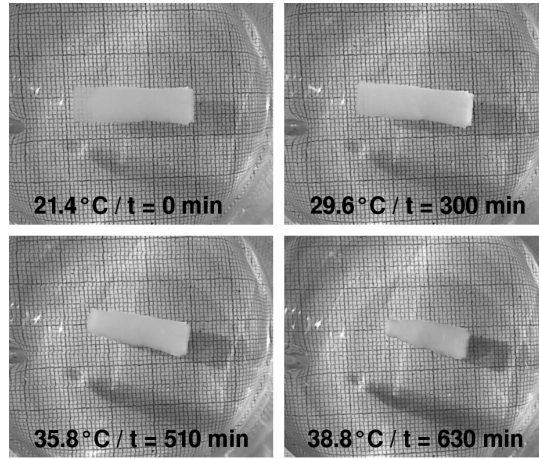


Figure 4.7: Images of the poly(NIPAM) macrogel during the determination of the swelling curve with a constant heating rate of  $1^\circ\text{C}$  per 30 minutes

ment and a calculation of the swelling ratio  $\alpha$  according to equation 4.1, it was possible to represent the swelling behaviour graphically (see figure 4.8).  $L_h$  is the width/length of the gel at a certain temperature and  $L_0$  is the width/length at initial measurement conditions.

$$\alpha = \frac{L_h}{L_0} \quad (4.1)$$

The swelling ratio was determined at four different positions of the macrogel, once in the length and three times in width at a high, medium and low crosslinker density. Here, the area with the highest crosslinking density shows the lowest deswelling behaviour (black curve), as expected. With decreasing content of the crosslinker BIS the swelling behaviour of the macrogel increases (see green and blue curve in figure 4.8). Furthermore, only a slight change in length of the gel could be observed. Beside this, the investigation of the

height of the macrogel was not possible due to the experimental setup and the image processing technique.

In addition, it has to be mentioned that some of the differently crosslinked zones of the

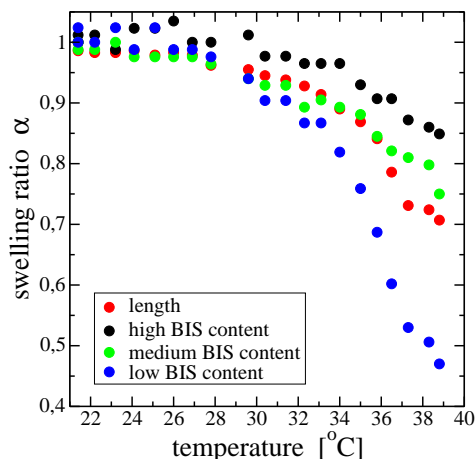


Figure 4.8: Swelling curves obtained from different areas of a macrogel with a continuous crosslinker gradient via image processing

macroscopic gel do not seem to be completely collapsed. This is manifested by the fact that the swelling curves of these regions (green and blue curve in figure 4.8) do not decay to a constant final value at temperatures above the VPTT of poly(NIPAM) ( $\sim 32^\circ\text{C}$ ). Consequently, an equilibration time of 30 minutes after a temperature change of  $1^\circ\text{C}$  seems to be too short to bring the macrogel in a state of equilibrium. It was therefore of great interest to study the kinetics of the gel network collapse. The results obtained by these experiments are presented in the following section.

## 4.4 Deswelling kinetics of a crosslinker-gradient macrogel

For a kinetic study of the shrinking process, the gel was cut in a rectangle after the synthesis and equilibrated at room temperature for 24 hours. It was found that after the equilibration time a subsequent change in volume of the gel occurs (see figure 4.9). This change is due to the fact that the less crosslinked regions (left side of the gel) showed an additional swelling. For the following image analysis to determine the swelling behaviour



of the macrogel, this change in the gel dimensions has to be kept in mind.

For the investigation of the swelling behaviour, the gel was suddenly plunged into a

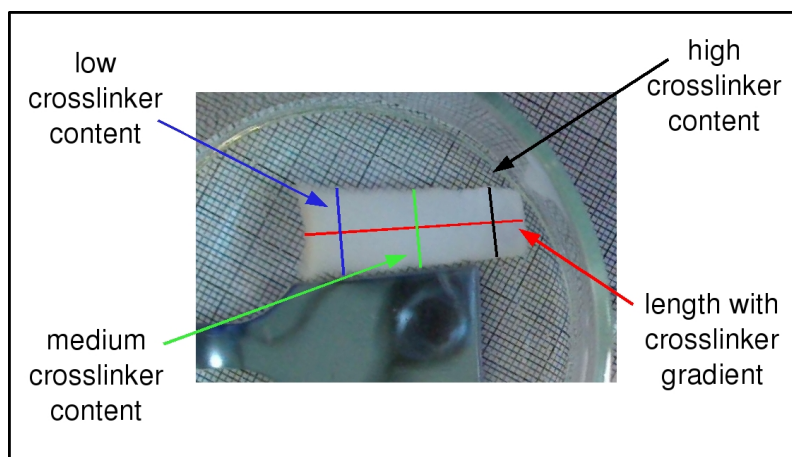


Figure 4.9: Poly(NIPAM) macrogel with BIS gradient after a equilibrium time of 24 hours at RT. The gel is used for the determination of the swelling kinetics.

preheated water bath at 40°C and the collapse of the polymer network was recorded within the first 15 minutes using a video camera. The further observation of deswelling was done by an automatic imaging process, which took a picture every hour. However, during this measurement the evaporation of the solvent at 40°C could not be prevented. If the solvent is refilled again, a decrease in the water bath temperature occurs and consequently swelling of the gel results. For this reason, the hourly photographs taken after the video sequence were finally not used for the determination of the swelling curves. To offer the possibility to measure the shrinking process of the macrogels for a long time, it is hence necessary to prevent the evaporation of the solvent. A solution for this problem could be to construct a closed measurement setup with a water-saturated atmosphere and a possibility to picture the temperature induced collapse of the gel.

To calculate the swelling ratio  $\alpha$  according to equation 4.1, every 10 seconds a picture was taken out of the video sequence and analyzed with the image processing software (Image Tool). Therefore, comparable to the previous experiment, the scale of the graph paper was transferred to a number of pixels and by means of this the calculation of  $\alpha$  was done. However, the use of the graph paper and distortion effects of the water bath

result here in a certain inaccuracy of the image interpretation. This inaccuracy has a stronger influence on small changes in the swelling ratio. The influence is rather small at high changes in the  $\alpha$  value (see following evaluation of the swelling curves).

Figure 4.10 shows the changes in the gel dimensions (once in the length and three

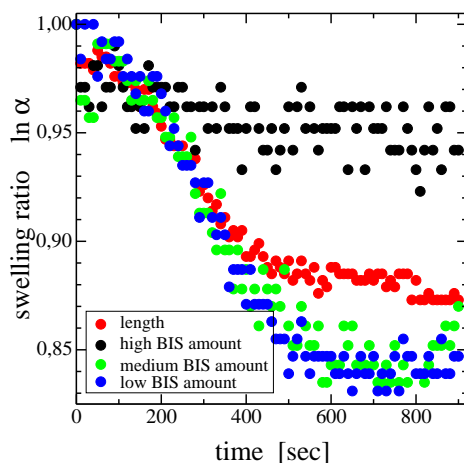


Figure 4.10: The swelling ratio  $\alpha$  from different position of the macrogels as a function of temperature obtained from the kinetic measurements.

times in the width) during the collapse of the poly(NIPAM) network with a continuous crosslinker gradient at 40°C. During the first ten minutes of the deswelling process, the swelling ratio  $\alpha$  of the length (red curve) decreases to a nearly constant value within the experimental errors. Comparing the width measurements at three different areas of the macrogel (that means at three different crosslinking densities), it is obvious that the domain with the highest BIS amount only shows a small change in the  $\alpha$ -value (black curve). The strong fluctuation of the data points is caused by the error of the measurement. As mentioned before, due to the image processing of the video sequence, small changes in the  $\alpha$ -value are afflicted with a higher error. Nevertheless, from figure 4.10 it is easy to see that during the first 400 seconds of the measurement, the swelling curve decreases slightly and the swelling ratio drops to a constant value.

Looking at the swelling curves of the macrogel regions with a medium (green curve) and a high (blue curve) crosslinker content, so a strong decrease of  $\alpha$  is obvious. Both swelling curves show approximately the same temporal decay and drop at the end of

the measurement nearly to a constant value. An explanation for this similar swelling behaviour could be, that indeed during the synthesis of this macrogel a crosslinking gradient is formed, but the difference of the BIS amount in the medium and high crosslinker region is not as big as expected. The removing of the capillary after the preparation of the BIS gradient, with which the reaction tube was filled, could also induce a mixing of the crosslinking agent. By an averaging of the width from the three different zones of the gel, a swelling curve was obtained, which is comparable to that of the length. Such behaviour was expected since the change in length reflects the overall swelling of the crosslinker gradient macrogel.

In summary, from the measured collapse of the macrogel network it was possible

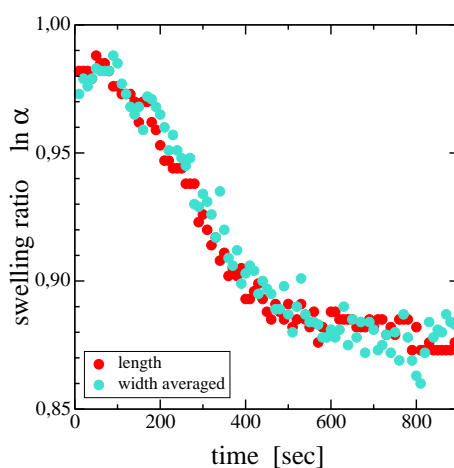


Figure 4.11: The swelling ratio  $\alpha$  from the length and the averaged width of the macrogels as a function of temperature obtained from the kinetic measurements.

to identify areas with a different crosslinking density. These areas showed a different deswelling behaviour related to the incorporated BIS amount. Hence, the regions with a high crosslinking density shrink only slightly, while the gel network containing a medium to a low amount of BIS showed a significant decrease in volume.

The aim of this kinetic measurement was to determine how long a macroscopic gel network with the dimension of some cubic centimeters needs to reach its equilibrium state after a spontaneous change in temperature above the VPTT. From the swelling curves in figure 4.10 it seems, that the  $\alpha$ -values of the four analyzed regions with different

crosslinker density drop within the measurement time to a constant value. This would mean, that within a time of 15 minutes the gel network completely collapses to this equilibrium state at 40°C. But from comparison with the swelling curves of figure 4.8 a different behaviour was expected. These contrary results can be caused by the fact, that directly before the kinetic measurement the macrogel was equilibrated at RT for 24 hours and for the determination of the swelling curve with a constant heating rate, the gel was used as received from the synthesis. A second reason for the discrepancy could be that for both measurements of the swelling behaviour, gels from different synthesis have been used.

Tanaka and coworkers studied the swelling kinetics of macroscopic gels in detail.<sup>20,124</sup> For example, they showed that the swelling or shrinking of a macroscopic gel with a non-spherical shape is not only based on pure diffusion processes.<sup>124</sup> In the case of a long cylindrical gel (diameter 1.35 mm; length/diameter = 30) they established that a change in diameter is directly related to a change in length. To describe the swelling kinetics, they developed a two-process approach based on the total energy of the gel, which can be divided into a bulk energy term and a shear energy term. A change in the bulk energy describes the swelling of the cylindrical gel to a certain diameter. This volume change is a pure diffusional process. Hence, the shear energy of the system increases and to compensate this energy, the gel tries to relax by an increase in length and a decrease in diameter (volume stays constant). For the swelling studies, they synthesized poly(NIPAM) gels in a micropipette and determined the swelling in radius and length when the gel was plunged into water directly after the synthesis. The fitting procedure of the swelling curves was done by the first three terms of the following equations:

$$u_{diameter}(a, t) = \Delta \sum_n B_n \exp[-t/\tau_n], \quad (4.2)$$

$$u_{length}(z, t) = \Delta \frac{z}{a} \sum_n B_n \exp[-t/\tau_n]. \quad (4.3)$$

Here,  $u(a, t)$  and  $u(z, t)$  is the displacement vector in the direction of the diameter and the length,  $\Delta$  is the total change of the gel radius,  $a$  and  $z$  are the initial radius and

length of the gel and  $\tau$  the relaxation time. Further, Li et al. defined the relaxation time of cylindrical gels as:<sup>124</sup>

$$\tau_n = \frac{a^2}{D_e \alpha_n^2} \quad \text{with } D_e = \frac{2}{3} D_0, \quad (4.4)$$

with  $D_e$  as the apparent collective diffusion constant,  $\alpha_n$  as the eigenvalue and  $D_0$  as the collective diffusion constant. The theory developed by Li and Tanaka predicts that the first eigenvalue  $\alpha_1$  for a cylindrical macrogel is in the range between 0 and 2.74 and that  $B_1$  ranges from 0.573 to a value of 1<sup>124</sup> (for spherical gels:  $\alpha_1$ : 0 -  $\pi$ ,  $B_1$ : 0.608 - 1). Plotting  $\delta u/a$  vs. time, Li et al. obtained for a long cylindrical gel that the relaxation time for a change in length and diameter is nearly the same ( $\tau_{1,diameter} \sim 66$  min;  $\tau_{1,length} \sim 65$  min). In contrast to this, the relaxation time of a short cylinder (length = diameter) is in the range of  $\tau_1 \sim 39$  min, what is nearly the same as for a spherical gel, as the authors mentioned.<sup>124</sup> Moreover, the collective diffusion constant  $D_0$  was determined from the experimental values of  $B_1$  and  $\tau_1$  in combination with a theoretical calculation of  $\tau_1$  depending on the shear modulus  $R$ . Consequently, a value of  $D_0 = 2.9 \cdot 10^{-7}$  cm<sup>2</sup>/s was found, which is comparable to the diffusion constant measured by dynamic light scattering by Tanaka<sup>110</sup> and Peters.<sup>125</sup>

For a quantitative description of the data obtained from the kinetic measurements of the crosslinker gradient macrogel, a first approach was made to fit the decay of the swelling ratio  $\alpha$  with a single exponential function.

$$\alpha = \alpha_0 + b \cdot \exp(-t/\tau) \quad (4.5)$$

As presented in figure 4.12, the single exponential fit leads to a good description of the swelling curves. The obtained values for the relaxation time are  $\tau = 369$  s for the change in length,  $\tau = 517$  s for the width with a medium crosslinker content and  $\tau = 434$  s for the parts of the gel with a low crosslinker concentration.

Additionally, we tried to fit the swelling curves with a sum of three exponential functions, similar to the approach of Li et al. (see equation 4.2 and 4.3). For the fitting procedure we used equation 4.6. Here, we obtained for  $\tau_1$  nearly the same values as for  $\tau$  from the

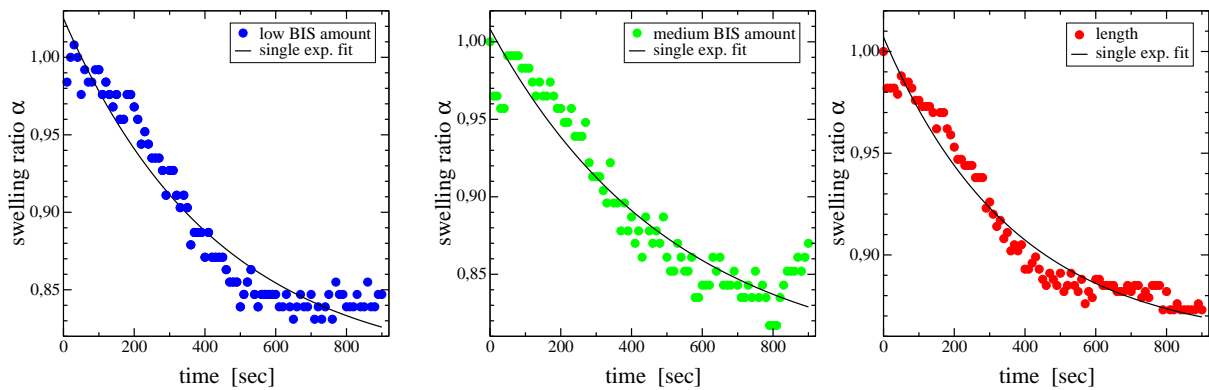


Figure 4.12: Experimental swelling curves from different position of the macrogels fitted with a single exponential function

fitting with a single exponential function (see equation 4.5).

$$\alpha = \alpha_0 + b \cdot \exp(-t/\tau_1) + c \cdot \exp(-t/\tau_2) + d \cdot \exp(-t/\tau_3). \quad (4.6)$$

To determine the diffusion constant from the swelling curves of the different areas of the crosslinker gradient macrogel, we used the value for the shear modulus  $R$  from the publication of Li<sup>124</sup> ( $R = 0.35$ ), determined from this the first eigenvalue  $\alpha_1$  ( $\alpha_1 \sim 2.2$ ) and calculated the collective diffusion constant  $D_0$  according to equation 4.4 (used values are listed in table 4.1). This results in values of  $D_0 \sim 2.92 \cdot 10^{-4} \text{ cm}^2/\text{s}$  for the area of the gels with a medium crosslinker content,  $D_0 \sim 2.02 \cdot 10^{-3} \text{ cm}^2/\text{s}$  for the area of the gels with a low crosslinker content (results also listed in table 4.1). These values deviate strongly from Tanaka's results and therefore further investigations are needed to understand this differences.

Nevertheless, within the basic experiments on preparing a macroscopic gel with a crosslinker gradient, the use of a commercially available peristaltic pump allows the synthesis of stable macrogels. With this technique it was possible to build up a crosslinker gradient from 5 mol% to 20 mol% BIS in the network. But with this preparation method it is also possible to synthesize gels with a higher crosslinking density.

The determination of the swelling ratio  $\alpha$  from the photographs or the video sequence is connected to a certain inaccuracy caused by the use of the graph paper as scaling bar

Table 4.1: Experimental results for the relaxation rate  $\Gamma$  and the collective diffusion constant  $D_0$  of the different zones of the macrogel. Additionally, the values used from the literature for the calculation of  $D_0$  are listed.<sup>124</sup>

gel area	relaxation rate	$a$	$R$	$\alpha_1$	$D_0$
low BIS content	434 s	0.64 cm	0.35	2.2	$2.92 \cdot 10^{-4} \text{ cm}^2/\text{s}$
medium BIS content	517 s	0.58 cm	0.35	2.2	$2.02 \cdot 10^{-4} \text{ cm}^2/\text{s}$
length	367 s	3.34 cm	/	/	/

and due to distortion effects of the water bath. Nevertheless, it was shown within this work that inside the synthesized macrogels, regions with different crosslinker density can be identified. The decrease of the swelling ratio of these gel regions with an increasing temperature reflects the thermosensitive behaviour of BIS crosslinked poly(NIPAM) gels. Depending on the area, where  $\alpha$  has been determined, the macrogel shows different degrees of deswelling. The regions with a high crosslinking density show only a smaller decrease in  $\alpha$ , as expected, while the low crosslinked regions decrease strongly in volume. This phenomenon still remains to be understood.

From previous studies a similar behaviour was found for microgel particles based on poly(NIPAM) crosslinked with BIS.<sup>2</sup> The swelling curves obtained by DLS, for the colloidal particles with a lower crosslinker content show a stronger deswelling behaviour. In contrast to this, the degree of deswelling was much lower if the microgel network is highly crosslinked.





# 5 Internal network dynamics of micro- and macrogels based on poly(NIPAM)

In the previous chapter, the swelling behaviour of macroscopic gels was followed by a change in the overall dimensions of the network structure using an image processing technique. In contrast, this chapter focuses on the internal network dynamics of crosslinked gels. Generally, to obtain a homogeneous distribution of the crosslinker in a gel, the way in which the gel has been formed is very important. In the case of NIPAM based microgels the synthesis is normally done by an emulsion polymerization at temperatures above the VPTT and hence, the crosslinker BIS is consumed faster than the NIPAM monomer.<sup>22</sup> In contrast to this, macrogels mainly show a statistical distribution of the monomer and crosslinker<sup>24</sup> and therefore a higher homogeneity of the network structure.

In this work, micro- and macrogels consisting of NIPAM and butenoic acid (BAc) with BIS as crosslinking agent are used and due to the incorporation of the COOH-groups into the gel network an additional sensitivity to pH can be achieved.<sup>32,33,35,52,126</sup> As already mentioned, due to the different synthesis conditions during preparation of the micro- and macrogels a different local network structure and consequently, differences in the local network motion are expected. To study such local motions on a lengthscale of nanometers, neutron spin-echo (NSE) is a well suited scattering technique.

## 5.1 Characterization of the microgel particles and their VPT

In the left graph of figure 5.1 a typical intensity time autocorrelation function is shown. The PCS experiments reveal the low polydispersity of the microgel synthesized in this study. This is obvious from the narrow relaxation rate distribution  $G(\Gamma)$  as shown in the right graph of figure 5.1.

In the case of only translational diffusion, a plot of the maximum of the relaxation rate

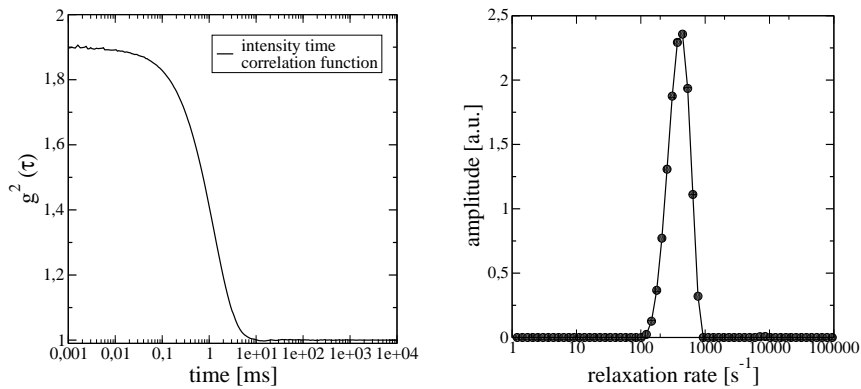


Figure 5.1: Obtained autocorrelation function (left) and relaxation rate distribution (right) of the poly(NIPAM-co-BAc) microgel at  $20^{\circ}\text{C}$ , scattering angle of  $60^{\circ}$  and a pH value of 5.5

$\Gamma$  vs.  $q^2$  results in a linear dependence according to eq. 2.9. The microgel poly(NIPAM-co-BAc) at a pH of 2 and also 5.5 perfectly follows the prediction of eq. 2.9. Therefore it is straightforward to calculate the translational diffusion coefficient  $D^T$  and the hydrodynamic radius  $R_h$  can be subsequently computed using the Stokes-Einstein equation. The results are shown in table 5.1.

In Fig. 5.2 the hydrodynamic radius of the microgel poly(NIPAM-co-BAc) at a pH of 5.5 and 2.0 as a function of temperature is shown. The VPTT of poly(NIPAM-co-BAc) at pH of 5.5 is taken as the point of inflection of the swelling curve (dashed line). The swelling curve of the microgel at a pH value of 2.0 could not be fully measured, since the colloidal particles aggregate at the beginning of the volume phase transition (see figure 5.2 blue

Table 5.1: Summary of the PCS results for the poly(NIPAM-co-BAC) microgels at two different pH values

sample name	pH	$D^T$	$R_h(20^\circ\text{C})$	VPTT
poly(NIPAM-co-BAC)	5.5	$1.59 \cdot 10^{-12} \text{ m}^2/\text{s}$	134 nm	$\sim 40^\circ\text{C}$
poly(NIPAM-co-BAC)	2.0	$2.12 \cdot 10^{-12} \text{ m}^2/\text{s}$	101 nm	/

dots). However, the part of the curve which was accessible at pH 2.0 is in good approximation identical with the swelling curve of the respective poly(NIPAM) homopolymer particle (VPTT at  $32^\circ\text{C}$ ). The squares in figure 5.2 represent the inverse of the swelling ratio  $\alpha$ , which was calculated as mentioned in earlier studies<sup>2,127</sup> by using equation 2.12.

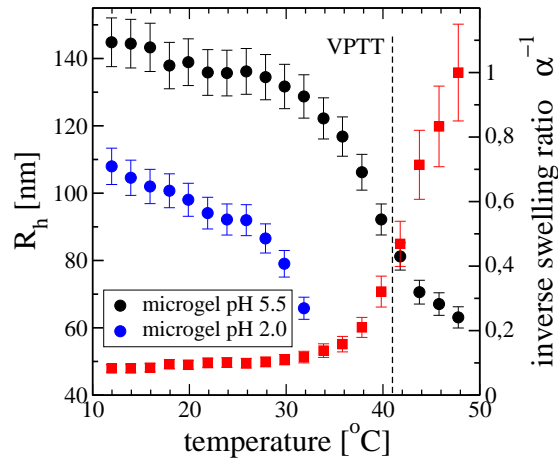


Figure 5.2: Swelling curve of the poly(NIPAM-co-BAC) microgel at pH 5.5 and 2.0; in addition also the inverse swelling ratio  $\alpha^{-1}$  at pH 5.5 is given

## 5.2 A comparative NSE study

The focus of the NSE experiment presented here, is on the internal dynamics of chemically similar micro- and macrogels. In this context, the ensemble averaged intermediate scattering functions  $\langle S(q, t) \rangle_E$  for a copolymer micro- and macrogel at two different pH values at several different  $q$ -values is measured. It should be noted, that all measurements were

done at a temperature of  $293.1 \pm 0.1$  K. Hence, the NIPAM based gels are in the swollen state. The obtained scattering functions are shown in fig. 5.3.

It is obvious that at low  $q$ -values ( $q = 0.05 - 0.11 \text{ \AA}^{-1}$ ) the measurable Fourier time

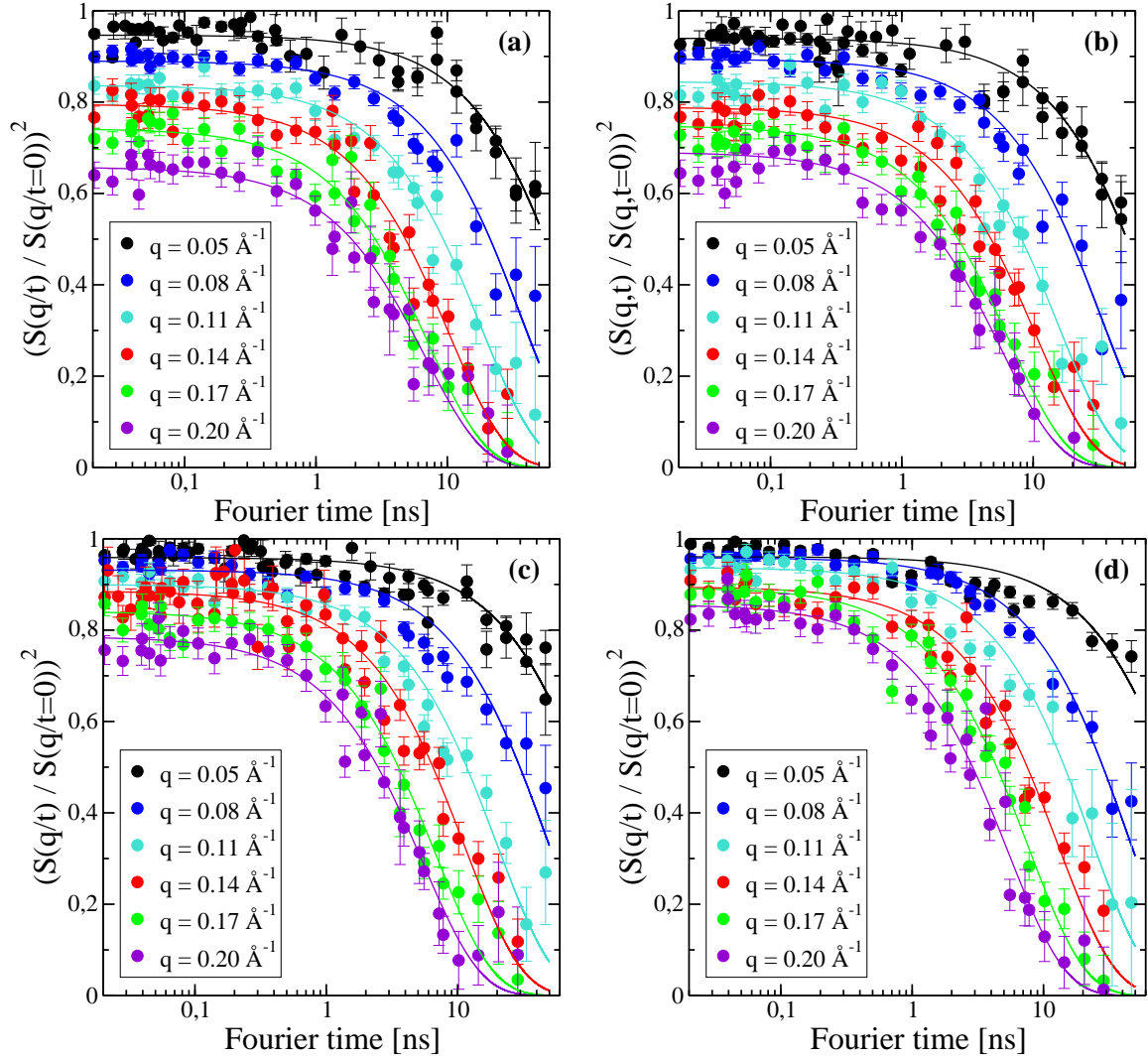


Figure 5.3: Normalised NSE intermediate scattering functions  $S(q,t)/S(q,t=0)$  at different  $q$ -values, obtained for the poly(NIPAM-co-BAc) microgel (a)(b) at pH 5.5 and 2.0 and for the macrogel (c)(d) at the same pH values.

at IN11 is too small to obtain the complete decay of  $\langle S(q,t) \rangle_E$ . But at  $q$ -values larger than  $0.14 \text{ \AA}^{-1}$  the scattering functions decay to zero. This is similar compared to our previous experiments,<sup>31</sup> but was different in a study by Koizumi et al.<sup>128</sup> This issue will

be discussed later.

The simplest way to analyse the  $S(q, t)$  is, to assume that the gels behave ergodically. In this case, the  $S(q, t)$  should not show a  $q$ -dependent baseline<sup>29,110</sup> and the decay of the scattering function could be easily fitted by a single exponential function (see equation 2.29). It was already shown by our group<sup>31</sup> that the internal motion of microgels can be resolved by NSE and that on the very short length scale probed in this experiment the fluctuations seem to decay totally, at least within the experimental precession. Hence, also in the present case it is straightforward to fit the data for the poly(NIPAM-co-BAC) microgels at pH 5.5 and pH 2.0 with a single exponential function. The results are shown in figure 5.3.

However, in a combined NSE/SANS experiment of Koizumi et al. a different behaviour of a macroscopic poly(NIPAM) gel is reported.<sup>128</sup> Using a poly(NIPAM) gel (crosslinked with about 0.26 mol%) and two different NSE setups (IN15 in Grenoble, France, and FRM2 in Jülich, Germany) they achieved to measure  $S(q, t)/S(q, t = 0)$  in a Fourier time window up to 190 ns and in a  $q$ -range from  $0.035 \text{ \AA}^{-1}$  to  $0.16 \text{ \AA}^{-1}$  (see figure 5.4).

Koizumi and coworkers found out, that the decay of the NSE scattering function at

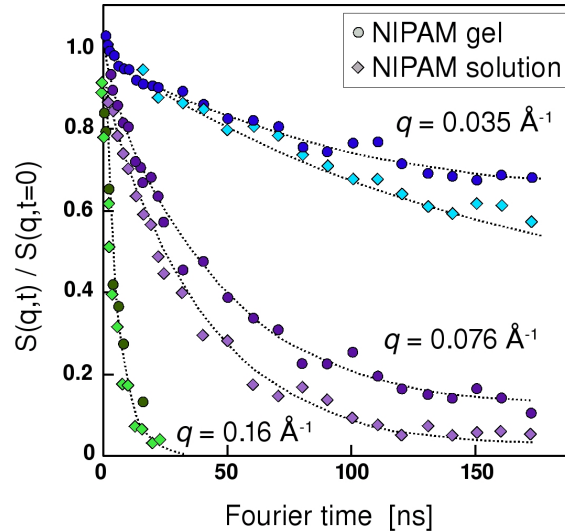


Figure 5.4: NSE decay curves  $S(q, t)/S(q, t = 0)$  at  $q=0.035, 0.076$  and  $0.16 \text{ \AA}^{-1}$ , obtained for the swollen poly(NIPAM) gel and solution at  $28^\circ\text{C}$  (redrawn based on the publication of Koizumi<sup>128</sup>).

lower  $q$  ( $< 0.05 \text{ \AA}^{-1}$ ) could be described by a  $q^2$ -dependency, corresponding to a collective diffusion. Whereas for higher  $q$ -values ( $> 0.05 \text{ \AA}^{-1}$ ) the curve decays according  $\sim q^3$ , corresponding to a Zimm type internal chain motion. Due to the low amount of crosslinker used by Koizumi et al. the chains move like free polymer chains in a good solvent. Therefore, the normalized intermediate scattering function is given by

$$S(q, t)/S(q, t = 0) \sim \exp[-(\Gamma t)^\beta] \quad (5.1)$$

with the exponent  $\beta$  is  $2/3$  for Zimm single chain motion and  $1$  for collective diffusion.<sup>128</sup> Here, the use of an exponential function without a  $q$ -dependent baseline is comparable to our results and indicates a pseudo-ergodic behaviour of the gels on the length scale of the NSE experiment. However, in contrast to the work of Koizumi we obtained in equation 5.1a a value of  $1$  for  $\beta$  and the relaxation rates follow a  $\sim q^2$  for a diffusional mode. A reason for this contrary behaviour could be the crosslinking density in the gels. We used a crosslinker content of  $5 \text{ mol\%}$ , which results in a rather rigid gel network. Using only  $0.26 \text{ mol\%}$ , as Koizumi did, a relatively soft and fluid like gel is obtained. Obviously, using such a low crosslinking density in the poly(NIPAM) gel, the polymer chains between the junction points behave like chains in solution would do.

Due to the fact, that the NSE scattering curves of our poly(NIPAM-co-BAC) macrogel are phenomenologically very similar to those of the corresponding microgel, we also tried to fit these  $S(q, t)$  with a single exponential function. This led to a good description of the measured  $S(q, t)$  (results are shown in figure 5.3). Apparently, also the macroscopic gel shows the pseudo-ergodic behaviour on the length scale of the NSE experiment, despite of the fact that in DLS experiments on these systems the non-ergodicity has a strong impact.<sup>29</sup> Hence, at least in our experiment also for the macrogel  $q \cdot \xi \gg 1$  holds.

A contrary behaviour for poly(fluorosilicone) (PFS) gels was obtained by Hecht and Geissler.<sup>129</sup> They compared the decay of the intermediate scattering function of a uncrosslinked PFS solution and the corresponding crosslinked gel. It has to be mentioned here, that from the details of the gel preparation it was not possible to determine the crosslinking density.<sup>130</sup> For the polymer solution they found out, that the NSE curves relax to zero, while for the gel the intermediate scattering functions decay to a constant

value that increases with decreasing  $q$ . In this case, the baseline dependent decay was described by

$$A(t = 0) = A_s(q) + A_f(q) \cdot \exp(-\Gamma t) \quad (5.2)$$

with  $A(0) = 1$ ,  $A_s(q)$  is the constant baseline and  $A_f(q)$  is the relative amplitude of the fluctuating component.<sup>129</sup> From the relaxation rate  $\Gamma$  they determined the diffusion

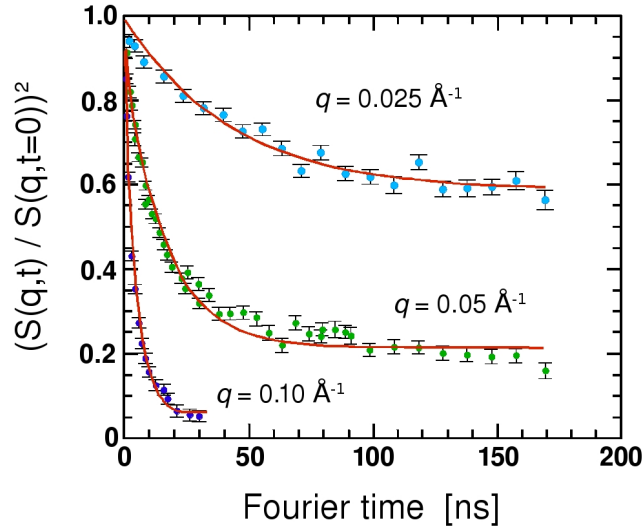


Figure 5.5: Neutron spin-echo decay from a poly(fluorosilicone) gel swollen in acetone for the different wavevectors (redrawn based on the publication of Hecht<sup>129</sup>).

coefficient  $D_G$  of the crosslinked PFS gel according to  $\Gamma = D_G q^2$  and obtained a value of  $(2.5 \pm 0.4) \cdot 10^{-10} \text{ m}^2/\text{s}$ . Further dynamic light scattering experiments of the PFS gel were done. The analysis of the intensity correlation functions using a heterodyne model<sup>131</sup> results in similar values of  $D_G$  as obtained in the NSE measurement. This is why we also tried to fit the data of the present study using equation 5.2. However, this does not lead to a satisfying description of the poly(NIPAM-co-BAC) NSE curves. Beside this, the value of  $D_G$  obtained from Geissler et al. is an order of magnitude higher than our values for  $D_G$  of the micro- and macrogel (see results in the later discussion). A calculation of the correlation length  $\xi$  with the data from Geissler results in  $\xi = 2.8 \text{ nm}$ . With regard to the fact, that our macroscopic poly(NIPAM-co-BAC) gels show pseudo-ergodic behaviour on the length scale of the NSE experiment, it is possible for larger  $q$ -values ( $q = 0.05 - 0.5$

$\text{\AA}^{-1}$ ) to resolve faster dynamic processes, such as chain segment movements between the crosslinkers. Figure 5.6 summarises all NSE relaxation rates for the poly(NIPAM-co-BAC) microgel at pH 5.5 and 2.0 and for the corresponding macrogel at the same two pH values. The  $\Gamma$  values are plotted as a function of  $q^2$ . According to equation 2.29 for a diffusional mode a linear dependence is expected.

Looking at figure 5.6, first of all it is obvious that the frequencies for the microgels

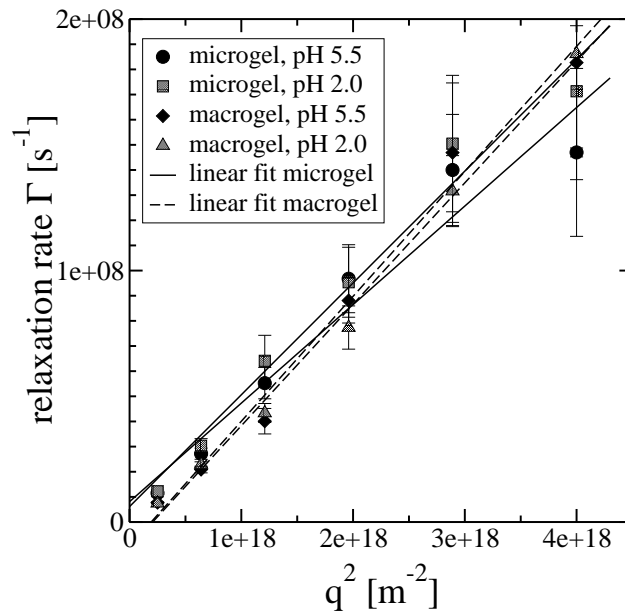


Figure 5.6: Plot of the relaxation rates  $\Gamma$  vs.  $q^2$  for the micro- and macrogel at two different pH values

and the homologous macrogel do not differ very much. This was surprising because we expected larger differences related to the higher inhomogeneity of the microgel network. Nevertheless, the differences are of the order of 10%, only. Within the experimental precision the data for all experiments follow the prediction and the linear fits go through zero taking the error into account.

From the slope, the network diffusion coefficients  $D_G$  were calculated. The values are given in table 5.2. All values are of the same order of magnitude. The values for the poly(NIPAM-co-BAC) macrogel are about 10-20% higher compared to the microgel. All the computed diffusion coefficients are similar compared to previously published data for poly(NIPAM) based micro-<sup>31</sup> and macrogels. For the microgel with a crosslinker



density of 5 mol% investigated by Kratz et al. a value for the diffusion coefficient  $D_G$  of  $3.16 \cdot 10^{-11} m^2/s$  was found.

Another point, which should be noted is the fact that a change in pH seems to have a significant influence on the microgel, whereas for the macrogel within the experimental precision no change in  $D_G$  can be evidenced. This is due to the much stronger mechanical constraints in the macrogel, which prevent the macrogel from shrinking upon the decrease in pH from 5.5 to 2.0.

$D_G$  represents the dynamics of the collective diffusion of the network in the micro- as

Table 5.2: Summary of the NSE results for the poly(NIPAM-co-BAC) macro- and micro-gels

sample name	pH	$D_G$	$\xi_{coll}$
poly(NIPAM-co-BAC) microgel	5.5	$3.92 \cdot 10^{-11} m^2/s$	4.4 nm
poly(NIPAM-co-BAC) microgel	2.0	$4.45 \cdot 10^{-11} m^2/s$	3.9 nm
poly(NIPAM-co-BAC) macrogel	5.5	$4.97 \cdot 10^{-11} m^2/s$	3.5 nm
poly(NIPAM-co-BAC) macrogel	2.0	$4.83 \cdot 10^{-11} m^2/s$	3.6 nm

well as in the respective homologous macrogel. The dynamic correlation length  $\xi$  of this network motion can be estimated from  $D_G$  by.<sup>102</sup>

$$\xi = \frac{kT}{6\pi\eta D_G} \quad (5.3)$$

where  $k$  is the Boltzmann constant,  $T$  the temperature (here  $293.2 \pm 0.1 K$ ) and  $\eta$  the viscosity of the solvent ( $D_2O$  ( $20^\circ C$ ) = 1.25 mPa·s). The obtained values for  $\xi$  are summarized in table 5.2. Similar results were obtained by Shibayama<sup>120</sup> using DLS experiments on macrogels. In this case the crosslinker density was about 1.2 mol% and acrylic acid was used as a comonomer. This might allow to compare these data to our systems containing butenoic acid. In a light scattering experiment the non-ergodicity of gels has to be taken into account. This is why the theory of Pusey and van Megen<sup>29</sup> was used by Shibayama to analyse the DLS data. The value of the apparent diffusion coefficient  $D_A$  obtained in this way is about  $2.7 \cdot 10^{-11} m^2/s$ , which is in the same range

as the  $D_G$  of our micro- and macrogels. Therefore, it could be shown that the results from DLS experiments of gels (non-ergodic behaviour) are in good agreement with the results of NSE measurements, where gels behave pseudo-ergodically on the length scale probed by the neutrons.

# 6 NIPAM-co-NtBAM Copolymer

## Microgels

It is well known, that thermosensitive microgels based on poly(NIPAM) undergo a reversible volume phase transition at a temperature of  $\sim 32^\circ\text{C}$ . By the copolymerization of NIPAM with other monomers, it is possible to influence this phase transition and an additional sensitivity to pH or ionic strength can be created. Many researchers reported the preparations of NIPAM based copolymer microgels containing comonomers with charged groups, like acrylic acid<sup>26,32-34</sup> or methacrylic acid.<sup>35,36</sup> Using such hydrophilic monomers, the phase transition temperature is shifted to higher values. In contrast to this, with the addition of hydrophobic comonomers to poly(NIPAM), the transition temperature can be decreased.<sup>132</sup>

In the following chapter the volume phase transition of poly(NIPAM-co-*N-tert*-butylacrylamide) copolymer microgels as a function of the comonomer content is studied in detail applying different scattering techniques (light and neutron scattering). It is expected, that due to the copolymerization of NIPAM with the more hydrophobic monomer NtBAM the transition temperature can be shifted to lower values. Further, the swelling curves obtained on the basis of DLS measurements are analyzed using the theoretical model of Flory and Rehner.

### 6.1 Overall size and shape of the microgel particles

The microgel particles presented here consist of NIPAM with different contents of the comonomer, *N-tert*-butylacrylamide (NtBAM), to create microgels with a VPTT differing

from that of pure NIPAM. To get information about the size and the polydispersity of the obtained particles, DLS was used. First, the intensity autocorrelation functions for all copolymer microgels were recorded as a function of  $q$  and subsequently analyzed with CONTIN.<sup>84,85</sup>

In Fig. 6.2, typical relaxation rate distributions for the microgels at a scattering angle

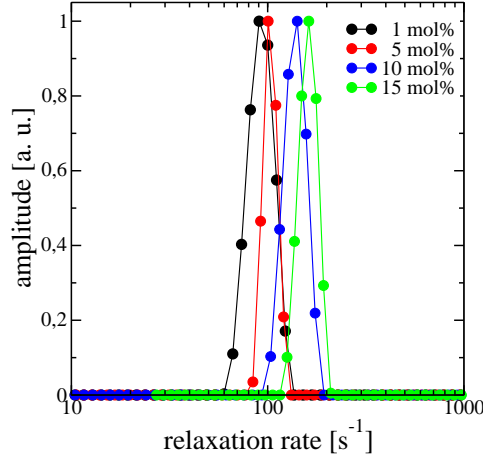


Figure 6.1: Distribution of the relaxation rates as computed by a CONTIN analysis for the different poly(NIPAM-co-NtBAM) microgels

of  $45^\circ$  are given; these show a narrow distribution corresponding to a low polydispersity of the particles. The maximum of  $G(\Gamma)$  shifts towards higher values of  $\Gamma$  with increasing content of the comonomer NtBAM. According to Eq. 2.9, a plot of  $\Gamma$  vs.  $q^2$  should result in a linear dependence (see Fig. 6.2) if the particles show only translational diffusion. The data for all prepared samples perfectly fulfill Eq. 2.9, and all linear fits go through the origin within the experimental precision. Hence, no non-diffusive modes contribute to the decay of the intermediate scattering functions.

The hydrodynamic radii of the copolymer microgel particles were calculated from the translational diffusion coefficient  $D^T$  according to the Stokes-Einstein equation (Eq. 2.11). A summary of the obtained radii is given in Table 6.1. From these data, it is clear that under the same experimental conditions during the synthesis the particle size decrease with increasing amount of NtBAM in the copolymer microgel. The same trend was observed by Bae and Lyon.<sup>51,52</sup> However, the microgel particles synthesized here by performing

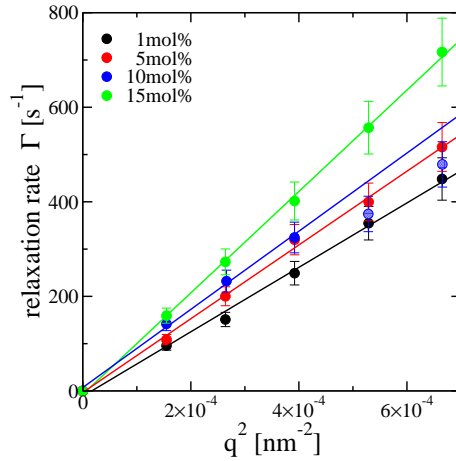


Figure 6.2: Relaxation rates of poly(NIPAM-co-NtBAM) microgels with different comonomer content as a function of  $q^2$  (the dotted point were not included in the linear regression because of aggregation of the particles) The slope of the linear fits is used to calculate  $D^T$ .

a surfactant-free emulsion polymerization are generally bigger than those studied in the previous works.<sup>51,52</sup> As already mentioned, the microgels prepared in the present work exhibit hydrodynamic radii at room temperature in the range from 315 nm for sample CM-9901 to 200 nm for sample CM-8515. For a direct comparison, the DLS measurements of the poly(NIPAM-co-NtBAM) copolymer with approximately 10 mol% NtBAM from Bea et al. can be used. They plotted the particle diameter distribution of the copolymer at four different temperatures to give an overview of the polydispersity and the particle dimensions. At a temperature of 29.9°C, the graph shows a sharp peak at a diameter of 113 nm, which is significantly smaller than the microgels prepared in this work, which exhibit a hydrodynamic diameter of about 287 nm (see Fig. 6.5, triangle curve at 29.9°C). Hence, it is straightforward to conclude that the particle size is strongly influenced by the interfacial tension during the synthesis.

The samples were also investigated by SEM and TEM at room temperature. These imaging techniques provide additional information about the homogeneity of the microgel particles in the totally collapsed state. In Fig. 6.3, some characteristic SEM and TEM images for the four copolymer microgels are shown. The micrographs from all samples

Table 6.1: Composition of the synthesized copolymer microgels and summary of the DLS results

sample name	NIPAM (100-x)	NtBAM (x)	$R_h$ (nm)	VPTT [°C]
CM-9901	99 mol%	1 mol%	315	32
CM-9505	95 mol%	5 mol%	274	30
CM-9010	90 mol%	10 mol%	235	26
CM-8515	85 mol%	15 mol%	200	24

show apparently spherical particles with a narrow size distribution.

The previously mentioned microscopy methods show the microgel particles in the dried

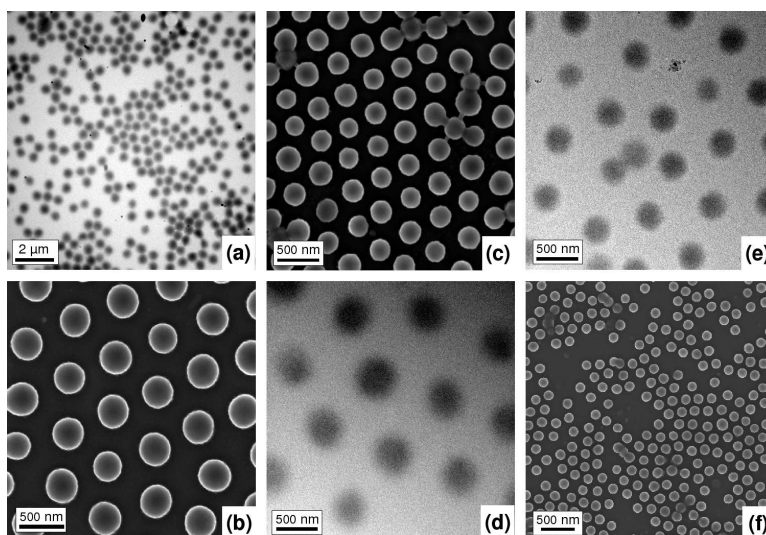


Figure 6.3: TEM and SEM pictures of PNIPAM with different comonomer content. (a) and (b): 1 mol%; (c): 5 mol%; (d): 10 mol%; (e) and (f): 15 mol%.

and hence, almost the fully collapsed state. Cryo-TEM can be employed to image the particles in the swollen state. A typical cryo-TEM image of sample CM-9010 is shown in Fig. 6.4. Using an image processing and analysis software (Image J, V.1.42), it is possible to determine the size distributions of the different copolymer microgel particles in the swollen state. Hence, the resulting particle radius can be directly compared with the

hydrodynamic radius of the DLS measurements. The experimentally obtained particle size distribution can be fitted using a Gaussian radius distribution function leading to a diameter of 240 nm. This is in very good agreement with the DLS results for the respective sample (237 nm).

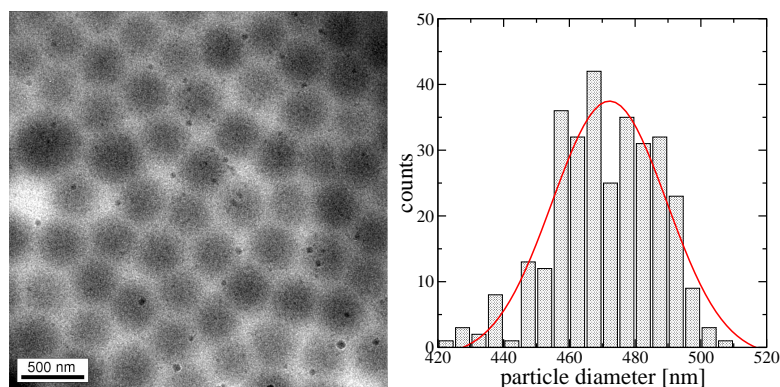


Figure 6.4: Cryo-TEM image of poly(NIPAM-co-NtBAM) with 10 mol% comonomer and corresponding particle size distribution (sample CM-9010).

## 6.2 Swelling behaviour

The extent of the temperature-induced particle swelling was characterized by DLS. Using this technique, the hydrodynamic radius,  $R_h$ , of the copolymer microgel particles was determined within a temperature range from  $T = 10^\circ\text{C}$  to  $44^\circ\text{C}$  and plotted against the temperature. To compare the swelling capacity for the different copolymer microgels, the swelling ratio  $\alpha$  according to Eq. 2.12 has also been calculated.

Figure 6.5 (a) shows the differences of the swelling behaviour for the poly(NIPAM-co-NtBAM) microgels dispersed in water. It is well documented in the literature<sup>7</sup> that pure poly(NIPAM) microgels exhibit a VPTT at  $32^\circ\text{C}$ . To exclude an influence of the crosslinker density on the volume phase transition,<sup>2,133</sup> the concentration of BIS was constant in all feed solutions (5 mol% respective to total monomer concentration).

The copolymer microgel CM-9901 shows nearly the same transition temperature as poly(NIPAM) homopolymer microgels, but already a comonomer amount of 5 mol% shifts the VPTT to lower temperatures, in this case to 30°C. A much higher effect is achieved using NtBAM contents of 10 mol% (VPTT  $\sim$  26°C) and 15 mol% (VPTT  $\sim$  24°C). This effect is most likely caused by the higher hydrophobicity of NtBAM compared to NIPAM. At the phase transition temperature, pure PNIPAM microgels change abruptly from being hydrophilic to a more hydrophobic state. This is due to the presence of the hydrophilic amide groups and the hydrophobic isopropyl group on the side chain. With the introduction of higher amounts of NtBAM, the hydrophobicity of the polymer network increases. Such a decrease in VPTT upon incorporation of hydrophobic comonomers was already observed previously for *tert*-butylacrylate.<sup>132</sup>

Furthermore, the swelling curves as well as the swelling ratios in Fig. 6.5(b) suggest that the size of the microgel particles does not strongly influence the swelling behaviour. The decrease of the swelling ratio  $\alpha$  from a value of 0.8 to values significantly below 0.1 in Fig. 6.5(b) reveals the high swelling capacity of these microgels. If the microgels are not in the totally collapsed state at temperatures above the volume phase transition temperature, the swelling ratio would not exhibit such a drastic decrease.

In the study of Bea et al., it is mentioned that from a NtBAM-content of 60 wt%, the volume phase transition does not occur. In connection with this, they determined the phase behaviour of several poly(NIPAM-co-NtBAM) particles in a temperature range between 0°C and 40°C. For the copolymer with approximately 10 mol% NtBAM, they measured a transition temperature around 32°C; in contrast to this, we determined the VPTT for a sample with 10 mol% NtBAM (CM-9010) to be 26°C. A reason for this discrepancy could be the definition of the transition temperature. In the literature, often the inflexion point of the swelling curve (second derivative = 0) is described as the VPTT and is at 32°C.<sup>36</sup> Bea et al. probably defined the transition temperature for pure poly(NIPAM) at the  $\Theta$ -temperature at 35°C. The  $\Theta$ -temperature is the temperature at which hydrodynamic radius approaches to its minimum.

To compare our results with that of Lyon and co-workers, we have to take into account



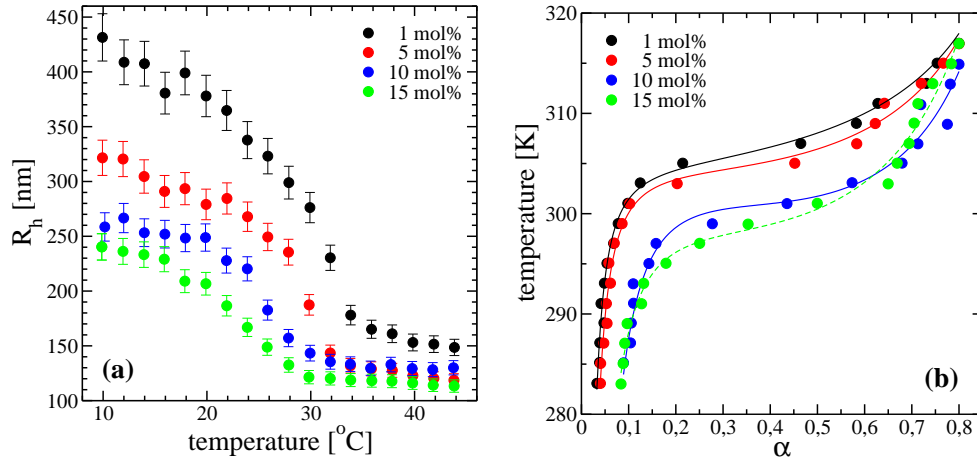


Figure 6.5: Swelling curves (a) and swelling ratio  $\alpha$  (b) with corresponding Flory-Rehner fits of the copolymer microgels with NtBAM content of 1 mol% (square), 5 mol% (diamond), 10 mol% (triangle) and 15 mol% (circle).

that they synthesized poly(NIPAM-co-NtBAM) microgels with 5 mol% acrylic acid. The swelling curves of their NIPAm/TBAm/AAC copolymers at pH 3.5 are partly comparable to our obtained data, which is shown in Fig. 6.5(a). Basically, the overall profiles of the swelling curves and the VPTT are similar, but it is noticeable that the volume phase transition obtained in the present contribution is broader than mentioned in literature. For a more detailed consideration of the swelling behaviour of the copolymer microgels, the swelling ratio  $\alpha$ , determined by Eq. 2.12, can be fitted in terms of the Flory-Rehner theory (FRT).<sup>88</sup> A comparison of the different fitting parameters allows to test the suitability of the FRT for uncharged copolymer microgels. In addition, we want to point out that there is a modified FRT used by Wu et al.,<sup>134,135</sup> which was originally developed by Prausnitz et al.<sup>136</sup> to describe the swelling behaviour for heterogeneous PNIPAM or PAM gels in water. The modification was done by taking into account that in the feed solution of the synthesis, two different monomer concentrations (cross-linker/monomer and total monomer/water) influence the segments length between the junction points of the network. This number of segments is directly incorporated in the elastic contribution to the chemical potential. Due to the effect that in our systems three different polymerizable units are present and that the cross-linker/total monomer ratio as well as the

concentration of monomer in water in the feed solution was constant for all four copolymer microgels, we decided to analyse the swelling behaviour by the simple FRT.

Eq. 2.19 was used to model the temperature/ $\alpha$ -diagrams, and the obtained fits are presented in Fig. 6.5(b). The resulting fitting parameters are summarized in the table 6.2. The  $\alpha$ -values for each temperature/ $\alpha$ -diagram have been multiplied by 0.8 to take into account, that the totally collapsed microgel particles still contain about 20 wt% water. This value is incorporated in Eq. 2.19 by  $\phi_0$  and is kept constant for all systems. A similar approach was already used by Crassous et al.<sup>90</sup>

In the case of the sample CM-8515, the observed  $\alpha$ -values could not be fitted satisfy-

Table 6.2: Results of the Flory-Rehner analysis of the swelling curves

sample name	NtBAM	$\phi_0$	$N_{gel}$	$\chi_2$	A	$\Theta$ [K]	VPTT [K]
CM-9901	1mol%	0.8	220	0.205	-14.104	305	305
CM-9505	5mol%	0.8	209	0.423	-10.718	306	303
CM-9010	10mol%	0.8	80	0.745	-7.009	307	299
CM-8515	15mol%	0.8	/	/	/	/	297

ingly using the FRT. For the other curves, the agreement was much better. Hence, in the following, the data set of the copolymer microgel with 15 mol% NtBAM is not included in the analysis. This already indicates that the validity of Eq. 2.19 for a description of copolymer particles is limited to lower comonomer content. The additional mixing contribution to the free energy is neglected. Therefore the treatment most likely fails for the highest NtBAM content. However, for the lower comonomer contents, the rather simple FRT still seems to work reasonably well.

The first variable fit parameter discussed here is  $N_{gel}$ , which is the average degree of polymerization of the polymer chain between the crosslinks. A high  $N_{gel}$  value stands for a weakly cross-linked polymer network, while low values reveal a high cross-linker density. Since the total amount of monomer (NIPAM and NtBAM together) in relation to the cross-linker amount was constant for all synthesized microgels, it is expected that the value for  $N_{gel}$  is nearly constant for the copolymers. These considerations nicely agree

with the values of the copolymers with 1 mol% and 5 mol% NtBAM ( $N_{gel} = 220$  and 200), but for CM-9010  $N_{gel}$  differs significantly ( $N_{gel} = 80$ ). A possible reason could be the actual amount of incorporated comonomer in the microgel. Assuming that the originally used content of NtBAM is not totally copolymerized in the microgel, the monomer/BIS ratio changes much more with increasing comonomer content. Consequently, the value for  $N_{gel}$  changes, namely to low values with increasing content of NtBAM.

As mentioned in literature, a change in the cross-linker density can result either in a slight increase<sup>2,133</sup> or in a not noticeable effect on the VPTT.<sup>25,137</sup> However, a visible shift of the VPTT to higher temperatures in the swelling curves (see Fig. 6.5(a)) resulting from a change in the cross-linker density can not be reached here, because at high NtBAM amounts the influence of the comonomer on the transition temperature dominates. Another explanation is of course the beginning break down of the validity of the FRT due to already too high comonomer content.

Additionally, we tried to fit the temperature-dependent swelling ratios with a constant value for  $N_{gel}$  in the FRT. This leads only to a good description of  $\alpha$  for the copolymer microgels with 1 mol% and 5 mol% NtBAM and is a further indication for a change in the monomer/BIS ratio.

A central fit parameter in Eq. 2.19 is the temperature dependent part of the interaction parameter  $\chi_2$ ,<sup>138</sup> which is connected with the volume fraction of the polymer  $\phi$  in Eq. 2.17. As shown in Table 6.2 the value for  $\chi_2$  changes from 0.2 to 0.7 with increasing content of NtBAM in the copolymer microgel. This trend in  $\chi_2$  can be explained by an increase of the interactions between the polymer and the solvent. By incorporation of the comonomer NtBAM, the whole microgel becomes more and more hydrophobic, and hence, the interaction between the polymer network and the surrounding solvent becomes increasingly unfavourable.

Another parameter which should be discussed is  $\Theta$ .  $\Theta$  is the spinodal temperature of the microgel particles, and the collapse is complete at this temperature. For pure poly(NIPAM) microgels, the  $\Theta$ -temperature with a value of 35°C<sup>51</sup> is about three degree higher than the VPTT<sup>36</sup> defined via the point of inflection of the swelling curve. The

values observed for  $\Theta$  for the copolymer microgels CM-9901, CM-9505 and CM-9010 differ strongly with increasing content of NtBAM (see Table 6.2) and the values obtained from the FRT fit increase with growing content of the comonomer. This is the opposite behaviour of the VPTT which is found to decrease in all samples. At present, no explanation for this observation can be given, but it might also be an artifact caused by the limits of the FRT.

### 6.3 Internal structure of the NIPAM-co-NtBAM copolymer microgels

SANS measurements are a good way to study the changes in the internal structure in poly(NIPAM) microgels across the volume phase transition. The obtained spectra of the four different poly(NIPAM-co-NtBAM) copolymers below and above the VPTT are presented in fig. 6.6. Similar scattering curves for slightly different microgels were already observed before.<sup>16, 25, 127</sup>

The scattering profiles of the poly(NIPAM-co-NtBAM) microgels in the swollen state (at 15.0°C) were fitted with eq. 2.26. The solid lines in fig. 6.6 show the best fits. A satisfying representation of the experimental SANS data is obtained. From these fits the correlation length  $\xi$  of the copolymer microgel network can be directly calculated, which is considered to be related to the blob size<sup>102</sup> and describes the ensemble average correlation of the polymer network. The obtained values for  $\xi$  are summarized in tab. 6.3 and are between 2.6 nm and 3.7 nm for the swollen poly(NIPAM-co-NtBAM) microgels. A dependence of the network correlation length on the increasing comonomer content of the poly(NIPAM-co-NtBAM) microgels could not be observed. Similar values for the correlation length were found for pure PNIPAM microgel particles with varying cross-linker content (1.47 to 7.33% BIS).<sup>25</sup> At a temperature of 15.9 °C values of 2.3 to 3.6 nm for  $\xi$  were obtained for the homopolymer microgels. The correlation lengths obtained for PNIPAM macrogels by Shibayama et al.<sup>7</sup> are in the same range as our data for the copolymer microgels. The SANS experiments at a temperature of 23 °C showed  $\xi$  values

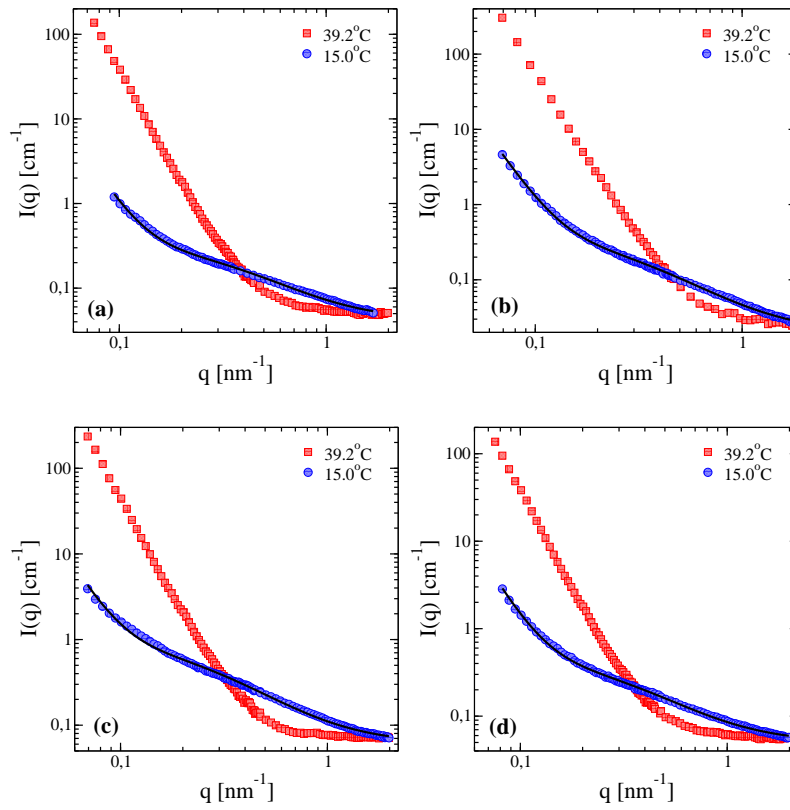


Figure 6.6: SANS profiles of the poly(NIPAM-co-NtBAM) microgels with different comonomer content at 15.0°C and 39.2°C; (a) CM-9901, (b) CM-9505, (c) CM-9010, (d) CM-8515.

for the macrogel form 0.78 to about 4 nm.

As shown in fig. 6.6 the scattering behaviour of the copolymer microgels above the

Table 6.3: Network correlation length  $\xi$  of the four investigated copolymer microgels at a temperature of 15°C

sample name	comonomer content	$I(q)$ [ $cm^{-1}$ ]	$\xi$ [nm]
CM-9901	1 mol%	0.2	2.6
CM-9505	5 mol%	0.3	3.1
CM-9010	10 mol%	0.7	3.7
CM-8515	15 mol%	0.2	2.6

VPTT (squares) differs strongly from that at lower temperatures (circles). As mentioned before, the particles are totally collapsed at these temperatures, and the intermediate  $q$ -region can normally be described by eq. 2.27. The scattering profile of poly(NIPAM-co-NtBAM) with 5 mol% comonomer at a temperature of 39.2°C and the corresponding fit with  $I(q) \propto q^{-4}$  are shown in fig. 6.7 (fit: blue curve). Looking at the graphs, it becomes clear that the decrease of the scattering intensity  $I(q)$  could not be successfully described by a simple  $q^{-4}$  decay. Here, we observed a  $q$ -dependence that differs slightly from the ideal Porod behaviour. A linear fit of  $\log I(q)$  vs.  $\log q$  with SASfit<sup>139</sup> results in  $\alpha < -4.4$  for the scattering intensity  $I(q) \propto q^\alpha$  (see fig. 6.7, triangle curve).

This is in agreement with previous results for pure poly(NIPAM) microgels with different

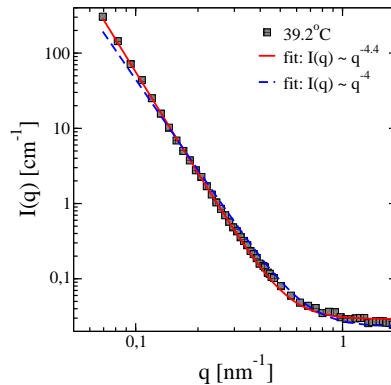


Figure 6.7: SANS profile of poly(NIPAM-co-NtBAM) with 5 mol% comonomer and the obtained fits by a ideal and a modified Porod behaviour.

cross-linker densities<sup>25</sup> and also similar to findings by Barbero et al.<sup>88</sup> The deviation from the  $q^{-4}$  dependence in the Porod region results from a certain surface roughness of the microgel particles and the more complex theoretical model by Wong<sup>105</sup> can be applied to fit the SANS data. In this model, Wong assumes that a two-component inhomogeneous system (here in this context the microgel particles in the totally collapsed state as the one component and the solvent water as the second) consists of areas with rough walls instead of smooth. For this three-dimensional system, the scattering intensity in the Porod region is modified by an additional term (see eq. 6.1), including  $x$  as the parameter

which characterizes the roughness.

$$I(q) \propto \frac{a}{q^{3+x}} + \frac{b}{q^4}. \quad (6.1)$$

If the roughness of the scattering interface is unimportant up to the length scale of  $1/q$  the first term of eq. 6.1 can be omitted and  $I(q) \propto q^{-4}$ .<sup>105</sup>

Hence, also in the following, the SANS profiles of the poly(NIPAM-co-NtBAM) microgels at temperatures above the VPTT were fitted using eq. 6.1. From these fits, we obtained a value for  $x$  which is 1.4 for all SANS profiles.

The surface roughness of the particles is independent from the comonomer content in the microgels. One possible reason for a more or less rough interface between the totally collapsed microgel particles and the surrounding solvent might be flexible terminal polymer chains at the particle surface. These chains additionally stabilize the colloidal microgel solutions under good solvent conditions.





# 7 Microgels and magnetic particles

Screening the literature, several works treating the incorporation of iron oxide based magnetic nanoparticles can be found.<sup>46,140–142</sup> However, less is known about cobalt or nickel containing smart microgels. In order to obtain core-shell hybrid microgels, different approaches have been employed in the present work. At first cobalt nanoparticles have been coated with silica (see section 7.1) and then modified to build up the microgel shell. Furthermore Ni nanoparticles have been synthesized and coated with silica or polystyrene (see section 7.2). In addition, in a different approach nickel particles have also been synthesized directly inside a microgel network.

## 7.1 Co-Nanoparticles

The magnetic Co@SiO<sub>2</sub> nanoparticles were prepared by a two step synthesis. The replacement of air by N<sub>2</sub> gas during the first step of the preparation prevented oxidation of the cobalt core in aqueous solution. Directly afterwards, APTMS and TEOS was added to grow a silica shell on the cobalt seed particles via the well known Stöber synthesis. In this case, the silica shell offers two important functions. On the one hand it prevents the magnetic particles from aggregation and on the other hand it protects the oxidation sensitive cobalt core. By changing the ratio between citric acid and Co<sup>2+</sup> we observed similar results as Kobayashi et al.<sup>113</sup> and Salgueiriño-Maceira et al.<sup>143</sup> The obtained particles with different molar ratios of citrate/Co<sup>2+</sup> (from 0.005 to 0.5) are characterized by TEM and the pictures are shown in figure 7.1. The cobalt core shows a good contrast in the TEM images due a high electron density of cobalt. Hence a clear boundary between the core and the SiO<sub>2</sub> shell is visible.

In the case of the particles with a thin SiO<sub>2</sub> shell and a large Co core ([citric

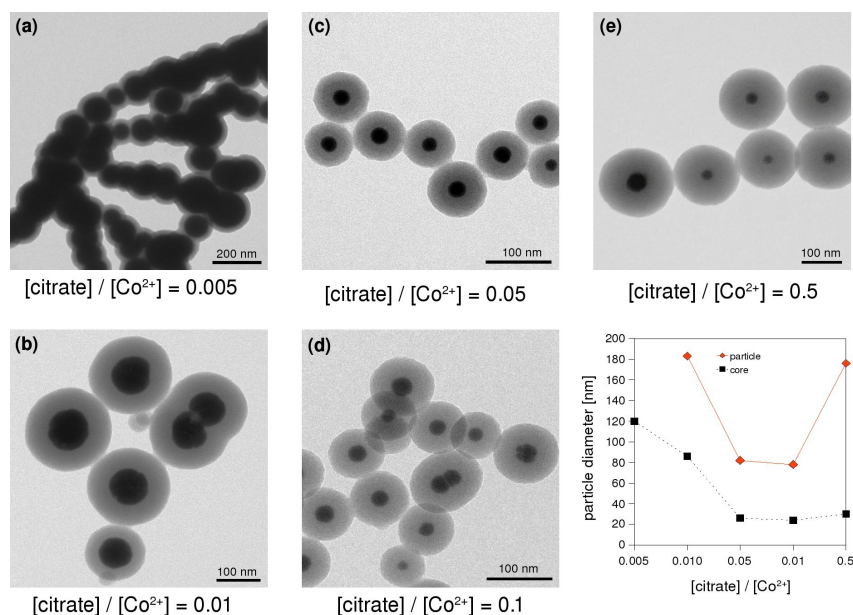


Figure 7.1: TEM images of Co@SiO<sub>2</sub> nanoparticles with varying molar ratio of [citrate]/[Co<sup>2+</sup>]: (a) 0.005, (b) 0.01, (c) 0.05, (d) 0.1, (e) 0.5 and averaged core and particle diameter

acid]/[Co<sup>2+</sup>] = 0.005) (see figure 7.1(a)) it was unfortunately not possible to produce well separated particles.<sup>143</sup> Most times worm-like structures are formed. This indicates that the Co particles aggregate during the first step of the synthesis due to magnetic interactions and the silica shell is then created around the worms. Without the addition of APTMS during the shell synthesis as a connecting agent between the metallic core and the growing SiO<sub>2</sub>, well separated particles could be obtained, but with a non uniform SiO<sub>2</sub> shell (see figure 7.2).

Using higher molar ratios of citric acid/Co<sup>2+</sup> a wide variety of experiments was done to study the influence of the two components. It should be noted, that core-shell particles with a nearly monodisperse size distribution independent of the citrate/Co<sup>2+</sup> ratio could be obtained. With an increase of the molar ratio, the particle diameter and also the core diameter decrease. Only at ratio of citric acid/Co<sup>2+</sup> = 0.5 the diameter of the silica shell increases strongly, while the size of the core stayed constant (see figure 7.1 (e)). A possible reason for this might be the used amount of TEOS during the synthesis. It is,

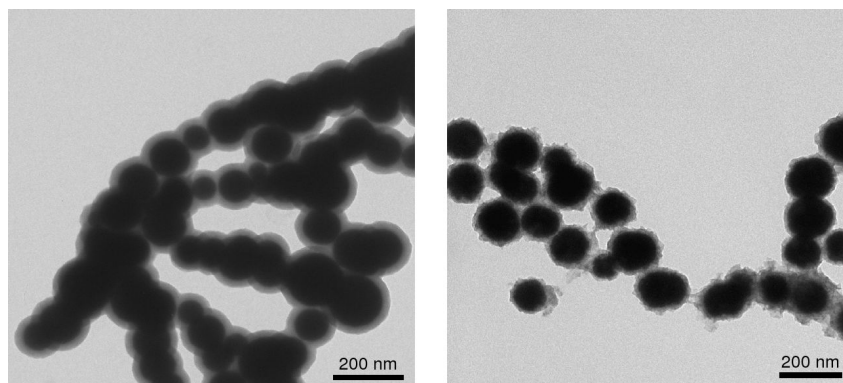


Figure 7.2: Comparison of  $\text{Co@SiO}_2$  nanoparticles synthesized without (left) and with APTMS (right)

however, necessary that during all syntheses only the citric acid/ $\text{Co}^{2+}$  ratio is changed and the APTMS/TEOS ratio is held constant. Nevertheless, a slightly higher amount of TEOS would strongly affect the thickness of the  $\text{SiO}_2$  layer. In this context it should be also mentioned that by a secondary addition of ammonia and TEOS a further growth of the  $\text{SiO}_2$  shell can be achieved.

The  $\text{Co@SiO}_2$  particles shown in figure 7.3 have been functionalized with 3-(Trimethoxysilyl)propyl methacrylate (MPS) and were used as core material for the polymerization of crosslinked NIPAM. These images reveal that the magnetic particles show the same structure as the original particles after the modification with MPS. An attempt to identify the presence of the MPS layer by IR spectroscopy or elemental analysis failed due to resolution limits of these techniques and the very low amount of MPS on the  $\text{Co@SiO}_2$  surface.

To build core-shell particles the polymerization of NIPAM and BIS on the surface of the MPS-modified magnetic particles was done analogously to a microgel synthesis in water and at a temperature of  $70^\circ\text{C}$ . Afterwards, TEM images (also cryo-TEM) were used to study the incorporation of the  $\text{Co@SiO}_2$  particles into the microgel. Figure 7.4 (a) is a snapshot of the sample of polymer modified magnetic particles and reveals the presence of different kinds of species: original  $\text{Co@SiO}_2$  particles, hollow spheres and particles with a non-uniform surface. In addition, it has to be mentioned, that the main part of the

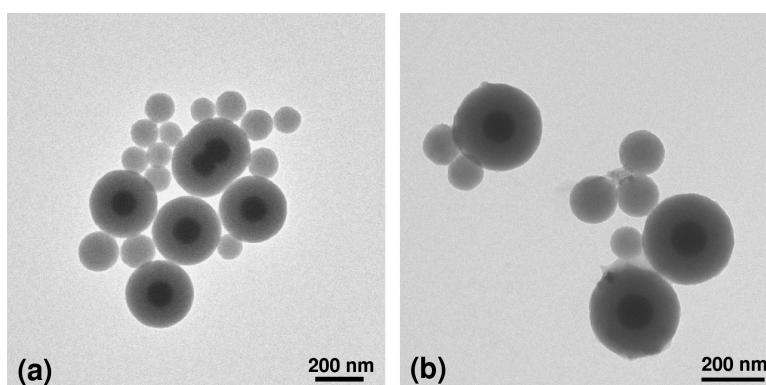


Figure 7.3: TEM images of Co@SiO<sub>2</sub> nanoparticles with a citrate/Co<sup>2+</sup> ratio of 0.1 before (a) and after the coating with MPS (b)

sample shows Co@SiO<sub>2</sub> particles without any poly(NIPAM) shell. Moreover, apparently the original Co@SiO<sub>2</sub> particles have a larger diameter compared to those having a non-uniform shell. This would be only possible if the SiO<sub>2</sub> layer is partially reduced during the polymerization of NIPAM.

In order to answer the question whether the non-uniform shell in the TEM image consists of a collapsed poly(NIPAM) shell or not, cryo-TEM measurements have been made. But within this experiment it was unfortunately not possible to determine a microgel shell in the swollen state and generally the presence of poly(NIPAM) around the Co@SiO<sub>2</sub> particles. Beside this, the cryo-TEM image (figure 7.4 (b)) also prove the formation of hollow particles and some additional crystalline structures. Similar structures have been investigated by Zhang et. al.<sup>144</sup> They synthesized cobalt flowerlike architectures using hydrothermal reduction of cobalt chloride hexahydrate. An important intermediate in this synthesis is Co(OH)<sub>2</sub>, which subsequently controls the transformation of cobalt nanoplates into flowers. Therefore, it could be that at a reaction temperature of 70°C during the polymerization of NIPAM the cobalt core is washed out. Due to the aqueous reaction medium and residual oxygen in the water, the cobalt could be oxidized and rearranges as Co(OH)<sub>2</sub> in the form of flowers. That would mean, however, that the SiO<sub>2</sub> layer around the core is too porous to form a suitable protection shell for the cobalt against oxidation.

Further repetitions of the NIPAM-coating with other Co@SiO<sub>2</sub> particles as core mate-

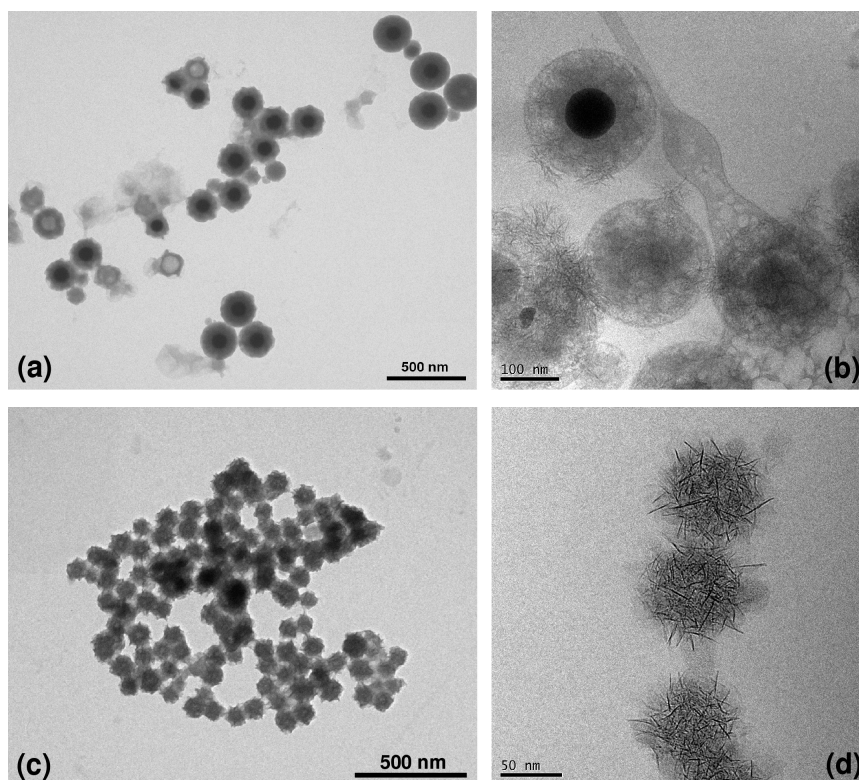


Figure 7.4: Co@SiO<sub>2</sub> particles after the synthesis of the poly(NIPAM) shell; the images show no formation of core-shell particles, but new flower-like structures are created

rial showed similar results (figure 7.4(c) and (d)), but no formation of core-shell particles as mentioned in literature with iron oxide@poly(NIPAM),<sup>145</sup> Au@poly(NIPAM)<sup>42</sup> or silica@poly(NIPAM).<sup>48</sup>

To prove the formation of Co(OH)<sub>2</sub> flowerlike structures by oxidation of the metallic cobalt from the core, wide angle x-ray scattering measurement (WAXS) of the nanoparticle solution have to be done. Unfortunately, it was not possible to do such experiments at our institute during the time of this work. Therefore, we will address this problem in the future.

## 7.2 Ni-Nanoparticles

In order to prepare hybrid microgels with a magnetic component, an attempt was made to use nickel as the magnetic material instead of cobalt. For the synthesis of the initial nickel nanoparticles, a well working method of Grzelczak et al.<sup>146</sup> was used. Afterwards different approaches have been employed to prevent the particles from oxidation and to incorporate them into microgels.

### 7.2.1 Magnetic nickel nanoparticle

As already mentioned in section 3.2.4.1, the synthesis starts with the preparation of platinum seeds. After the synthesis of the platinum seeds, different molar ratios of the seed particles were mixed with a nickel/hydrazine solution. An immediate change in colour of these six different solutions indicates the formation of the nickel nanoparticles, grown on the platinum seeds. A photograph of the solutions is shown in figure 7.5. The varying coloration of the solutions from brown (molar ratio of  $\sim 10$ ) to grey (molar ratio of  $\sim 100$ ) suggests that Ni particles of different sizes have been formed. This fact was confirmed by transmission electron microscopy (TEM) and the results are similar to those of Grzelczak et al.<sup>146</sup>

Using this Pt seed particle based technique, it was possible to synthesize relatively uniform nickel nanoparticles with different sizes. The average particle diameter of the Pt@Ni nanoparticles obtained with different molar ratios of  $\text{Ni}^{2+}/\text{Pt}^0$  was determined by analysing the TEM images with an image processing and analysis software (Image J, V.1.42). As a result, the average particle diameter was found to vary from  $\sim 20$  nm ( $\text{Ni}^{2+}/\text{Pt}^0 \sim 10$ ) to  $\sim 41$  nm ( $\text{Ni}^{2+}/\text{Pt}^0 \sim 100$ ). Due to their ferromagnetic behaviour the particles are not well separated in the TEM images and arrange in groups or form chains (see figure 7.6).

Beside this, a long-time experiment of nearly a year showed that the Pt@Ni nanoparticles stabilized with hexadecyltrimethylammonium bromide (CTAB) in solution undergo an aging process. Comparing the TEM images of freshly synthesized particles with older ones, it is clear that the morphology of the nanoparticles changes (see figure 7.7). A pos-

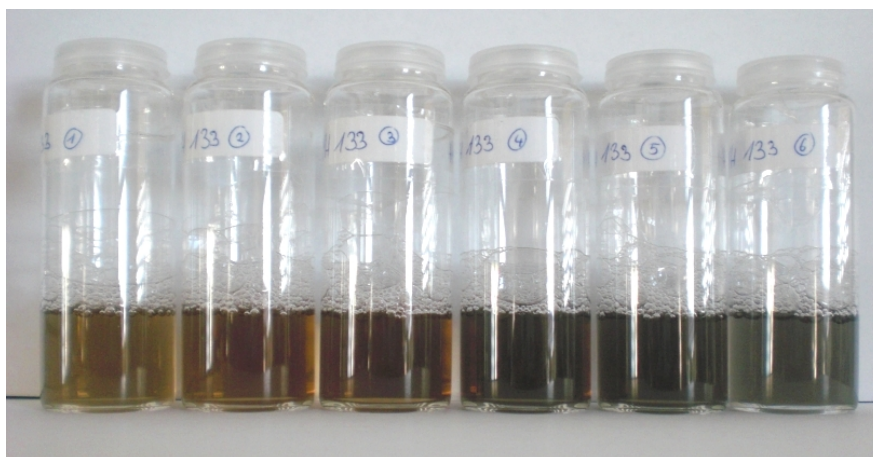


Figure 7.5: Nickel nanoparticles in solution with different particle diameters from 20 nm (left) to 41 nm (right)

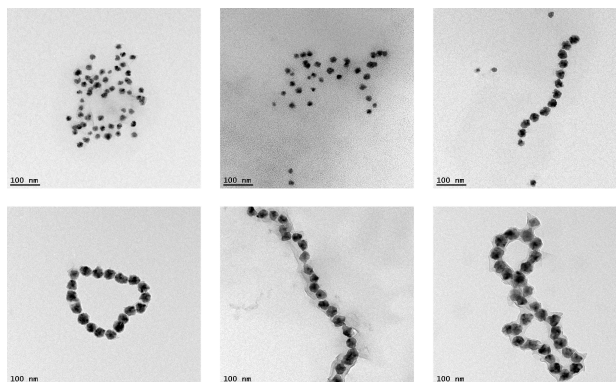


Figure 7.6: TEM images of Pt@Ni nanoparticles prepared using different ratios of platinum seeds to nickel solution ( $\text{Ni}^{2+}/\text{Pt}^0 \sim 10, 12, 20, 40, 80, 100$ )

sible reason could be oxidation of the metallic nickel to nickel oxides ( $\text{NiO}_x$ ) and nickel hydroxide ( $\text{Ni}(\text{OH})_2$ ).

Because of the strong binding of CTAB on the nanoparticle surface<sup>74</sup> and the loss of colloidal stability after removing the surfactant, it was tried to synthesize the Pt@Ni particles using a different stabilizing agent. As described in literature, the formation of Pt nanoparticles in presence of polyvinyl pyrrolidone (PVP) is possible.<sup>147</sup> After reduction of hexachloroplatinic acid hexahydrate ( $\text{H}_2\text{PtCl}_6 \cdot \text{H}_2\text{O}$ ) in a PVP solution, the solution went gray, what indicates the formation of Pt nanoparticles. By further addition of a nickel/hydrazine solution, no significant change in colour could be observed. An anal-

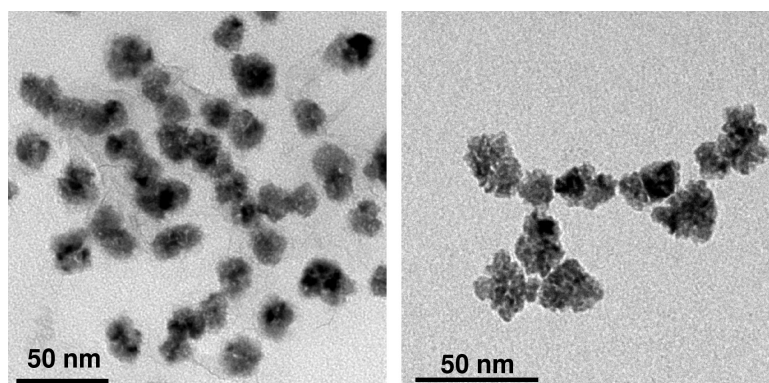


Figure 7.7: Aging process of the Pt@Ni nanoparticles; left: freshly made particles; right: particles after one year of storage

ysis of TEM images before and after the reduction of nickel showed that polydisperse Pt nanoparticles have been formed, but no growth of nickel on these seeds was achieved (figure 7.8). These results confirm the results of Grzelczak et al.,<sup>146</sup> which consider the presence of CTAB molecules for the deposition of nickel on the Pt seed particles a necessary pre-requisite.

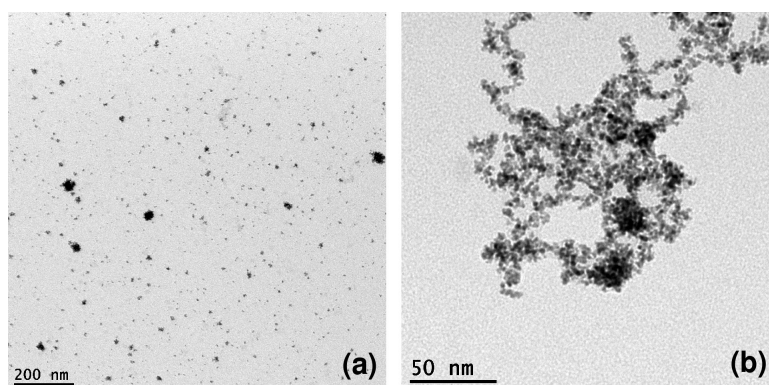


Figure 7.8: TEM images of Pt nanoparticles synthesized with PVP as surfactant (a) and Ni growth on Pt seed particles (b)



## 7.2.2 Coating techniques of Pt@Ni nanoparticles

To build up core-shell hybrid microgels, it is necessary to modify the precursor Pt@Ni nanoparticles with an additional shell, because a direct synthesis of poly(NIPAM) on Pt@Ni is not possible. This shell should not only protect the magnetic particles from aggregation and further oxidation, but should mainly allow a grafting-from polymerization of NIPAM around them. In this context, two different approaches were used. First, an attempt was made to surround the Pt@Ni particles with a silica layer and the second way to synthesize the shell is based on a coating technique with crosslinked polystyrene (PS).<sup>42</sup>

### 7.2.2.1 Silica-coating

Since the above mentioned Pt@Ni particles have a high  $\zeta$ -potential (+53 mV), a direct coating with silica using the well known Stöber method is not possible, because the transfer of the particles into ethanol would be not successful.<sup>74</sup> Reducing the surface potential of the magnetic particles by exchange of CTAB with another adequate component would allow the transfer to ethanol and subsequently the controlled hydrolysis of TEOS to form a silica shell. For a stabilization of nanoparticles and a further coating with silica the amphiphilic, nonionic polymer PVP was already successfully used.<sup>148</sup> To replace CTAB from the Pt@Ni surface with poly(vinylpyrrolidone) (PVP) a layer-by-layer technique was invented by Pastoriza-Santos et al.<sup>74</sup> In this process differently charged polyelectrolyte layers (poly(styrene sulphonate) (PSS), poly(allylamine hydrochloride) (PAH) and PVP) are stepwise precipitated on the nanoparticle surface (see figure 7.9). After removing an excess of surfactant, the particles can be transferred to an alcohol/water mixture and subsequently coated with silica.

Figure 7.10 shows as a result an uncontrolled deposition of silica around the Pt@Ni@PSS@PAH@PVP nanoparticles obtained by this layer-by-layer technique. Big aggregates of pure silica are formed and only partially nanoparticles are incorporated in a silica shell. In the enlarged section of the TEM image (right picture) the magnetic particles are easily identified, but always several particles are arranged in groups and coated

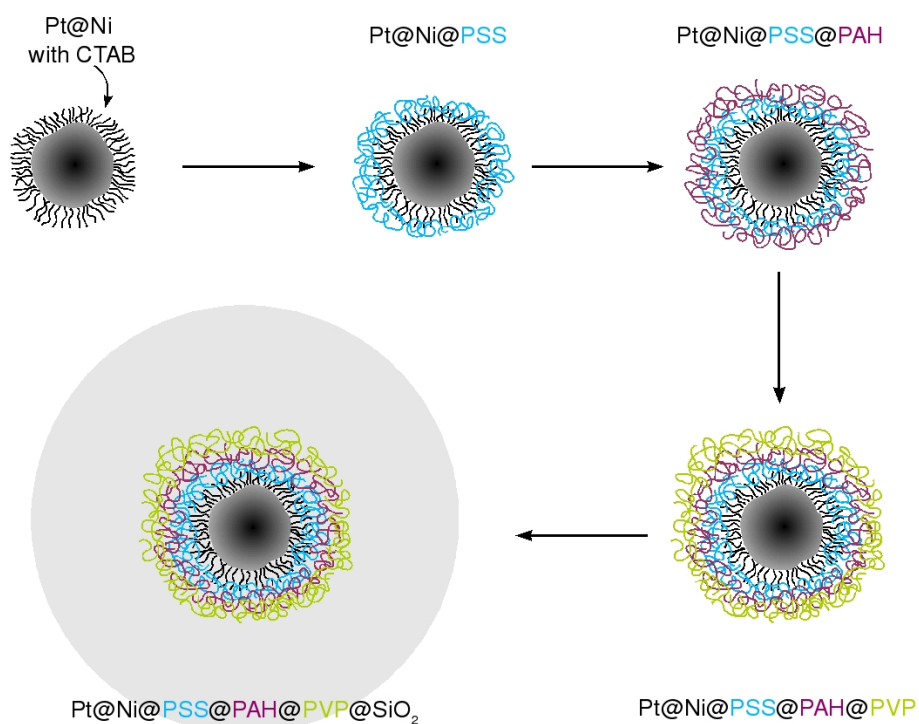


Figure 7.9: Scheme of the different preparation steps of the silica coating of Pt@Ni nanoparticles using a layer-by-layer technique

by a continuous silica layer. This might be related to the strong magnetic moment of the Pt@Ni, which favours the formation of nanoparticle groups. A controlled condensation of TEOS around separated particles as described in literature could not be achieved.<sup>74</sup> Also the deposition of a silica shells with a well defined thickness was unfortunately not possible within these experiments. Also by several experiments, no comparable or better result as described above could be obtained. This fact clearly shows, how sensitive this layer-by-layer technique is. In addition to the initially selected concentration of Pt@Ni particles, the reaction conditions of each individual polyelectrolyte coating step influence the complete following coating process. This includes:

- \* duration and frequency of the ultrasonic treatment of the polyelectrolytes and the magnetic nanoparticles
- \* addition rate of the polyelectrolyte solutions
- \* removing the excess of surfactant by centrifugation

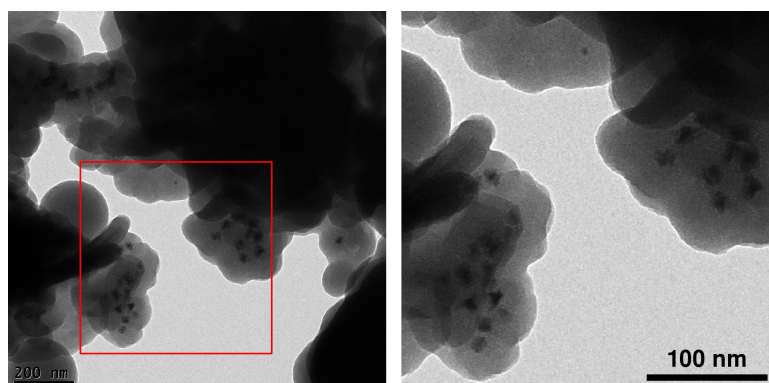


Figure 7.10: Magnetic nickel nanoparticles coated with silica using a layer-by-layer technique with oppositely charged polyelectrolytes

- \* transfer to the alcohol/water mixture; if the remaining surface charge is too positive, aggregation occurs
- \* amount of TEOS to obtain well separated particles

### 7.2.2.2 PS-coating

The modification of Pt@Ni nanoparticles with styrene was carried out in two separate experiments differing in the amount of used styrene and divinyl benzene (DVB) using a method investigated by Contreras-Cáceres et al. for the coating of CTAB stabilized gold nanoparticles.<sup>42</sup> Figure 7.11(a) and (b) show the TEM images of the Pt@Ni particles before and after the coating with a low amount of crosslinked polystyrene. The formation of a PS-shell around the particles can not be clearly verified by TEM. The shape of the modified particles shows a slightly less squared structure than the precursor nanoparticles, which could be an indication for the formation of a PS-shell. However, within the accuracy of the TEM it was not possible to determine an increase of the particle diameter. For this reason the coating procedure was repeated with a ten times higher amount of PS and DVB. Again, a comparison of the TEM images before and after the modification did not indicate the formation of a PS layer (see figure 7.11(c)). Besides this, a non-negligible amount of free PS latices was produced.

Assuming that in the first experiment a thin shell of PS/DVB has been formed around

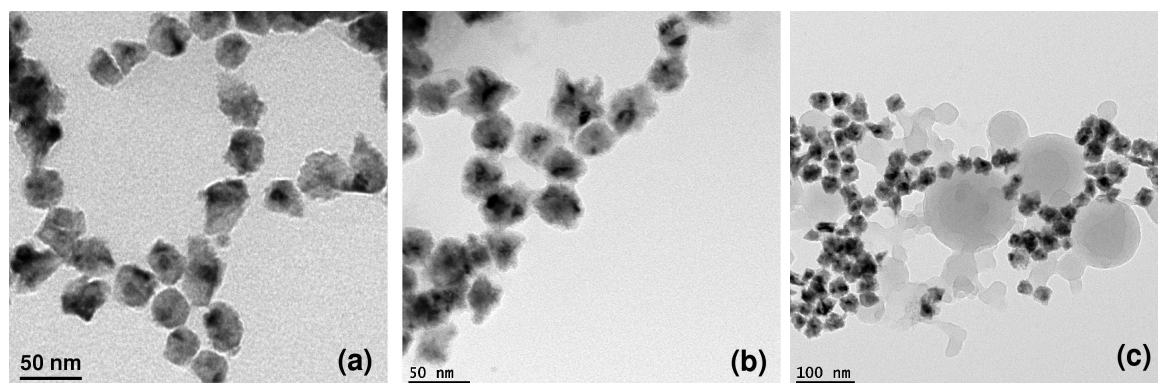


Figure 7.11: Coating of Pt@Ni nanoparticles with crosslinked polystyrene; (a) pure Pt@Ni nanoparticles, (b) Pt@Ni coated with a low amount of PS/DVB, (c) magnetic particles coated with a high amount PS/DVB

the Pt@Ni core, it has been tried to create a shell of crosslinked NIPAM around these magnetic precursor particles.<sup>42</sup> After the polymerization of NIPAM/BIS a white reaction mixture was obtained. Attaching a magnet to the outside of the reaction vessel results in a slightly gray precipitate at the glass, while the remaining microgel solution stayed white. This fact suggests that a high amount of free poly(NIPAM) microgel particles without a Pt@Ni core was build. To investigate a possible formation of magnetic core-shell particles TEM was used. Figure 7.12(a) shows an image of the magnetic precipitate, which was separated by a magnet from the residual microgel solution. Due to the high scattering contrast of the nickel, the microgel particles are hardly identified, but the TEM image clearly shows that the magnetic particles have not been incorporated into the microgel. A micrograph of the residual poly(NIPAM) solution (figure 7.12(b)) also proves the formation of Pt@Ni-free microgel particles. This might be traced back to the strong magnetic moment of the nanoparticles, which favours the formation of aggregates, but also indicates an incomplete or even not existing modification of the Pt@Ni surface with crosslinked PS.

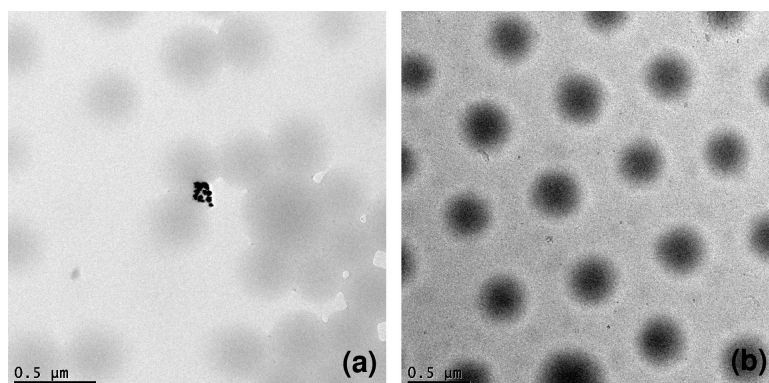


Figure 7.12: Modification of Pt@Ni@PS/DVB particles with a shell based on poly(NIPAM); the images show no incorporation of the magnetic particles into the microgel

### 7.2.3 Direct synthesis of Ni-nanoparticles in microgels

To synthesize the platinum seed particles directly in a microgel network, a weakly positively charged microgel is necessary due to the negatively charged  $\text{PtCl}_4^{-2}$  ions. For the later coating of the Pt seeds with nickel, the surfactant CTAB is essential. Hence, a poly(NIPAM) microgel using an emulsion polymerization with CTAB and V50 as initiator (also positively charged) was prepared. In the next step, the Pt salt was dissolved in the microgel solution and reduced with  $\text{NaBH}_4$ . After ten minutes reaction time, the solution turns slightly grey, which could indicate the formation of Pt nanoparticles. To confirm the formation of the Pt seeds in the microgel network, TEM images were taken. The results are shown in figure 7.13.

Due to the high scattering contrast of the Pt nanoparticles in TEM, the poly(NIPAM) particles are difficult to identify. So at a low magnification (7.13(a)) the colloidal particles of the microgel can be identified as spherical dark gray shadows in the background and the nanoparticles are hard to see, because of their size. The TEM image with a higher magnification (7.13(b)) shows that the Pt particles have not been incorporated into the microgels and big groups of free nanoparticles are found.

To test how far it is possible to coat the Pt cores with nickel in the presence of CTAB stabilized microgel particles, a nickel salt solution was added and reduced with hydrazine.

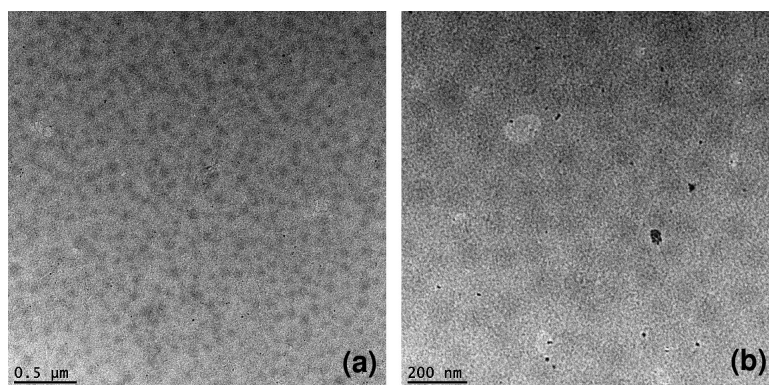


Figure 7.13: Synthesis of Pt seed particles in presence of a weakly positively charged microgel

The TEM images demonstrate that this way to synthesize Pt@Ni magnetic particles was not successful.

# 8 Summary and future perspectives

## Crosslinker gradient macrogels and deswelling kinetics

After the development of a well-suited technique to prepare macroscopic gels with a crosslinker gradient, the swelling behaviour of the gels was studied by means of image analysis and the swelling ratio  $\alpha$  could be determined for different zones of the gel. Kinetic measurements showed that the areas with a low and medium crosslinker content, as well as the length of the gel, exhibit strong and rather fast changes of the volume. The highly crosslinked areas undergo only limited swelling. Within the accessible measurement time, the swelling curves decayed finally to a constant value and it was possible to fit the decrease in the swelling ratio with functions proposed by Li and Tanaka<sup>124</sup> in order to obtain the relaxation time of the shrinking process. The obtained values for  $\tau$  from the zones with a low and a medium BIS content, as well as from the length, were in a range of some hundreds seconds. The following calculation of the collective diffusion constant  $D_0$  is based on assumptions from the literature<sup>124</sup> and yields values of  $D_0 \sim 2.92 \cdot 10^{-4} \text{ cm}^2/\text{s}$  for the area with a low BIS content and  $D_0 \sim 2.02 \cdot 10^{-4} \text{ cm}^2/\text{s}$  for the area with a medium BIS content. However, these values differ strongly from Tanaka's results and thus further detailed studies are necessary to explain these considerable difference for the collective diffusion constant.

## Internal dynamics of macro- and microgels

The internal network motion in a macrogel and a homologous microgel based on poly(NIPAM-co-BAC) are compared by neutron spin-echo experiments. The microgel was synthesized by a surfactant supported emulsion polymerization. Hence, the network

is created nearly under bulk conditions. The preparation of the macrogel was made under good solvent conditions. Due to this, it was expected to have a significantly higher network inhomogeneity in the microgel compared to the macrogel, which was supposed to cause strong differences in the local network motion.

However, the found differences in the network dynamics between micro- and macrogels were only in the range of 10-20%. This was surprisingly low, indicating that the morphology and the coupling of the chain motion does not differ too much between homologous micro- and macrogels. The absolute values of the diffusion coefficient for both poly(NIPAM-co-BAC) systems are in the same range compared to previous works on similarly crosslinked gels. Changes of the pH seem to have a stronger influence on the copolymer microgel. For the macrogel no significant change in the local network motion was found upon a decrease of pH.

In the future we wish to extend these experiments to different crosslinker concentrations in poly(NIPAM) homopolymer as well as in copolymer systems. Furthermore, the temperature dependence of the internal dynamics during the phase transition will be studied for responsive micro- and homologous macrogels. Another interesting point for future work will be the comparison of DLS results with NSE experiments. In DLS the non-ergodicity has to be taken into account, whereas in NSE up to a certain point the systems behave ergodically on a local scale.

### **Poly(NIPAM-co-NtBAM) copolymer microgels**

In this part of the thesis, copolymer microgels based on the thermoresponsive poly(NIPAM) in combination with the comonomer NtBAM were prepared. The colloidal particles obtained by the use of a surfactant-free emulsion polymerization exhibit a narrow particle size distribution and a swelling behaviour depending on the comonomer content. For all poly(NIPAM-co-NtBAM) microgels the volume phase transition temperature is lower compared to that of pure poly(NIPAM) (VPTT  $\sim 32^\circ\text{C}$ ) and the particle size decreases with increasing *N-tert*-butylacrylamide content.



---

Furthermore, the swelling behaviour of the particles with a comonomer content of up to 10 mol% could be described using the Flory-Rehner theory. However, some of the obtained parameters show a comonomer dependence, which is difficult to rationalise. For the highest NtBAM content the model fails. However, for low contents (up to 10 mol%) of an uncharged comonomer the theory is still applicable and gives a satisfying description of the swelling behaviour.

The local structure of the colloidal microgel particles was investigated by small angle neutron scattering. The network correlation length  $\xi$  is found to be approximately 3 nm for all synthesized copolymer systems. This suggests that the NtBAM comonomer has no significant influence on the network morphology, since this value is similar as the values found for homopolymer microgels.

A first approximation of the scattering intensity  $I(q)$  of the totally collapsed particles ( $T > VPTT$ ) by an ideal Porod law ( $I(q) \propto q^{-4}$ ) does not lead to a satisfying representation of the SANS profiles. Taking into account, that the poly(NIPAM-co-NtBAM) microgels exhibit dangling polymer chains at the microgel/water interface, the scattering of the surface roughness has to be added to the ideal Porod behaviour. Finally, this modification of the Porod law leads to a good description of the scattering profiles of the investigated copolymer systems and hence, it seems that the microgel particles exhibit a slightly higher roughness compared to previously studied pure poly(NIPAM) particles.

This chapter of the work has shown that the phase transition behaviour of poly(NIPAM) can easily be modified by copolymerization of NIPAM with different comonomers. The approach to describe the phase transition of the uncharged poly(NIPAM-co-NtBAM) systems using the Flory-Rehner theory resulted in a satisfying description only for low comonomer contents (up to 10 mol%). Hence, the Flory-Rehner approach should be modified to include the case of uncharged comonomers properly. Furthermore, the distribution of the comonomer NtBAM inside the microgel network is still unknown and would be of great interest. Here, contrast variation neutron scattering allows to study whether the monomers in the copolymer are randomly distributed or if the polymerization of one component is favoured and consequently a gradient copolymer is formed. Generally,

this technique is based on the fact that one monomer of the system is deuterated and with certain solvent mixtures of H<sub>2</sub>O/D<sub>2</sub>O the scattering from one component will be equal to that of the solvent. Thus, the so-called "matched" component in solution is invisible for the neutrons and the distribution of the second component can be determined.

### **Magnetic microgel hybrid systems**

In order to prepare hybrid microgel particles with a magnetic component, an approach was made to combine cobalt or nickel nanoparticles with NIPAM based microgels. In the case of cobalt, it was possible to prepare well-defined Co nanoparticles covered with a silica shell using a simple two-step synthesis. Both, the size of the core, as well as the silica shell thickness can be controlled by the synthetic procedure. For the poly(NIPAM) shell synthesis, the surface of the particles has been functionalized by 3-(Trimethoxysilyl)propyl methacrylate (MPS) and subsequently, the synthesis of the crosslinked poly(NIPAM) shell around the Co@SiO<sub>2</sub> particles was done using a simple emulsion polymerization. TEM images and also cryo-TEM images unfortunately showed that the formation of Co@SiO<sub>2</sub>@poly(NIPAM) was not successful. Beside this, the formation of hollow particles and some additional flowerlike structures was shown. Therefore, it is assumed that the SiO<sub>2</sub> layer around the cobalt core is too porous to form a suitable protection shell against oxidation and consequently during the polymerization reaction at 70°C the cobalt is washed out.

To prove this assumption, further investigations on the hollow particles and the flowerlike structures are necessary. Here, the problem arises that it is not possible to separate the different obtained structures (original Co@SiO<sub>2</sub>, hollow particles and flowerlike structures). Therefore, they can not be characterized independently. Using for example wide-angle X-ray scattering for solutions, this could provide an indication if the flowerlike particles exhibit a crystalline structure and if this consists of cobalt hydroxide.

Furthermore, to protect the cobalt core against oxidation during the synthesis of the microgel shell, an approach could be made to create an additional shell around the

---

Co@SiO<sub>2</sub> particles, which is impermeable for oxygen. Here, for example, a thin shell of polystyrene could be used, since the protection of nanoparticles with crosslinked styrene has already been reported in the literature.<sup>42</sup>

In the case of hybrid materials based on nickel nanoparticles and poly(NIPAM) as thermosensitive microgel, different approaches have been pursued. First of all, the preparation of CTAB stabilized nickel nanoparticles with different sizes analogous to a synthesis of Grzelczak et al.<sup>146</sup> was successful and the obtained particles could be well characterized with TEM. It was shown that the particles stored in CTAB solution undergo an aging process due to oxidation and consequently, the morphology of the nanoparticles changes. To prevent the sensitive magnetic nickel nanoparticles from oxidation and to modify them for the polymerization of NIPAM, different coating techniques have been applied. We first tried to construct Ni@SiO<sub>2</sub> particles using a layer-by-layer technique with various polyelectrolytes (PSS, PAH and PVP). Here, the surfactant CTAB is replaced by oppositely charged polyelectrolytes and with this surface modification, the nickel particles are prepared for a controlled condensation of TEOS around particles. Unfortunately, this coating procedure leads to an uncontrolled deposition of silica around the Pt@Ni@PSS@PAH@PVP nanoparticles and big aggregates of pure silica are formed. Furthermore, several experiments demonstrated the sensitivity of the LbL technique with respect to reaction conditions and therefore, it was not possible to obtain well-separated Ni@SiO<sub>2</sub> core-shell particles during the time of this work. Moreover, an attempt was made to cover the nickel nanoparticles surface with polystyrene and to synthesize a poly(NIPAM) shell around these modified particles. However, with this method only nickel-free microgel particles and aggregates of pure nickel particles could be obtained. Nevertheless, in order to prepare magnetic nickel hybrid microgels, we tried to synthesize the particles directly inside the microgel network. Therefore, poly(NIPAM) particles with CTAB as surfactant have been synthesized, followed by the reduction of PtCl<sub>4</sub><sup>2-</sup> inside the microgel network to create the seed particles for the subsequently formation of the nickel particles. The TEM images unfortunately showed that the Pt particles have not

been incorporated into the microgel and aggregates of free Pt nanoparticles are found. One possible approach for a successful synthesis of Pt@Ni in poly(NIPAM) would be to use a nearly surfactant free microgel. Therefore, the CTAB has to be removed from the microgel by ultrafiltration. The formation of the platinum seed particles outside of the microgel could than be prevented, since only the positive charges in the gel network can interact with the  $\text{PtCl}_4^{-2}$  ions. However, it is questionable whether a nickel growth on the Pt seed particles is possible without any CTAB stabilization.

# Bibliography

- [1] E. Geissler and A. M. Hecht. The poisson ratio of polymer gels. *Macromolecules*, 13:1276–1280, 1980.
- [2] T. Hellweg, C. D. Dewhurst, E. Brückner, K. Kratz, and W. Eimer. Colloidal crystals made of poly(*N*-isopropylacrylamide) microgel particles. *Colloid & Polymer Sci.*, 278(10):972–978, 2000.
- [3] S. Nayak and L. A. Lyon. Soft nanotechnology with soft nanoparticles. *Angew. Chem. Int. Ed.*, 44:7686–7708, 2005.
- [4] B. Vincent, M. Bradley and G. Burnett. Uptake and release of surfactants from polyampholyte microgel particles. *Colloid and Polymer Science*, 287:345–350, 2009.
- [5] R. F. S. Freitas and E. L. Cussler. Temperature sensitive gels as extraction solvents. *Chem. Eng. Sci.*, 42:97–103, 1987.
- [6] T. R. Hoare and D. S. Kohane. Hydrogels in drug delivery: Progress and challenges. *Polymer*, 49:1993–2007, 2008.
- [7] M. Shibayama, T. Tanaka, and C. C. Han. Small angle neutron scattering study on poly(*N*-isopropylacrylamide) gels near their volume-phase transition. *J. Chem. Phys.*, 97(9):6829–6841, 1992.
- [8] C. Wu and S. Zhou. Volume phase transition of swollen gels: Discontinuous or continuous. *Macromolecules*, 30:574–576, 1997.

- 
- [9] R. Pelton. Temperature-sensitive aqueous microgels. *Adv. Colloid Interf. Sci.*, 85:1–33, 2000.
- [10] S. Höfl, L. Zitzler, T. Hellweg, S. Herminghaus, and F. Mugele. Volume phase transition of smart microgels in bulk solution and adsorbed at an interface: A combined AFM, dynamic light, and small angle neutron scattering study. *Polymer*, 48:245–254, 2007.
- [11] Y. Hirokawa and T. Tanaka. Volume phase transition in a nonionic gel. *J. Chem. Phys.*, 81(12):6379–6380, 1984.
- [12] M. Shibayama, F. Ikkai, S. Inamoto, S. Nomura, and C. C. Han. pH and salt concentration dependence of the microstructure of poly(*N*-isopropylacrylamide-co-acrylic acid) gels. *J. Chem. Phys.*, 105(10):4358–4366, 1996.
- [13] M. Karg, I. Pastoriza-Santos, B. Rodriguez-González, R. von Klitzing, S. Wellert, and T. Hellweg. Temperature, pH, and ionic strength induced changes of the swelling behavior of PNIPAM-poly(allylacetic acid) copolymer microgels. *Langmuir*, 24(12):6300–6306, 2008.
- [14] Z. Meng, M. H. Smith, and L. A. Lyon. Temperature-programmed synthesis of micron-sized multi-responsive microgels. *Colloid Polym. Sci.*, 287:277–285, 2009.
- [15] Th. Hellweg. *Nanoscale Materials*, chapter Properties of NIPAM-Based Intelligent Microgel Particles: Investigated Using Scattering Methods, pages 209–225. Kluwer Academic Publishers, Dordrecht, 1st edition, 2003.
- [16] H. M. Crowther, B. R. Saunders, S. J. Mears, T. Cosgrove, B. Vincent, S. M. King, and G.-E. Yu. Poly(NIPAM) microgel particle de-swelling: a light scattering and small-angle neutron scattering study. *Colloids and Surfaces A: Physicochemical and Engineering Aspects*, 152:327–333, 1999.
- [17] A. Fernandez-Nieves, J. S. van Duijneveldt, A. Fernandez-Barbero, B. Vincent, and

- F. J. de las Nieves. Structure formation from mesoscopic soft particles. *Phys. Rev. E*, 64(5):051603/1–10, 2001.
- [18] S. Nayak, S. B. Debord, and L. A. Lyon. Investigations into the deswelling dynamics and thermodynamics of thermoresponsive microgel composite films. *Langmuir*, 19:7374–7379, 2003.
- [19] M. Karg and T. Hellweg. New "smart" poly(NIPAM) microgels and nanoparticle microgel hybrids: Properties and advances in characterisation. *Current Opinion in colloid and Interface Science*, 14:438–450, 2009.
- [20] T. Tanaka and D. J. Fillmore. Kinetics of swelling of gels. *J. Chem. Phys.*, 70(3):1214–1218, 1979.
- [21] Y. Li and T. Tanaka. Study of the universality class of the gel network system. *J. Chem. Phys.*, 90:5161–5166, 1989.
- [22] X. Wu, R. H. Pelton, A. E. Hamielec, D. R. Woods, and W. McPhee. The kinetics of poly(*N*-isopropylacrylamide) microgel latex formation. *Colloid & Polymer Science*, 272:467–477, 1994.
- [23] M. Stieger, W. Richtering, J. S. Pedersen, and P. Lindner. Small-angle neutron scattering study of structural changes in temperature sensitive microgel colloid. *J. Chem. Phys.*, 120(13):6197–6206, 2004.
- [24] A.-M. Hecht, R. Duplessix, and E. Geissler. Structural inhomogeneities in the range 2.5-2500 Å in polyacrylamide gels. *Macromolecules*, 18:2167–2173, 1985.
- [25] K. Kratz, Th. Hellweg, and W. Eimer. Structural changes in PNIPAM microgel particles as seen by SANS, DLS, and EM techniques. *Polymer*, 42(15):6531–6539, 2001.
- [26] S. Schmidt, H. Motschmann, T. Hellweg, and R. von Klitzing. Thermoresponsive surfaces by spin-coating of PNIPAM-co-PAA microgels. a combined AFM and ellipsometry study. *POLYMER*, 49:749–756, 2008.

- 
- [27] S. Kazakov, M. Kaholek, D. Kudasheva, I. Teraoka, M. K. Cowman, and K. Levon. Poly(*N*-isopropylacrylamide-co-1-vinylimidazole) hydrogel nanoparticles prepared and hydrophobically modified in liposome reactors: Atomic force microscopy and dynamic light scattering study. *Langmuir*, 19(19):8086–8093, 2003.
- [28] C. Wu and S. Zhou. Light scattering study of spherical poly(*N*-isopropylacrylamide) microgels. *J. Macromol. Sci.*, B36:345–355, 1997.
- [29] P. N. Pusey and W. van Megen. Dynamic light scattering by non-ergodic media. *Physica A*, 157:705–741, 1989.
- [30] A. Koike, T. Yamamura, and N. Nemoto. Dynamic light scattering of CTAB: NaSal threadlike micelles in the semidilute regime. II. effect of surfactant concentration. *Colloid & Polymer Science*, 272:955–961, 1994.
- [31] Th. Hellweg, K. Kratz, S. Pouget, and W. Eimer. Internal dynamics in colloidal PNIPAM microgel particles immobilised in a mesoscopic crystal. *Colloids and Surfaces A*, 202(2-3):223–232, 2002.
- [32] K. Kratz, Th. Hellweg, and W. Eimer. Influence of charge density on the swelling of colloidal poly(*N*-isopropylacrylamide-co-acrylic acid) microgels. *Colloids & Surfaces A*, 170(2-3):137–149, June 2000.
- [33] J.-H. Kim and M. Ballauff. The volume transition in thermosensitive core-shell latex particles containing charged groups. *Colloid Polym. Sci.*, 277:1210–1214, 1999.
- [34] M. J. Snowden, B. Z. Chowdhry, B. Vincent, and G. E. Morris. Colloidal copolymer microgels of *N*-isopropylacrylamide and acrylic acid: pH, ionic strength and temperature effects. *J. Chem. Soc., Faraday Trans.*, 92:5013–5016, 1996.
- [35] T. Hoare and R. Pelton. Highly pH and temperature responsive microgels functionalized with vinylacetic acid. *Macromolecules*, 37:2544–2550, 2004.



- 
- [36] B. R. Saunders, H. M. Crowther, and B. Vincent. Poly((methyl methacrylate)-co-(methacrylic acid)) microgel particles: Swelling control using pH, cononsolvency, and osmotic deswelling. *Macromolecules*, 30:482–487, 1997.
- [37] I. Berndt and W. Richtering. Doubly temperature sensitive core-shell microgels. *Macromolecules*, 36:8780–8785, 2003.
- [38] D. Suzuki, J. G. McGrath, H. Kawaguchi, and L. A. Lyon. Colloidal crystals of thermosensitive, core/shell hybrid microgels. *J. Phys. Chem. C*, 111:5667–5672, 2007.
- [39] D. J. Kim, S. M. Kang, B. Kong, W.-J. Kim, H.-J. Paik, and I. S. Choi. Formation of thermoresponsive gold nanoparticle/PNIPAAm hybrids by surface-initiated, atom transfer radical polymerization in aqueous media. *Macromol. Chem. Phys.*, 206:1941–1946, 2005.
- [40] M. Karg, I. Pastoriza-Santos, J. Perez-Juste, T. Hellweg, and L. M. Liz-Marzan. Nanorod-coated PNIPAM microgels: Thermoresponsive optical properties. *Small*, 3(7):1222–1229, 2007.
- [41] M. Karg, Y. Lu, E. Carbó-Argibay, I. Pastoriza-Santos, J. Pérez-Juste, and L. M. Liz-Marzán. Multi-responsive hybrid colloids based on gold nanorods and poly-(NIPAM-co-allyl-acetic acid) microgels: temperature- and pH-tunable plasmon resonance. *Langmuir*, 25:3163–3167, 2009.
- [42] R. Contreras-Cáceres, A. Sánchez-Iglesia, M. Karg, I. Pastoriza-Santos, J. Pérez-Juste, J. Pacifico, T. Hellweg, A. Fernández-Barbero, and L. M. Liz-Marzán. Encapsulation and growth of gold nanoparticles in thermoresponsive microgels. *Adv. Mater.*, 20:1666–1670, 2008.
- [43] M. Ballauff and Y. Lu. "Smart" nanoparticles: Preparation, characterization and applications. *Polymer*, 48:1815–1823, 2007.

- 
- [44] D. Suzuki and H. Kawaguchi. Hybrid microgels with reversibly changeable multiple color. *Langmuir*, 22:3818–3822, 2006.
- [45] Y. Mei, Y. Lu, F. Polzer, M. Ballauff, and M. Drechsler. Catalytic activity of palladium nanoparticles encapsulated in spherical polyelectrolyte brushes and core-shell microgels. *Chem. Mater.*, 19:1062–1069, 2007.
- [46] S. Bhattacharya, F. Eckert, V. Boyko, and A. Pich. Temperature-, pH-, and magnetic-field-sensitive hybrid microgels. *Small*, 3(4):650–657, 2007.
- [47] M. Karg, I. Pastoriza-Santos, L. M. Liz-Marzán, and T. Hellweg. A versatile approach for the preparation of thermosensitive PNIPAM core-shell microgels with nanoparticle cores. *Chem. Phys. Chem.*, 7:2298–2301, 2006.
- [48] M. Karg, S. Wellert, I. Pastoriza-Santos, A. Lapp, L. M. Liz-Marzán, and T. Hellweg. Thermoresponsive core-shell microgels with silica nanoparticle cores: size, structure, and volume phase transition of the polymer shell. *Phys. Chem. Chem. Phys.*, 10:6708 – 6716, 2008.
- [49] S. Koizumi, M. Monkenbusch, D. Richter, D. Schwahn, B. Farago, and M. Annaka. Frozen concentration fluctuations in a poly(*N*-isopropylacrylamide) gel studied by neutron spin-echo and small-angle neutron scattering. *Appl. Phys. A*, 74:S399–S401, 2002.
- [50] J. Adelsberger, A. Kulkarni, A. Jain, W. Wang, A. M. Bivigou-Koumba, P. Busch, V. Pipich, O. Holderer, T. Hellweg, A. Laschewsky, P. Müller-Buschbaum, and C. M. Papadakis. Thermoresponsive PS-*b*-PNIPAM-*b*-PS micelles: Aggregation behavior, segmental dynamics, and thermal response. *Macromolecules*, 43:2490–2501, 2010.
- [51] Y. D. Yi and Y. C. Bae. Volume-phase transition of submicron-sized *N*-isopropylacrylamide/*N*-*tert*-butylacrylamide particles by photon correlation spectroscopy. *Journal of Applied Polymer Science*, 67:2087–2092, 1998.

- 
- [52] J. D. Debord and L. A. Lyon. Synthesis and characterization of pH-responsive copolymer microgels with tunable volume phase transition temperatures. *Langmuir*, 19:7662–7664, 2003.
- [53] K. Dusek. *Responsive Gels: Volume Transitions I*, volume 109 of *Advances in Polymer Science*. Springer Verlag, Berlin, 1 edition, 1993.
- [54] K. Dusek. *Responsive Gels: Volume Transitions II*, volume 110 of *Advances in Polymer Science*. Springer Verlag, Berlin, 1 edition, 1993.
- [55] T. Hoare and R. Pelton. Characterizing charge and crosslinker distributions in polyelectrolyte microgels. *Current Opinion in Colloid & Interface Sci.*, 13:413–428, 2008.
- [56] P. Hazot, J. P. Chapel, C. Pichot, A. Elaissari, and T. Delair. Preparation of poly(*N*-ethylmethacrylamide) particles via an emulsion/precipitation process: The role of the crosslinker. *J. Polym. Sci.: Part A: Polym. Chem.*, 40:1808–1817, 2002.
- [57] S. Hirotsu, Y. Hirokawa, and T. Tanaka. Volume-phase transitions of ionized *N*-isopropylacrylamide gels. *J. Chem. Phys.*, 87(2):1392–1395, 1987.
- [58] P. J. Flory. *Principles of Polymer Chemistry*. Cornell University Press, Ithaca and London, 1953.
- [59] A. Z. Pich and H.-J. P. Adler. Composite aqueous microgels: an overview of recent advances in synthesis, characterization and application. *Polym. Int.*, 56:291–307, 2007.
- [60] M. Das, H. Zhang, and E. Kumacheva. Microgels: Old materials with new applications. *Annu. Rev. Mater. Res.*, 36:117–142, 2006.
- [61] A. M. Schmidt. Thermoresponsive magnetic colloids. *Colloid Polym. Sci.*, 285:953–966, 2007.

- 
- [62] B. Sierra-Martin, M. S. Romero-Cano, A. Fernandez-Nieves, and A. Fernandez-Barbero. Thermal control over the electrophoresis of soft colloidal particles. *Langmuir*, 22:3586–3590, 2006.
- [63] A. Fernandez-Nieves, A. Fernandez-Barbero, F. J. de las Nieves, and B. Vincent. Motion of microgel particles under an external electric field. *J. Phys.: Condens. Matter*, 12:3605–3614, 2000.
- [64] Sara Abalde-Cela, Paula Aldeanueva-Potel, Cintia Mateo-Mateo, Laura Rodríguez-Lorenzo, Ramón A. Alvarez-Puebla, and Luis M. Liz-Marzán. Surface-enhanced raman scattering biomedical applications of plasmonic colloidal particles. *J. R. Soc. Interface*, pages 1–16, 2010.
- [65] Shigan Chai, Jinzhi Zhang, Tingting Yang, Jianjun Yuan, and Shiyuan Cheng. Thermoresponsive microgel decorated with silica nanoparticles in shell: Biomimetic synthesis and drug release application. *Colloids and Surfaces A: Physicochem. Eng. Aspects*, 356:32–39, 2010.
- [66] A. Pich, A. Karak, Y. Lu, A. K. Ghosh, and H.-J. P. Adler. Preparation of hybrid microgels functionalized by silver nanoparticles. *Macromol. Rapid Commun.*, 27:344–350, 2006.
- [67] Y. Lu, Y. Mei, M. Drechsler, and M. Ballauff. Thermoresponsive core-shell particles as carriers for Ag nanoparticles: Modulating the catalytic activity by a phase transition in networks. *Angew. Chem. Int. Ed.*, 45:813–816, 2006.
- [68] M. Agrawal, J. Rubio-Retama, N. E. Zafeiropoulos, N. Gaponik, S. Gupta, V. Cimrova, V. Lesnyak, E. Lopez-Cabarcos, S. Tzavalas, R. Rojas-Reyna, A. Eychmüller, and M. Stamm. Switchable photoluminescence of cdte nanocrystals by temperature-responsive microgels. *Langmuir*, 24:9820–9824, 2008.
- [69] M. Bradley, N. Bruno, and B. Vincent. Distribution of CdSe quantum dots within swollen polystyrene microgel particles using confocal microscopy. *Langmuir*, 21:2750–2753, 2005.

- 
- [70] Stefano Sacanna and Albert P. Philipse. A generic single-step synthesis of monodisperse core/shell colloids based on spontaneous pickering emulsification. *Adv. Mater.*, 19:3824–3826, 2007.
- [71] A. Pich, Y. Lu, V. Boyko, K.-F. Arndt, and H.-J. P. Adler. Thermo-sensitive poly(*N*-vinylcaprolactam-co-acetoacetoxyethyl methacrylate) microgels: 3. incorporation of polypyrrole by selective microgel swelling in ethanol–water mixtures. *Polymer*, 45:1079–1087, 2004.
- [72] Y. Lu, Y. Mei, M. Ballauff, and M. Drechsler. Thermoresponsive core-shell particles as carrier systems for metallic nanoparticles. *J. Phys. Chem. B*, 110:3930–3937, 2006.
- [73] M. Das, N. Sanson, D. Fava, and E. Kumacheva. Microgels loaded with gold nanorods: Photothermally triggered volume phase transition under physiological conditions. *Langmuir*, 23:196–201, 2007.
- [74] I. Pastoriza-Santos, J. Pérez-Juste, and L. M. Liz-Marzán. Silica-coating and hydrophobation of CTAB-stabilized gold nanorods. *Chem. Mater.*, 18:2465–2467, 2006.
- [75] C. Lofton and W. Sigmund. Mechanisms controlling crystal habits of gold and silver colloids. *Adv. Funct. Mater.*, 15:1197–1208, 2005.
- [76] N. Malikova, I. Pastoriza-Santos, M. Schierhorn, N. A. Kotov, and L. M. Liz-Marzán. Layer-by-layer assembly of mixed spherical and planar gold nanoparticles: Control of interparticle interactions. *Langmuir*, 18:3694–3697, 2002.
- [77] Jill E. Millstone, Sungho Park, Kevin L. Shuford, Lidong Qin, George C. Schatz, and Chad A. Mirkin. Observation of a quadrupole plasmon mode for a colloidal solution of gold nanoprisms. *J. Am. Chem. Soc.*, 127:5312–5313, 2005.
- [78] B. J. Berne and R. Pecora. *Dynamic Light Scattering*. John Wiley & sons, Inc., New York, 1976.

- 
- [79] J.-HZ-Xue, d.J. Pine, S.T. Milner, X.-I. Wu, and P.M. Chaikin. Nonergodicity and light scattering from polymer gels. *Physical Review A*, 46(10):6550–6563, 1992.
- [80] Hidemitsu Furukawa, Kazuyuki Horie, Ryunosuke Nozaki, and Mamoru Okada. Swelling-induced modulation of static and dynamic fluctuations in polyacrylamide gels observed by scanning microscopic light scattering. *Physical Review E*, 68:031406, 2003.
- [81] B. Chu. *Laser Light Scattering*. Academic Press, Inc., New York, 1974.
- [82] D. E. Koppel. Analysis of macromolecular polydispersity in intensity correlation spectroscopy: The method of cumulants. *J. Chem. Phys.*, 57(11):4814–4820, 1972.
- [83] C. B. Barger. Measurement of continuous distribution of spherical particles by intensity correlation spectroscopy: Analysis by cumulants. *J. Chem. Phys.*, 61(5):2134–2138, 1974.
- [84] S. W. Provencher. A constrained regularization method for inverting data represented by linear algebraic or integral equations. *Computer Physics Com.*, 27:213–217, 1982.
- [85] S. W. Provencher. Contin: a general purpose constrained regularization program for inverting noisy linear algebraic and integral equations. *Computer Physics Com.*, 27:229–242, 1982.
- [86] T. Tanaka, E. Sato, Y. Hirokawa, S. Hirotsu, and J. Peetermans. Critical kinetics of volume phase transition of gels. *Phys. Rev. Lett.*, 55:2455–2458, 1985.
- [87] M. Shibayama. Spatial inhomogeneity and dynamic fluctuations of polymer gels. *Macromol. Chem. Phys.*, 199:1–30, 1998.
- [88] A. Fernandez-Barbero, A. Fernandez-Nieves, I. Grillo, and E. Lopez-Cabarcos. Structural modifications in the swelling of inhomogeneous microgels by light and neutron scattering. *Phys. Rev. E*, 66(5):051803/1–10, 2002.

- 
- [89] P. J. Flory. Thermodynamics of polymer solutions. *Discussions of the Faraday Society*, (49):7–29, 1970.
- [90] J. J. Crassous, A. Wittmann, M. Siebenbürger, M. Schrunner, M. Drechsler, and M. Ballauff. Direct imaging of temperature-sensitive core-shell latexes by cryogenic transmission electron microscopy. *Colloid Polym Sci*, 286:805–812, 2008.
- [91] Joseph P. Cook and D. Jason Riley. The effect of perchlorate ions on a pyridine-based microgel. *Advances in Colloid and Interface Science*, 147:69–73, 2009.
- [92] P. J. Flory and J. Rehner. Statistical mechanics of cross-linked polymer networks. I. rubberlike elasticity. *J. Chem. Phys.*, 11(11):512–520, 1943.
- [93] S. Hirotsu. Static and time-dependent properties of polymer gels around the volume phase transition. *Phase Transitions*, 47:183–240, 1994.
- [94] B.E. Eichinger and P.J. Flory. Thermodynamics of polymer solutions. *Trans. Faraday Soc*, 64:2035–2052, 1968.
- [95] Shunsuke Hirotsu. Softening of bulk modulus and negative poisson’s ratio near the volume phase transition of polymer gels. *J. Chern. Phys., Vol. 94, No.5, 1 March 1991*, 94:3950–3957, 1991.
- [96] P. A. L. Fernandes, S. Schmidt, M. Zeiser, A. Fery, and T. Hellweg. Swelling and mechanical properties of polymer gels with cross-linking gradient. *Soft Matter*, 6:3455–3458, 2010.
- [97] J. S. Higgins and H. C. Benoit. *Polymers and Neutron Scattering*. Clarendon Press, Oxford, 2 edition, 1996.
- [98] C. J. Carlile and B. T. M. Willis. *Experimental Neutron Scattering*. Oxford Univ. Press, 2009.
- [99] R. Gilles, A. Ostermann, C. Schanzer, B. Krimmer, and W. Petry. The concept of the new small-angle scattering instrument SANS-1 at the FRM II. *Physica B*, 385:1174–1176, 2006.

- 
- [100] M. Shibayama, T. Tanaka, and C. C. Han. Small-angle neutron scattering study on weakly charged temperature sensitive polymer gels. *J. Chem. Phys.*, 97(9):6842–6854, 1992.
- [101] E. Geisler, F. Horkay, and A.-M. Hecht. Scattering from network polydispersity in polymer gels. *Phys. Rev. Lett.*, 71(4):645–648, 1993.
- [102] P.-G. de Gennes. *Scaling Concepts in Polymer Physics*. Cornell University Press, Ithaca and London, 1979.
- [103] W. Brown, Z. Pu, and R. Rymden. Size and shape of nonionic amphiphile micelles: NMR self-diffusion and static and quasi-elastic light-scattering measurements on  $C_{12}E_5$ ,  $C_{12}E_7$ , and  $C_{12}E_8$  in aqueous solution. *J. Phys. Chem.*, 92:6086–6094, 1988.
- [104] K. Kratz, A. Lapp, W. Eimer, and T. Hellweg. Volume phase transition and structure of TREGDMA, EGDMA, and BIS cross-linked PNIPAM microgels: A small angle neutron and dynamic light scattering study. *Colloids & Surfaces A*, 197(1-3):55–67, January 2002.
- [105] P. Wong. Scattering by inhomogeneous systems with rough internal surfaces: Porous solids and random-field ising systems. *Phys. Rev. B*, 32(11):7417–7424, 1985.
- [106] F. Mezei, editor. *Neutron Spin Echo*, volume 124 of *Lecture Notes in Physics*. Springer Verlag, Berlin, 1980.
- [107] F. Mezei, C. Pappas, and T. Gutberlet. *Neutron Spin Echo Spectroscopy*, volume 601 of *Lecture Notes in Physics*. Springer, Heidelberg, 1 edition, 2003.
- [108] F. Mezei. Neutron spin echo: A new concept in polarized thermal neutron techniques. *Z. Physik*, 255:146–160, 1972.
- [109] O. Holderer, M. Monkenbusch, R. Schätzler, H. Kleines, W. Westerhausen, and D. Richter. The JCNS neutron spin-echo spectrometer J-NSE at the FRM II. *Meas. Sci. Technol.*, 19:034022, 2008.



- 
- [110] T. Tanaka, L. O. Hocker, and G. B. Benedek. Spectrum of light scattered from a viscoelastic gel. *J. Chem. Phys.*, 59:5151–5159, 1973.
- [111] T. Tanaka. Dynamics of critical concentration fluctuations. *Phys. Rev. A*, 17(2):763–766, 1978.
- [112] R. H. Pelton and P. Chibante. Preparation of aqueous lattices with *N*-isopropylacrylamide. *Colloids and Surfaces*, 20:247–256, 1986.
- [113] M. Konno B. Rodriguez-Gonzalez Y. Kobayashi, M. Horie and L. M. Liz-Marzán. Preparation and properties of silica-coated cobalt nanoparticles. *J. Phys. Chem. B*, 107:7420–74205, 2003.
- [114] B. Rodriguez-Gonzalez-M. Spasova I. Barsukov M. Farle M. Grzelczak, J. Perez-Juste and L. M. Liz-Marzán. Pt-catalyzed growth of Ni nanoparticles in aqueous CTAB solution. *Chem. Mater.*, 20:5399–5405, 2008.
- [115] A. Radulescu. KWS-2 - the high-intensity SANS diffractometer of JCNS at FRM II. In *Trends and Perspectives in Neutron Scattering on Soft Matter*, Tutzing, 05.10.2009 - 08.10.2009.
- [116] G. D. Wignall and F. S. Bates. Absolute calibration of small-angle neutron scattering data. *J Appl Crystallogr*, 20:28–40, 1987.
- [117] T. P. Russell, J. S. Lin, S. Spooner, and G. D. Wignall. Intercalibration of small-angle x-ray and neutron scattering data. *J Appl Crystallogr*, 21:629–638, 1988.
- [118] B. Farago. Recent neutron spin-echo developments at the ILL (IN11 and IN15). *Physica B*, 267:270–276, 1999.
- [119] UTHSCSA Image Tool, version 3.0, University of Texas, Health Science Center in San Antonio, USA; Sept. 2010.
- [120] M. Shibayama, Y. Fujikawa, and S. Nomura. Dynamic light scattering study of poly(*N*-isopropyl-acrylamide-co-acrylic acid) gels. *Macromolecules*, 29:6535–6540, 1996.

- 
- [121] M. Shibayama, K. Kawakubo, F. Ikkai, and M. Imai. Small-angle neutron scattering study on charged gels in deformed state. *Macromolecules*, 31:2586–2592, 1998.
- [122] J. Gao and B. J. Frisken. Cross-linker-free *N*-isopropylacrylamide gel nanospheres. *Langmuir*, 19:5212–5216, 2003.
- [123] J. Gao and B. J. Frisken. Influence of reaction conditions on the synthesis of self-cross-linked *N*-isopropylacrylamide microgels. *Langmuir*, 19:5217–5222, 2003.
- [124] Youg Li and Toyochi Tanaka. Kinetics of swelling and shrinking of gels. *J. Chem. Phys.*, 92:1365–1371, 1990.
- [125] A. Peters and S. J. Candau. Kinetics of swelling of polyacrylamide gels. *Macromolecules*, 19:1952–1955, 1986.
- [126] G. E. Morris, B. Vincent, and M. J. Snowden. Adsorption of lead ions onto *N*-isopropylacrylamide and acrylic acid copolymer microgels. *J. Colloid Inter. Sci.*, 190(1):198–205, 1997.
- [127] K. Kratz, Th. Hellweg, and W. Eimer. Effect of connectivity and charge density on the swelling and local structural properties of colloidal pnipa microgels. *Ber. Bunsenges. Phys. Chem.*, 102:1603–1608, 1998.
- [128] S. Koizumi, M. Monkenbusch, D. Richter, D. Schwahn, and Bela Farago. Concentration fluctuations in polymer gel investigated by neutron scattering: Static inhomogeneity in swollen gel. *J. Chem. Phys.*, 121:12721–12731, 2004.
- [129] A.-M. Hecht, F. Horkay, P. Schleger, and E. Geissler. Thermal fluctuations in polymer gels investigated by neutron spin echo and dynamic light scattering. *Macromolecules*, 35:8552–8555, 2002.
- [130] A.-M. Hecht, F. Horkay, and E. Geissler. Neutron scattering investigation on a bimodal polymer gel. *J. Phys. Chem. B*, 105:5637–5642, 2001.
- [131] W. Brown. *Dynamic Light Scattering: The Method and Some Applications*. Clarendon Press, Oxford, 1993.

- 
- [132] Qing-Song Zhang, Liu-Sheng Zha, Jing-Hong Ma, and Bo-Run Liang. Synthesis and characterization of novel, temperature-sensitive microgels based on *N*-isopropylacrylamide and *tert*-butyl acrylate. *Journal of Applied Polymer Science*, 103:2962–2967, 2007.
- [133] B. Sierra-Martin, Y. Choi, M. S. Romero-Cano, T. Cosgrove, B. Vincent, and A. Fernandez-Barbero. Microscopic signature of a microgel volume phase transition. *Macromolecules*, 38:10782–10787, 2005.
- [134] J. Wu, G. Huang, and Z. Hu. Interparticle potential and the phase behavior of temperature-sensitive microgel dispersions. *Macromolecules*, 36:440–448, 2003.
- [135] H. Wu, M. Lattuada, P. Sandkühler, J. Sefcik, and M. Morbidelli. Role of sedimentation and buoyancy on the kinetics of diffusion limited colloidal aggregation. *Langmuir*, 19:10710–10718, 2003.
- [136] Toshiaki Hino and John M. Prausnitz. Swelling equilibria for heterogeneous polyacrylamide gels. *Journal of Applied Polymer Science*, 62:1635–1640, 1996.
- [137] H. Senff and W. Richtering. Influence of cross-linker density on rheological properties of temperature-sensitive microgel suspensions. *Colloid Polym. Sci.*, 278:830–840, 2000.
- [138] B. Erman and P.J. Flory. Critical phenomena and transitions in swollen polymer networks and in linear macromolecules. *Macromolecules*, 19:2342–2353, 1986.
- [139] J. Kohlbrecher. *SASfit: A program for fitting simple structural models to small angle scattering data*. Paul Scherrer Institut, Laboratory for Neutron Scattering, CH-5232 Villigen, Switzerland, 2008.
- [140] J. Rubio-Retama, N. E. Zafeiropoulos, C. Serafinelli, R. Rojas-Reyna, B. Voit, E. Lopez-Cabarcos, and M. Stamm. Synthesis and characterization of thermosensitive PNIPAM microgels covered with superparamagnetic Fe<sub>2</sub>O<sub>3</sub> nanoparticles. *Langmuir*, 23:10280–10285, 2007.

- 
- [141] J. E. Wong, A. Krishnakumar Gaharwar, D. Mueller-Schulte, D. Bahadur, and W. Richtering. Layer-by-layer assembly of a magnetic nanoparticle shell on a thermoresponsive microgel core. *J. Magnetism and Magnetic Mater.*, 311:219–223, 2007.
- [142] H. Kawaguchi. *Hydrogels: Biological Properties and Applications*. Springer, 2009.
- [143] V. Salgueirino-Maceira, M. A. Correa-Duarte, M. Farle, M. A. Lopez-Quintela, K. Sieradzki, and Rodolfo Diaz. Synthesis and characterization of large colloidal cobalt particles. *Langmuir*, 22:1455–1458, 2006.
- [144] Y.-J. Zhang, Y. Zhang, Z.-H. Wang, D. Li, T.-Y. Cui, W. Liu, and Z.-D. Z. Controlled synthesis of cobalt flowerlike architectures by a facile hydrothermal route. *Eur. J. Inorg. Chem.*, pages 2799–2738, 2008.
- [145] Matthias Karg. *Multi-Responsive Hybrid Colloids Based On Microgels And Nanoparticles*. PhD thesis, TU Berlin, Institut für Chemie, 2009.
- [146] M. Grzelczak, J. Pérez-Juste, P. Mulvaney, and L.M. Liz-Marzán. Shape control in gold nanoparticle synthesis. *Chem. Soc. Rev.*, 37:1783–1791, 2008.
- [147] M. M. Koebel, L. C. Jones, and G. A. Somorjai. Preparation of size-tunable, highly monodisperse PVP-protected Pt-nanoparticles by seed-mediated growth. *J Nanopart Res*, 10:1063–1069, 2008.
- [148] Ch. Graf, D. L. J. Vossen, A. Imhof, and A. van Blaaderen. A general method to coat colloidal particles with silica. *Langmuir* 2003, 19, 6693-6700, 19:6693–6700, 2003.

# List of Publications

1. **Y. Hertle**, M. Zeiser, C.Hasenöhrl, P. Busch and T. Hellweg. Responsive P(NIPAM-co-NtBAM) microgels: Flory-Rehner description of the swelling behaviour. *Colloid Polym. Sci.*, 288:1047-1059, 2010.
2. **Y. Hertle**, M. Zeiser, P. Fouquet, M. Maccarini and T. Hellweg. The internal network dynamics of poly(NIPAM) based copolymer micro- and macrogels: A comparative quasilelastic neutron scattering study. *J. Phys. Chem.*, submitted.

# Abbreviations

$\alpha$	swelling ratio
$\eta$	viscosity
$\lambda$	wavelength
$v$	molar volume of solvent
$\xi$	correlation length
$\tau$	Fourier time
$\phi$	polymer volume fraction
$\chi$	polymer-solvent interaction parameter
$\Gamma$	relaxation rate
$\Theta$	theta temperature
$\Pi$	osmotic pressure
AAc	acrylic acid
AFM	atomic force microscopy
AIBA	2,2'-azobis(2-methylbutyronitrile)
APS	ammonium peroxodisulfate
APTMS	(3-aminopropyl)trimethoxysilane
BAC	butenoic acid
BIS	<i>N,N'</i> -methylenebisacrylamide
CTAB	hexadecyltrimethylammonium bromide
DLS	dynamic light scattering
$D_T$	translational diffusion coefficient
DVB	divinylbenzene
e.g.	exempli gratia
et al.	et altera
FRM II	Forschungs-Neutronenquelle Heinz Maier-Leibnitz
FRT	Flory-Rehner theory
ICF	intensity correlation function

ILL	Institute Laue-Langevin
JCNS	Jlich centre for neutron science
$k_B$	Boltzmann constant
KPS	potassium peroxydisulfate
LbL	layer-by-layer
LCST	lower critical solution temperature
M	molar
MPS	3-(Trimethoxysilyl)propyl methacrylate
$M_W$	molecular weight
n	refractive index
$N_A$	Avogadro's number,
$N_{gel}$	average degree of polymerization between junction points,
NIPAM	<i>N</i> -isopropylacrylamide
NSE	Neutron spin echo
NtBAM	<i>N</i> -tert-butylacrylamide
OZ	Ornstein-Zernike
$P(q)$	particle form factor
PAH	poly(allylamine hydrochloride)
poly(NIPAM)	poly( <i>N</i> -isopropylacrylamide)
PS	polystyrene
PSS	poly(styrene sulphonate)
PVP	poly(vinylpyrrolidone)
$q$	scattering vector
$R_g$	radius of gyration
$R_h$	hydrodynamic radius
RT	room temperature
$S(q)$	interparticle structure factor
SANS	small angle neutron scattering
SDS	sodium dodecyl sulfate

SEM	scanning electron microscopy
SERS	Surface enhanced Raman spectroscopy
SLS	static light scattering
TEM	transmission electron microscopy
TEOS	tetraethyl orthosilicate
TMEDA	<i>N,N,N',N'</i> -Tetramethylethylenediamine
V	particle volume
VPT	volume phase transition
VPTT	volume phase transition temperature




# Erklärung zur Dissertation

Hiermit erkläre ich, dass ich die vorliegende Arbeit selbstständig verfasst und keine anderen als die von mir angegebenen Quellen und Hilfsmittel verwendet habe.

Ferner erkläre ich, dass ich anderweitig mit oder ohne Erfolg nicht versucht habe, diese Dissertation einzureichen. Ich habe außerdem keine gleichartige Doktorprüfung an einer Hochschule endgültig nicht bestanden.

Bayreuth, der 15. Dezember 2010

  
\_\_\_\_\_  
Yvonne Hertle